# Physiological and molecular studies of the chloroplast movements in the liverwort *Apopellia endiviifolia*

**2023. 3**

Department of Biological Production Science
United Graduate School of Agricultural Science
Tokyo University of Agriculture and Technology

**YONG LEE KIEN**

# Physiological and molecular studies of the chloroplast movements in the liverwort *Apopellia endiviifolia*

# 苔類ホソバミズゼニゴケにおける葉緑体運動の生理学的・分子生物学的研究

A Dissertation Presented

by

YONG LEE KIEN

Submitted to United Graduate School of Agricultural Science of Tokyo University of Agriculture and Technology

in partial fulfilment of the requirements for the degree of

DOCTOR OF PHILOSOPHY

March 2023

**DECLARATION OF ORIGINALITY**

I hereby declare that the thesis is based on my original work. All the quotations and citations have been duly acknowledged. No portion of the work referred to in this dissertation has been previously or concurrently submitted for any other degree programs in other institutions of higher learning.

YONG LEE KIEN

**ACKNOWLEDGEMENTS**

First and foremost, I would like to express my great gratitude and appreciation to my supervisor, Prof Yutaka Kodama, for his unceasing countenance, guidance, patience and motivation throughout my study and living in Japan. I am deeply grateful to him for providing helpful suggestions and comments on the draft documents leading to this thesis. His guidance will be remembered forever by me.

Moreover, I would like to extend my gratitude to my co-supervisors, Prof Toshiyuki Fukuhara and Dr Takeshi Kurokura for their guidance and support in my study. Great appreciation to Dr Gotoh Eiji (Kyushu University) for suggestions on the visualisation of chloroplast actin filaments in *A. endiviifolia*. My sincere thanks were also presented to the MEXT scholarship for providing financial support for my study and living in Japan.

Last but most importantly, I dedicated this thesis to my beloved family. I will not forget their sincere love, moral support, countless prayers and endless efforts during my entire journey in university. This piece of work is also dedicated to my fellow lab mates, for their helpful suggestions and discussion, also all the fun we have had in the journey of my postgraduate study.

## ABSTRACT

Chloroplast movements refer to the subcellular localisation of chloroplasts in plant cells that respond to ambient light and temperature. The relocation of chloroplasts optimises photosynthetic activity under different environmental conditions and supports plant growth and development to survive. These behavioural chloroplast movements under room temperature conditions have induced chloroplast to migrate to the anticlinal wall bordering with neighbouring cells in dark (dark-positioning response), accumulate towards weak light (accumulation response), and avoid strong light (avoidance response). While at low-temperature conditions, chloroplast moves away from the weak light (cold-avoidance response). In the present study, I identified a liverwort *Apopellia endiviifolia* with simple thalloid thalli comprising uniformly developed chloroplasts without any air chamber. From the thallus, clear views of the four chloroplast responses were observed. Moreover, the light-dependent chloroplast responses including accumulation, avoidance and cold-avoidance in *A. endiviifolia* were only reacted to blue light irradiation, indicating mediation from the blue light photoreceptor phototropin. A single copy phototropin gene of *A. endiviifolia* (*AePHOT*) was identified through the next-generation RNA sequencing and Southern blot analysis, similar to the *MpPHOT* gene in the closely related liverwort *Marchantia polymorpha* that perform a simple signalling pathway. These results showed a beneficial combination of the simple thalloid thallus and single copy *AePHOT* gene in *A. endiviifolia*, which can be useful for the following study of chloroplast movements.

To further understand the functional role of the *AePHOT* gene in regulating the chloroplast movements, I performed a comparative analysis on the transient expression of *AePHOT* and *MpPHOT* in *A. endiviifolia* and *M. polymorpha*. I have cross-introduced the plasmids of AePHOT or MpPHOT into the thalli of *A. endiviifolia* and gemmalings of *M. polymorpha* by particle bombardment. Avoidance response from the transient overexpression of the *AePHOT* gene was observed in the AePHOT-transformed cells of *A. endiviifolia* under weak blue light (BL) at 22°C. This result has confirmed the functions of the *AePHOT* gene in *A. endiviifolia*. However, the avoidance response was not induced in AePHOT-transformed cells of *M. polymorpha*, indicating incompatibility of *AePHOT* to *M. polymorpha*. This observation showed the species specificity of *AePHOT* that only functions in *A. endiviifolia*. On the other hand, the transient overexpression of *MpPHOT* has induced avoidance responses in both MpPHOT-transformed cells of *A. endiviifolia* and *M. polymorpha* under the weak BL conditions, showing the compatible function of *MpPHOT* in *A. endiviifolia*.

As *AePHOT* signalling in the chloroplast movements of *A. endiviifolia* has been demonstrated, cytoskeleton components employed in the downstream pathway that facilitate the chloroplast movements were investigated. To date, two cytoskeleton components, microtubules and actin filaments have been reported to move chloroplasts in plant cells. Through the respective fluorescent localisations, I observed the microtubules and actin filaments in the thallus cells of *A. endiviifolia*. The visualisation of microtubules and actin filaments was specifically disrupted by the microtubule and actin filament polymerisation inhibitors oryzalin and latrunculin-A (lat-A), respectively. To find the responsible cytoskeleton components of the chloroplast movements in *A. endiviifolia*, the chloroplast positionings in the inhibitor-treated thalli with disrupted microtubules or actin filaments have been examined. In the oryzalin-treated thalli, light-dependent chloroplast responses including accumulation, avoidance and cold-

avoidance were induced unaffectedly despite the disrupted microtubules. Whereas, these chloroplast responses were inhibited in the lat-A-treated thalli, as the disrupted actin filaments have restricted the chloroplast mobility in the formation of chloroplast responses. These results indicate that the light-dependent chloroplast responses are regulated by actin filaments only, which is consistent with the photosynthetic organs reported in previous data. Additionally, a rapid dark-positioning response of *A. endiviifolia* that can be achieved after 3 h of dark incubation was demonstrated in the present study. This response was considered a faster reaction than in any reported plant species. Under the dark conditions, the dark-positioning response of *A. endiviifolia* was not inhibited by the disrupted microtubules, but by the disrupted actin filaments. This result proves the actin filament regulation in the dark-positioning response, and it is the first to be reported here.

In conclusion, my study demonstrated the beneficial characteristics of clear chloroplast observation and simple *AePHOT* signalling in *A. endiviifolia*. These characteristics thus facilitated the subsequent analysis to determine the mechanism of chloroplast movements in *A. endiviifolia*, where *AePHOT* signalling in mediating the chloroplast movements through the actin filament motility mechanism was shown. Moreover, the rapid dark-positioning response of *A. endiviifolia* was highlighted in the present study, as it shows the potential uses of *A. endiviifolia* as a model plant to elucidate the mechanism of dark-positioning response.

**TABLE OF CONTENTS**


ACKNOWLEDGEMENTS I

ABSTRACT II

LIST OF FIGURES VII

LIST OF TABLES XIII

CHAPTER 1 INTRODUCTION

1.1 Chloroplast movements in plants 1

1.2 Photoreceptor signalling for chloroplast movements 2

1.3 Importance of chloroplast movements to agriculture 3

1.4 Objectives of the study 3

1.5 Outline of the dissertation 4

CHAPTER 2 CHLOROPLAST RELOCATION MOVEMENTS IN THE LIVERWORT *APOPELLIA ENDIVIIFOLIA*

2.1 Background overview 5

2.2 Methodology

2.2.1 Plant materials and growth conditions 6

2.2.2 Genomic DNA and total RNA extraction of *A. endiviifolia* 6

2.2.3 Sex determination of *A. endiviifolia* 7

2.2.4 Histological observation of *A. endiviifolia* and *M. polymorpha* thalli 7

2.2.5 Treatments of dark, light and low-temperature 8

2.2.6 Observation and evaluation of chloroplast positioning 8

2.2.7 Observation of chloroplast positioning under red light microbeam irradiation 9

2.2.8 Time-lapse observation of chloroplast movements under blue light microbeam irradiation 9

2.2.9 Next-generation RNA sequencing analysis of *A. endiviifolia* 10

2.2.10 Cloning and analysis of the *AePHOT* gene from *A. endiviifolia* 10

2.2.11 Southern blot analysis of *AePHOT* 11

2.2.12 Quantitative real-time PCR of *AePHOT* 11

2.3 Results

2.3.1 Sex determination of *A. endiviifolia* 12

2.3.2 Morphological characteristics of *A. endiviifolia* thallus 12

2.3.3 Chloroplast responses of *A. endiviifolia* 13

2.3.4 Blue light-dependent chloroplast movements in *A. endiviifolia* 14

2.3.5 Single copy phototropin gene of *A. endiviifolia* (*AePHOT*) 15

2.3.6 Relative quantification of *AePHOT* expression level in different chloroplast responses 16

2.4 Discussion 16

2.5 Summary of key findings 18

CHAPTER 3 COMPARATIVE ANALYSIS OF *AEPHOT* AND *MPPHOT* EXPRESSIONS IN *APOPELLIA ENDIVIIFOLIA* AND *MARCHANTIA POLYMORPHA*

3.1 Background overview 36

3.2 Methodology

3.2.1 Plant materials and growth conditions 37

3.2.2 Plasmid construction 37

3.2.3 Particle bombardment of *A. endiviifolia* and *M. polymorpha* 37

3.2.4 Observation and assessment of chloroplast positionings in transformed cell 38

3.3 Results

3.3.1 AePHOT and MpPHOT functions in *A. endiviifolia* 38

3.3.2 AePHOT and MpPHOT functions in *M. polymorpha* 39

3.4 Discussion 39

3.5 Summary of key findings 40

CHAPTER 4 ANALYSIS OF CYTOSKELETONS INVOLVED IN CHLOROPLAST MOVEMENTS OF *APOPELLIA ENDIVIIFOLIA*

4.1 Background overview 45

4.2 Methodology

4.2.1 Plant materials and growth conditions 46

4.2.2 Time-tracking observation of the dark-positioning response of *A. endiviifolia* 46

4.2.3 Treatments of microtubule and actin filament polymerisation inhibitors 46

4.2.4 Immunofluorescence staining of microtubules 47

4.2.5 Actin filament fluorescent marker amplification 47

4.2.6 Particle bombardment 48

4.2.7 Visualisation of microtubules and actin filaments of *A. endiviifolia* 48

4.2.8 Induction of chloroplast movements in *A. endiviifolia* 48

4.2.9 Observation and evaluation of chloroplast positioning 49

4.3 Results

4.3.1 Timeline of the dark-positioning response of *A. endiviifolia* 49

4.3.2 Visualisation of microtubules and actin filaments in *A. endiviifolia* 49

4.3.3 Depolymerisation of microtubules and actin filaments in *A. endiviifolia* 50

4.3.4 Chloroplast movements of *A. endiviifolia* are actin filament dependent 50

4.4 Discussion 51

4.5 Summary of key findings 53

CHAPTER 5 CONCLUSION AND PROSPECT FOR FUTURE STUDY 59

LIST OF REFERENCES

**LIST OF FIGURES**

**Figure 1.** Simple thalloid liverwort, *Apopellia endiviifolia*. Scale bar, 1 mm.

**Figure 2.** Light spectra of the light sources used in the present study. **A,** Light spectrum of white fluorescent light. **B,** Light spectrum of white LEDs. **C,** Light spectrum of blue LEDs. **D,** Light spectrum of red LEDs.

**Figure 3.** Restriction sites and probe for the Southern blot analysis of *AePHOT*. **A,** Two single restriction sites, EcoRV and EcoRI in the *AePHOT* mRNA were targeted to identify the *AePHOT* gene copy number. Black line, protein coding region; Blue lines, untranslated region (UTR); Red bars, restriction sites. **B,** Probe (583 bp DNA fragment) used for labelling was amplified from genomic DNA between LOV2 and kinase coding regions of *AePHOT*.

**Figure 4.** Sex determination of the isolated *A. endiviifolia*. PCR amplification was performed using primers for genes expressed in male (*PenB_Tua1* and *PenB_Raba1/11*) and female (*PenB_MT3*, *PenB_CYSP* and *PenB_MT2*) gametophytes with cDNA (**A**) and genomic DNA (**B**) from *A. endiviifolia*. The *Actin* gene (*PenB_ACT1*; accession number: DQ100290) of *A. endiviifolia* was used as a positive control. A 100-bp ladder (L) was used in the 2% TAE gel electrophoresis.

**Figure 5.** Transverse sections and chloroplast observation in *A. endiviifolia* and *M. polymorpha* thalli. **A**–**B,** Representative images of *A. endiviifolia* (**A**) and *M. polymorpha* (**B**) thalli. Black lines indicate the sectioning of the thallus. Scale bar, 1 mm. **C–F**, Transverse sections of *A. endiviifolia* (**C, E**) and *M. polymorpha* (**D, F**) thalli. Safranin red staining indicates the cell wall, and Alcian blue counterstaining indicates the intracellular contents. Scale bar, 200 μm. Asterisks indicate the developed air chamber in *M. polymorpha* thallus (**D, F**). **G–H,** Observation of chloroplasts through chlorophyll autofluorescence (red) by confocal laser scanning microscopy. The adaxial sides of *A. endiviifolia* (**G**) and *M. polymorpha* (**H**) thalli were observed. An arrow indicates the developed air chamber in *M. polymorpha* thallus (**H**). Scale bars, 20 μm.

**Figure 6.** Chloroplast responses of *A. endiviifolia* under the dark, different light intensity and low-temperature conditions. **A,** Dark-positioning response of *A. endiviifolia*. Detached thalli were incubated in the dark at 22°C, and the dark-positioning response was observed after 24 h, 48 h and 72 h. The accumulation response under 60 µmol photons $m^{-2}$ $s^{-1}$ of white light (weak WL) was observed before dark incubation. **B,** Evaluation of the dark-positioning response by the P/A ratio quantification. The graph shows a quantitative analysis of the chloroplast positioning in (**A**) based on the average P/A ratio from three replicates. **C**, Accumulation and avoidance responses of *A. endiviifolia*. Detached thalli were incubated under 10 to 210 µmol photons $m^{-2}$ $s^{-1}$ of WL at 22°C for 24 h; only representative images from thallus incubated under 80 to 150 µmol photons $m^{-2}$ $s^{-1}$ of WL were presented. The accumulation response was observed at <110 µmol photons $m^{-2}$ $s^{-1}$, and the avoidance response was observed at >120 µmol photons $m^{-2}$ $s^{-1}$ of WL irradiation. **D,** Evaluation of the accumulation and avoidance responses by the P/A ratio quantification. The graph shows a quantitative analysis of the chloroplast positioning in (**C**) based on the average P/A ratio from three replicates. The average P/A ratio of the dark-adapted thallus before treatment can be referred to the average P/A ratio of dark-positioning response at 24 h in (**B**). **E,** Cold-avoidance response in *A. endiviifolia*. Detached thalli were incubated under 60 µmol photons $m^{-2}$ $s^{-1}$ of WL at 22°C and 5°C for 24 h. The cold-avoidance response was induced at 5°C, whereas the accumulation response was induced at 22°C. **F,** Evaluation of the cold-avoidance response by the P/A ratio quantification. The graph shows a quantitative analysis of the chloroplast positioning in (**E**) based on the average P/A ratio from three replicates. Scale bars, 50 µm. Error bars represent standard deviation (N=3). Different alphabets (a and b) above the graph bars indicate significant differences (Tukey's HSD test for (**B**, **D**); Unpaired t-test for (**F**); $\alpha < 0.05$).

**Figure 7.** Dark-positioning response near the outermost anticlinal wall of *A. endiviifolia* thallus. Accumulation and dark-positioning response were induced after incubation under 60 µmol photons $m^{-2}$ $s^{-1}$ of white light and in the dark, respectively, for 24 h at 22°C. Arrowheads indicate no chloroplast localisation at the outermost anticlinal wall in the dark-positioning response. Scale bars, 50 µm.

**Figure 8.** Blue light-dependent chloroplast movements in *A. endiviifolia*. Detached thalli were incubated under 10 to 70 µmol photons $m^{-2}$ $s^{-1}$ of blue and red light at 22°C for 24 h. **A,** Quantitative analysis of chloroplast positioning resulting from blue light irradiation based on the average P/A ratio from three replicates. Different alphabets (a, b and c) above the graph bars indicate significant differences (Tukey's HSD test; $\alpha < 0.05$). **B,** Quantitative analysis of chloroplast positioning resulting from red light irradiation based on the average P/A ratio from three replicates in this study. The average P/A ratio of the dark-adapted thallus before treatment can be referred to the average P/A ratio of dark-positioning response at 24 h in Figure 6B.

**Figure 9.** Chloroplast movements in *A. endiviifolia* after red light (RL) microbeam irradiation. **A,** Observation of chloroplast positioning in the thallus cell before and after 90 min irradiation of weak RL microbeam (9 μmol photons $m^{-2}$ $s^{-1}$) at 22°C. **B,** Observation of chloroplast positioning in the thallus cell before and after 90 min irradiation of strong RL microbeam (227 μmol photons $m^{-2}$ $s^{-1}$) at 22°C. Scale bars, 30 μm. The black circle indicates the RL microbeam-irradiated spot.

**Figure 10.** Time-lapse imaging of chloroplast movements in *A. endiviifolia* under blue light (BL) microbeam irradiation. **A,** Accumulation response of chloroplasts towards the weak BL (30 μmol photons $m^{-2}$ $s^{-1}$) microbeam-irradiated spot in the thallus cell at 22°C. **B,** Quantitative analysis of the chloroplast moving distance in (**A**) calculated from the five numbered chloroplasts; the average distance of chloroplasts moved against time is shown in the graph. **C,** Avoidance response of the chloroplasts away from the strong BL (430 μmol photons $m^{-2}$ $s^{-1}$) microbeam-irradiated spot in the thallus cell at 22°C. **D,** Quantitative analysis of the chloroplast moving distance in (**C**) calculated from the five numbered chloroplasts; the average distance of chloroplasts moved against time is shown in the graph. **E,** Cold-avoidance response of the chloroplasts away from the weak BL (30 μmol photons $m^{-2}$ $s^{-1}$) microbeam-irradiated spot in the thallus cell at 5°C. **F,** Quantitative analysis of the chloroplast moving distance in (**E**) calculated from the five numbered chloroplasts; the average distance of chloroplasts moved against time is shown in the graph. Scale bars, 30 μm. The black circle indicates the BL microbeam-irradiated spot. Error bars represent standard deviation. The "r" indicates the correlation coefficient between the average distances of chloroplasts moved from the microbeam and irradiation time.

**Figure 11.** A single copy *PHOTOTROPIN* gene (*AePHOT*) of *A. endiviifolia*. **A,** Schematic illustration of AePHOT protein. aa, amino acids. **B,** Maximum likelihood phylogenetic tree of *A. endiviifolia*. Through the alignment of *AePHOT* sequences with ClustalW in Mega 7, phylogenetic relationships of *A. endiviifolia* (red border) with 47 non-vascular and vascular plants had assembled. The bootstrap values are indicated at the nodes. The bar represents 0.10 substitutions in each site. **C,** Southern blot analysis of *AePHOT*. A single band was shown in the lane denoted with EcoRI and EcoRV in the blot that was generated from EcoRI- and EcoRV-digested DNA products, respectively. The blot was hybridised by a probe of the *AePHOT* genomic fragment between the LOV2 and kinase coding regions (Figure 3B).

**Figure 12.** Alignment of *AePHOT* and *MpPHOT* nucleotide sequences (cDNA). The dark-shaded sequences indicate identical nucleotides between *AePHOT* and *MpPHOT*. The boxes indicate the coding regions of LOV1, LOV2, and kinase domains.

**Figure 13.** Alignment of AePHOT and MpPHOT protein sequences. The dark-shaded sequences indicate identical amino acids between AePHOT and MpPHOT. The boxes indicate the LOV1, LOV2, and kinase domains. Red arrowheads indicate the cysteine residues for FMN binding in the LOV1 and LOV2 domains of AePHOT and MpPHOT. The blue arrowhead indicates the aspartic acid residue, which is essential for the kinase function of AePHOT and MpPHOT.

**Figure 14.** Quantitative real-time PCR analysis of *AePHOT* gene expression. Relative expression levels (fold change values) of *AePHOT* in the dark, weak white light (WL), strong WL, and low temperature (5°C) with weak WL are shown in the graph. All transcript levels were normalised against *PenB_ACT1*. Error bars represent standard deviation. Different alphabets (a and b) above the graph bars indicate significant differences (Tukey's HSD test; $\alpha < 0.05$).

**Figure 15.** Time course of the avoidance and cold-avoidance responses of *A. endiviifolia*. **A,** Avoidance response of chloroplasts moving away from the irradiated strong BL microbeam (430 μmol photons $m^{-2}$ $s^{-1}$) in the thallus cell at 22°C. The arrows show chloroplasts moving towards the anticlinal wall separately. **B,** Cold-avoidance response of chloroplasts moving away from the irradiated weak BL microbeam (30 μmol photons $m^{-2}$ $s^{-1}$) in the thallus cell at 5°C. The arrows show chloroplasts gathering into a group (yellow dashed line) and moving away from the microbeam spot. Scale bars, 30 μm. The blue circle indicates the BL microbeam-irradiated spot. Images shown in this figure are taken from the time-lapse imaging in Figure 10C and 10E.

**Figure 16.** Observation of chloroplast positionings formed in the AePHOT- and MpPHOT-transformed cells of *A. endiviifolia* under weak blue light (25 μmol photons $m^{-2}$ $s^{-1}$) at 22°C. The AePHOT and MpPHOT with Citrine fluorescent marker were introduced into *A. endiviifolia* by particle bombardment. Mock refers to the control experiment that only introduced Citrine into *A. endiviifolia*. Citrine and chlorophyll fluorescence are shown as yellow and red, respectively. Scale bars, 25 μm.

**Figure 17.** Observation of chloroplast positionings formed in the MpPHOT- and AePHOT-transformed cells of *M. polymorpha* under weak blue light (25 μmol photons $m^{-2}$ $s^{-1}$) at 22°C. The MpPHOT and AePHOT with Citrine fluorescent marker were introduced into *M. polymorpha* by particle bombardment. Mock refers to the control experiment that only introduced Citrine into *M. polymorpha*. Citrine and chlorophyll fluorescence are shown as yellow and red, respectively. Scale bars, 25 μm.

**Figure 18.** Timeline of the dark-positioning response of *A. endiviifolia*. **A,** Representative images of the hourly dark induction of dark-positioning response in *A. endiviifolia* thalli. Scale bars, 50 µm. **B,** Evaluation of chloroplast positioning by the P/A ratio quantification. The average P/A ratio of chloroplasts positioning from the periclinal wall to the anticlinal wall in the dark-positioning response after every 30 min of dark incubation was tracked and quantified from three replicates. The declining P/A ratio implied the process of chloroplast movements in the dark-positioning response. Error bars represent standard deviation (N=3). Significant differences from 0 min with the range of 30 min ≤ t (time) ≤ 24 h ($P < 0.05$), 90 min ≤ t ≤ 24 h ($P < 0.01$), and 180 min ≤ t ≤ 24 h ($P < 0.001$); Tukey's HSD test; $\alpha < 0.05$.

**Figure 19.** Visualisation of microtubules and actin filaments in *A. endiviifolia*. **A**, Confocal z-stack image of microtubules in fluorescent-stained thallus section of *A. endiviifolia*. The thallus section of *A. endiviifolia* was stained by Alexa Fluor 488 fluorescent probe in immunofluorescence staining. **B**, Confocal z-stack image of actin filaments in *A. endiviifolia* transformed cells transiently expressing *Lifeact-Citrine*. **C**, Visualisation of chloroplast (cp-) actin filaments (white arrowhead) during the avoidance response of *A. endiviifolia* through *Lifeact-Citrine* expression. (**B, C**) The *Lifeact-Citrine* construct was introduced into *A. endiviifolia* by particle bombardment. Alexa Fluor 488, Lifeact-Citrine and chlorophyll fluorescence are shown as green, yellow, and red, respectively. Scale bars, 25 µm.

**Figure 20.** Depolymerisation of microtubules and actin filaments of *A. endiviifolia* by their respective inhibitors. **A**, Confocal z-stack image of microtubules in fluorescent-stained thallus section that pre-treated with dimethyl sulfoxide (control experiment) or oryzalin (microtubule depolymerisation inhibitor). **B**, Confocal z-stack image of actin filaments in *A. endiviifolia* transformed cells expressing *Lifeact-Citrine* treated with ethanol (control experiment) or latrunculin A (actin filament depolymerisation inhibitor). DMSO, 0.25% (v/v) dimethyl sulfoxide solution; Oryzalin, 10 µM oryzalin; EtOH, 0.25% (v/v) ethanol solution; Lat-A, 1 µM latrunculin A. Alexa Fluor 488, Lifeact-Citrine and chlorophyll fluorescence are shown as green, yellow, and red, respectively. Scale bars, 25 µm.

**Figure 21.** Determination of actin filament dependency of the accumulation, avoidance and cold-avoidance responses of *A. endiviifolia*. **A,** Representative images of chloroplast positioning induced in the inhibitor-treated thalli after incubation under weak blue light (25 μmol photons $m^{-2}$ $s^{-1}$) at 22°C for 24 h. The graph showed the quantitative analysis of the resulting chloroplast positionings based on the average P/A ratio from three replicates. **B,** Representative images of chloroplast positioning induced in the inhibitor-treated thalli after incubation under strong blue light (50 μmol photons $m^{-2}$ $s^{-1}$) at 22°C for 24 h. The graph showed the quantitative analysis of the resulting chloroplast positionings based on the average P/A ratio from three replicates. **C,** Representative images of chloroplast positioning induced in the inhibitor-treated thalli after incubation under weak blue light (25 μmol photons $m^{-2}$ $s^{-1}$) at 5°C for 24 h. The graph showed the quantitative analysis of the resulting chloroplast positionings based on the average P/A ratio from three replicates. DMSO, 0.25% (v/v) dimethyl sulfoxide solution; Oryzalin, 10 μM oryzalin; EtOH, 0.25% (v/v) ethanol solution; Lat-A, 1 μM latrunculin-A. Scale bars, 50 μm. Error bars represent standard deviation (N=3). Different alphabets (a and b) above the graph bars indicate significant differences (Tukey's HSD test; $\alpha < 0.05$).

**Figure 22.** Determination of actin filament dependency of the dark-positioning response of *A. endiviifolia*. **A,** Representative images of chloroplast positioning induced in the inhibitor-treated thalli after incubation in the dark at 22°C for 3 h. The graph showed the quantitative analysis of the resulting chloroplast positionings based on the average P/A ratio from three replicates. DMSO, 0.25% (v/v) dimethyl sulfoxide solution; Oryzalin, 10 μM oryzalin; EtOH, 0.25% (v/v) ethanol solution; Lat-A, 1 μM latrunculin A. Scale bars, 50 μm. Error bars represent standard deviation (N=3). Different alphabets (a and b) above the graph bar indicate significant differences (Tukey's HSD test; $\alpha < 0.05$).

**LIST OF TABLES**

**Table 1.** Primers used in the experiments described in Chapter 2.

**Table 2.** Quantification of chloroplast positionings resulted in the transformed cells of *A. endiviifolia* after incubation under weak blue light (25 μmol photons $m^{-2}$ $s^{-1}$) at 22°C for 24 h.

**Table 3.** Quantification of chloroplast positionings resulted in the transformed cells of *M. polymorpha* after incubation under weak blue light (25 μmol photons $m^{-2}$ $s^{-1}$) at 22°C for 24 h.

# CHAPTER 1
# INTRODUCTION

## 1.1 Chloroplast movements in plants

Chloroplast was named chlorophyll grains by Bohm in 1856 and the movement closely responded to the ambient light and temperature (Moore, 1888; Senn, 1908). Different chloroplast movements are induced under diverse environmental conditions to enhance photosynthesis efficiency for plant growth and development. Since the late 19$^{th}$ century, plant biologist Bernhard Frank defined the differences in chloroplast movements under light and dark conditions (Frank, 1872; Senn, 1908). Referring to these findings, plant taxonomist Gustav Senn performed a systematic analysis and classified ten different forms of chloroplast movements under different light intensities, wavelengths, and temperatures (Senn, 1908). These ten chloroplast movements were subsequently categorised into four main types to date (Senn, 1908; Kataoka, 1980). Under room temperature, dark-positioning response is induced in the dark where chloroplasts move to the anticlinal wall bordering with neighbouring cells in the liverwort *Marchantia polymorpha*, the moss *Physcomitrella patens* and the fern *Adiantum capillus-veneris*, yet to the bottoms of cells in the angiosperm *Arabidopsis thaliana* (Sato et al., 2001; Komatsu et al., 2014; Tsuboi & Wada, 2012a; Suetsugu et al., 2005). While weak light induces an accumulation response where chloroplasts move to the periclinal wall to perceive sufficient light for photosynthesis (Gotoh et al., 2018; Wada, 2016). In contrast, strong light induces an avoidance response where the chloroplast moves to the anticlinal wall to avoid any photodamages (Kasahara et al., 2002; Wada, 2016). At low-temperature conditions, cold-avoidance response is induced where chloroplasts move to the anticlinal to avoid cold-mediated photodamages despite under weak light conditions (Fujii et al., 2017; Kodama et al., 2008). The photodamages on chloroplasts would lead to the collapse of the chloroplast apparatus, thus reducing or inhibiting the photosynthetic activities of the plant (Izumi et al., 2017). Therefore, plants perform different chloroplast movement strategies to protect themselves from photodamages.

The chloroplast movements were observed from a few model plants such as the *A. thaliana*, *P. patens*, *A. capillus-veneris* and *M. polymorpha* (Kadota et al., 2000; Kagawa & Wada, 1994; Komatsu et al., 2014; Trojan & Gabrys, 1996). The photosynthetic organs of these model plants like leaves and thalli have been used to observe chloroplast movements, although some are morphologically complex. For instance, the cell surface layer of *A. thaliana* leaf contains epidermal cells with undeveloped chloroplasts, therefore the removal of the palisade mesophyll cells in the second cellular layer is required before observation. Moreover, the complex thalloid thallus of *M. polymorpha* contains different meristematic cells and air chambers that hinder chloroplast observation; hence the chloroplasts are usually observed from the pre-mature gemmalings (Komatsu et al., 2014; Shimamura, 2016). To improve the chloroplast observation, the morphologically simple protonemata and gametophyte prothallus of *P. patens* and *A. capillus-veneris* are used (Kadota et al., 2000; Kagawa & Wada, 1994; Kasahara et al., 2004). These morphologically simple photosynthetic organs show clear chloroplast views directly, particularly the single-cell layered protonemata of *P. patens* (Kadota et al., 2000; Kasahara et al., 2004). However, these species have high gene redundancy that will harden the analysis of the gene of interest as it requires multiple silencing of the redundant gene copies (Kagawa et al., 2004; Li et al., 2015). Therefore, a model plant with low gene redundancy as *M.*

*polymorpha* and producing morphological simple photosynthetic organs as *P. patens* is desired for chloroplast movement analysis (Komatsu et al., 2014; Kasahara et al., 2004). The combination of these beneficial characteristics is expected to be found in the simple thalloid liverwort *Apopellia endiviifolia* that categorised with low gene redundancy and grows simple morphological thalloid thallus (He-Nygren et al., 2006; Crandall-Stotler et al., 2005; Li et al., 2015).

### 1.2 Photoreceptor signalling for chloroplast movements

Two plant-specific photoreceptors, blue light (BL) photoreceptor phototropin (phot) or red light (RL) photoreceptor phytochrome were identified to mediate the chloroplast movements (Sakai et al., 2001; Kagawa et al., 2001; Jarillo et al., 2001; Kadota et al., 2000). Both phot and phytochrome were reported to monitor the chloroplast movements in *P. patens* simultaneously and this is an exceptional case (Kasahara et al., 2004; Kadota et al., 2000; Sato et al., 2001). Indeed, chloroplast movements in many plants were reported to be mediated by phot only (Sakai et al., 2001; Komatsu et al., 2014; Kasahara et al., 2004; Tsuboi et al., 2007; Yong et al., 2021). Phot composed of two LOV (light, oxygen, voltage) domains in the N-terminal region and a serine/threonine kinase in the C-terminal region (Briggs et al., 2001). An inactive flavin mononucleotide (FMN) chromophore was carried in each LOV domain and works as a signalling switch (Briggs et al., 2001). Once BL activated the LOV domain, the FMN chromophore binds with the LOV-conserved cysteine, creating conformation changes in the FMN chromophore structure (Christie et al., 1999; Christie, 2007). This structural alternation then activates the C-terminal kinase domain and triggers the downstream phot signalling to induce chloroplast movements through the actin-binding protein, CHLOROPLAST UNUSUAL POSITIONING (CHUP) (Christie et al., 1999; Takagi, 2003; Oikawa et al., 2003, 2008).

The *PHOT* gene has been identified with multiple copies in different plant species namely, two copies in *A. thaliana* (*AtPHOT1* and *AtPHOT2*), three copies in *A. capillus-veneris* (*AcPHOT1*, *AcPHOT2* and *AcNEOCHROME1*, a chimeric gene encoding phot with a phytochrome light-sensing domain) and seven copies in *P. patens* (*PpPHOT1A-1*, *PpPHOT1A-2*, *PpPHOT1A-3*, *PpPHOT1B*, *PpPHOT2B*, *PpPHOT2C-1* and *PpPHOT2C-2*) (Li et al., 2015; Sakai et al., 2001; Tsuboi et al., 2007). The multiple copies of *PHOT* genes in a plant reacted to different light intensities and their overlapped expression resulted in the observed chloroplast response. Taking the *A. thaliana* as an example, both *AtPHOT1* and *AtPHOT2* mediate the accumulation response simultaneously under weak light conditions, whereas only the *AtPHOT2* induces the avoidance response under strong conditions (Jarillo et al., 2001; Kagawa et al., 2001; Sakai et al., 2001). This type of complex *PHOT* signalling pathway hinders the elucidation process of the gene of interest, as it requires the silencing of other gene copies in advance. Therefore, a model plant with low gene redundancy that conducts a simple *PHOT* signalling pathway is needed.

### 1.3 Importance of chloroplast movements to agriculture

Chloroplast movements play an important role in enhancing the photosynthesis of plants. The movement is responsible to form the corresponding chloroplast responses under different environmental conditions to perceive light energy and protect from photodamages. With effective chloroplast responses, plants perform photosynthesis for development and adaptation to survive. Indeed, the chloroplast accumulation response under the weak light condition was proven to accelerate effective photosynthesis as well as plant production (Gotoh et al., 2018). In the artificial cultivation of the lettuce *Lactuca sativa*, leaf expansion was induced in response to the accumulation response under weak blue light conditions, whereas the avoidance response under strong blue light conditions induced the development of leaf thickness (Hikawa et al., 2019). These data highlight the mutual relationship between chloroplast movements and plant production, where the optimum conditions for accumulation response to get high crop production has been desired in many agricultural sectors. To achieve this goal, the construction of a closed cultivation environment with controllable light conditions like greenhouses has been designed (Xin et al., 2019). Along with the continued improvement in chloroplast movements and crop production, the issue of plantation difficulties and food shortages in the world could be solved in the future.

### 1.4 Objectives of the study

In the present study, I have analysed a simple thalloid liverwort *Apopellia endiviifolia* with low gene redundancy to demonstrate the clear chloroplasts observation and simple phototropin gene signalling (Shimamura, 2016; He-Nygren et al., 2006). The transverse section of simple thalloid thallus and chloroplast responses of *A. endiviifolia* under dark, different light and low-temperature conditions were observed. I have also conducted the next-generation RNA sequencing of *A. endiviifolia* to identify the phototropin (*AePHOT*) gene and determined the number of gene copies of *AePHOT* by Southern blot analysis. Subsequently, to further understand the functional role of *AePHOT* in mediating chloroplast movements, I compared the transient expression of *AePHOT* and *MpPHOT* in *A. endiviifolia* and *M. polymorpha*. Through the resulting chloroplast responses in the transformed cells, the function of *AePHOT* and the compatibility of *AePHOT* and *MpPHOT* can be determined. Additionally, I have coincidentally found the dark-positioning response of *A. endiviifolia* can be achieved within a short period than those reported in other plant species. Thus, I aim to find out the required time for the response to be completed in the dark incubation by time-tracking observation. If the dark-positioning response of *A. endiviifolia* is proven to achieve within a short period, this characteristic will be useful for the understanding of the response, since it is lack of studies to date. Furthermore, I also aim to visualise the cytoskeleton components, microtubules and actin filaments of *A. endiviifolia* and identify the one that is employed in regulating the chloroplast movements. Through the respective fluorescent probes, the microtubules and actin filaments of *A. endiviifolia* can be observed. By comparing the chloroplast positionings formed between the untreated and inhibitor-treated thalli with disrupted microtubules or actin filaments, I can determine which disrupted cytoskeleton has inhibited the chloroplast movements, and that is the one responsible for the movements.

### 1.5 Outline of the dissertation

This dissertation composes of six chapters. Chapter 1 is the general introduction that describes the research background of chloroplast movements and photoreceptor signalling, the importance of chloroplast movements to agriculture, also the objectives of the present study. Chapter 2 demonstrates the transverse section of the simple thalloid thallus and the chloroplast responses of *A. endiviifolia* under dark, different light and low-temperature conditions. The chapter also shows the identification of a single copy *AePHOT* gene of *A. endiviifolia* by RNA sequencing and Southern blot analysis, as well as the *AePHOT* expression analysis. Chapter 3 describes the understanding of the functional role of *AePHOT* in mediating chloroplast movements from the comparative analysis of *AePHOT* and *MpPHOT* transient expressions in *A. endiviifolia* and *M. polymorpha*. This chapter also shows the determination of the compatibility of *AePHOT* and *MpPHOT* in both species. Chapter 4 presents the result of the time-tracking observation of the dark-positioning response of *A. endiviifolia*. This chapter also shows the visualisation of the cytoskeleton components, microtubules and actin filaments of *A. endiviifolia*. Identification of the responsible cytoskeleton components employed in regulating the chloroplast movements of *A. endiviifolia* by inhibitor treatment was also described. Chapter 5 concludes all key findings of the present study and provides insights into the mechanisms of chloroplast movements of *A. endiviifolia*. This chapter also discusses the prospect of the potential uses of *A. endiviifolia*, particularly in elucidating the mechanism of chloroplast movements.

# CHAPTER 2

# CHLOROPLAST RELOCATION MOVEMENTS IN THE LIVERWORT *APOPELLIA ENDIVIIFOLIA*

## 2.1 Background overview

A simple thalloid liverwort *Apopellia endiviifolia* (Figure 1) which is homotypical named *Pellia endiviifolia* was mainly studied. It adapts in moist and shady habitats, belonging to the class of Jungermanniopsida in Marchantiophyta (He-Nygrén et al., 2006; Parzych et al., 2018). This species is dioecious liverwort where the male- and female-specific genes have been identified and the gene expression analyses in vegetative and reproductive development stages were also reported (Sierocka et al., 2011, 2014, 2020). Furthermore, *A. endiviifolia* was recognized as the basal lineage of land plant evolution after the common microRNAs (miRNAs) with algae that were not found in land plants have been identified through the miRNA micro-transcriptome analysis (Alaba et al., 2015). Besides the studies related to sex determination and phylogenetic evolution of *A. endiviifolia*, the purification function of this species in accumulating trace elements of iron and manganese contaminants from polluted water has also been reported (Parzych et al., 2018). These reported studies reveal various research directions to explore *A. endiviifolia*, and I am focusing on the chloroplast movements in the present study. As *A. endiviifolia* develops simple thalloid vegetative, it may provide a clear chloroplast positioning view from the thallus (Crandall-Stotler et al., 2005). Here, I observed the transverse section of the simple thalloid thallus of *A. endiviifolia*, and the dark-positioning, accumulation, avoidance, and cold-avoidance responses after incubation under dark, different light and low-temperature conditions. Additionally, *A. endiviifolia* belongs to the family of Marchantiophyta with the closely related species *Pellia neesiana* and *Marchantia polymorpha* that was categorised by a single phototropin (*PHOT*) gene trait (Li et al., 2015; He-Nygrén et al., 2006; Parzych et al., 2018). Therefore, *A. endiviifolia* may also has a single copy *PHOT* gene which will be identified through the next-generation RNA sequencing and Southern blot analysis in this study. The results could show the beneficial characteristic of *A. endiviifolia* in facilitating the study of chloroplast movements.

## 2.2 Methodology

### 2.2.1 Plant materials and growth conditions

Thalli of *Apopellia endiviifolia* were sampled and isolated from Utsunomiya City, Tochigi prefecture, Japan and named as Utsunomiya male 1 (UTm1) strain. The thalli were sterilised with 3% $H_2O_2$ and axenically propagated on a mineral growth medium (Sierocka et al., 2011). The mineral culture media were prepared from 0.5 g (0.1%) of fine fertilizer powder (Hyponex®), 250 µL (0.05%) of Gamborg's B5 vitamin, 5 g (1%) of sucrose (Wako Pure Chemical Industries, Ltd), 4 g (0.8%) of agar powder (BOP; SSK Sales Co., Ltd.), and adjusted to pH 7 to a final volume of 500 mL before autoclaved for 15 min at 121°C. Moreover, the male strain (Tak-1) of *M. polymorpha* was used in this study, and the subcultures of *M. polymorpha* were propagated on half-strength B5 culture media. The half-strength B5 culture media was prepared from 250 µL of Gamborg's B5 vitamin, 0.25 g of MES (2-(N-Morpholino) ethanesulfonic Acid; Nacalai Tesque Inc.), 5 g of sucrose (Wako Pure Chemical Industries, Ltd), 5 g of agar powder (BOP; SSK Sales Co., Ltd.), and adjusted to pH 5.5 to a final volume of 500 mL before autoclaved for 15 min at 121°C (Tsuboyama & Kodama, 2014). Both *A. endiviifolia* and *M. polymorpha* were propagated under continuous 60 µmol photons $m^{-2}$ $s^{-1}$ white light (FL40SW; NEC Corporation) at 22°C. One- to two-month-old thallus pieces of *A. endiviifolia* and *M. polymorpha* were used for all experiments.

### 2.2.2 Genomic DNA and total RNA extraction of *A. endiviifolia*

One-month-old thalli of *A. endiviifolia* were used to extract the genomic DNA and total RNA. For the extraction of genomic DNA, the cetyltrimethylammonium bromide (CTAB) method was applied (Tsuboyama & Kodama, 2014). About 3 g of frozen detached thalli were homogenised by pestle and mortar and added with 5 mL of 70°C CTAB buffer solution (a mixture of 1.5% CTAB, 75 mM Tris–HCl pH 8.0, 15 mM EDTA, and 1.05 M NaCl), following a 20 min shaking in a hybridisation incubator (HB100; TAITEC) at 55°C. After the incubation, the homogeneous mixture was mixed with 6 mL of chloroform at room temperature before centrifugation at 5000 rpm, 20°C for 10 min. The supernatant was transferred to a new falcon tube and then mixed well with 500 µL of 10% CTAB buffer solution (a mixture of 10% CTAB and 0.7 M NaCl) and 5 mL of chloroform before centrifugation at 5000 rpm, 20°C for 10 min. After that, the supernatant was transferred to a new falcon tube and incubated with 10 mL CTAB precipitation buffer solution (a mixture of 1% CTAB, 50 mM Tris–HCl pH8.0 and 10 mM EDTA) for an hour. The mixture was centrifuged at 10000 rpm, 4°C for 20 min after the incubation, later all supernatant was removed, and the DNA precipitate was dissolved in 500 µL of 1M NaCl. To precipitate the DNA pellets, 500 µL of isopropanol was added, followed by centrifugation at 13000 rpm, 4°C for 5 min. The DNA pellets were cleaned with 70% ethanol before being resuspended in 500 µL of Tris-EDTA buffer with 20 mg/mL RNase A (Sigma-Aldrich®) and incubated at 37°C for an hour. After the incubation, the mixture was diffused with 500 µL of chloroform and centrifuged at 13000 rpm, 4°C for 5 min. The supernatant was collected and added with 50 µL of 3M NaOAc and 500 µL of isopropanol before centrifugation at 13000 rpm, 4°C for 5 min. The supernatant was removed, and the precipitated DNA pellets were cleaned with 70% ethanol before dissolution in 50 µL of sterilised distilled water. For the extraction of total RNA, the Invitrogen™ Trizol™ Reagent (Thermo Fisher Scientific) was used to obtain RNA pellets referring to the manufacturer's protocol (Chomczynski, 1993). The RNA pellets were then purified by

RNeasy Plant Mini kit (Qiagen®). The concentration of DNA solution and RNA eluate were measured using the Nanodrop One Spectrophotometer (Thermo Fisher Scientific) before storing at -80°C.

### 2.2.3 Sex determination of *A. endiviifolia*

To identify the sex of *A. endiviifolia* in the present study, primer sets used for Polymerase Chain Reaction (PCR) amplification of the genes expressed in male (*PenB_Tua1 and PenB_Raba1/11*) and female (*PenB_MT3*, *PenB_CYSP* and *PenB_MT3*) gametophytes were generated (Table 1) (Sierocka et al., 2011, 2014). The actin gene (*PenB_ACT1*; accession number: DQ100290) of *A. endiviifolia* was used as a positive control. Complementary DNA (cDNA) was amplified from the extracted RNA of *A. endiviifolia* by Reverse Transcription (RT-) PCR using ReverTra Ace® (Toyobo Co. Ltd). The cDNA and genomic DNA of *A. endiviifolia* were subjected to PCR amplification with the primer sets and PrimeSTAR® Max DNA Polymerase (Takara Bio). All PCR thermal cycles were completed by GeneAmp® PCR System 9700 (Perkin-Elmer). The sizes of the amplified DNA fragments were verified by 2% TAE agarose gel electrophoresis with a 100-base pair DNA ladder (NEB3231; New England Biolabs). The PCR products were extracted from the gel by HiYieldTM Gel/ PCR DNA Fragments Extraction Kits (RBC Bioscience) and further purified by ExoSAP-IT™ (United States Biochemical). Male and female gametophyte genes of *A. endiviifolia* in the purified PCR products were checked by sequencing with BigDye® Terminator v3.1 Cycle Sequencing Kit (Applied Biosystem).

### 2.2.4 Histological observation of *A. endiviifolia* and *M. polymorpha* thalli

One-month-old *A. endiviifolia* and *M. polymorpha* thalli were collected for paraffin fixation and tissue embedding. The detached thalli were fixed in FAA (5% formaldehyde, 5% acetic acid and 50% ethanol) and embedded in paraffin (ParaplastPlus; Leica Biosystems) in moulds to form blocks. The blocks were sectioned transversely with an RM2245 rotary microtome (Leica Biosystems) to 10 μm thickness and mounted on glass slides. The sectioned tissues were dewaxed with Histoclear (National Diagnostics) and rehydrated through an ethanol series (100%, 90%, 70% and 50%). The tissues were stained with Safranin O stain (0.1% in 50% ethanol) and Alcian Blue counterstain (0.1% in water) (Buda et al., 2013). After the staining process, the tissues were dehydrated in an ethanol series (50%, 70%, 95% and 100%) and submerged in Histoclear (National Diagnostics) for 20 min. The dehydrated tissues were observed under a BX60 light microscope (Olympus), and the images (1300×1024 pixels) were captured with a DP72 digital camera (Olympus).

### 2.2.5 Treatments of dark, light and low-temperature

Five detached thalli of *A. endiviifolia* were placed horizontally on a culture medium and incubated in darkness at 22°C for 24 h by a temperature-controlled incubator (IJ100 or IJ101, Yamato Scientific). The dark-adapted thalli were then incubated under different light conditions for 24 h before chloroplast observation. For light treatments, white, blue and red light-emitting diodes (LEDs) (white LED- H2WW, blue LED-BB45, red LED-RHB; CCS) were used to irradiate the detached thalli at 22°C. A light spectrometer (C-7000; Sekonic) was used to measure the light spectrum of the LEDs (Figure 2). To find the light intensity and light quality inducing accumulation and avoidance response of *A. endiviifolia*, light intensities of each coloured LED from every 10 μmol photons $m^{-2}$ $s^{-1}$ were applied in incubation. The light intensities of each coloured LED were adjusted using a light meter (LI-250A; LI-COR Bioscience). Furthermore, light-adapted thalli of *A. endiviifolia* that had preincubated under the weak white light (WL) of 60 μmol photons $m^{-2}$ $s^{-1}$ at 22°C for 24 h were used for low-temperature and dark treatments. The light-adapted thalli were incubated under weak WL at 5°C for 24 h in the low-temperature treatment and incubated with no supplemental light at 22°C for 24 h, 48 h and 72 h in the dark treatment. All treatments were repeated thrice, and the resulting chloroplast responses in *A. endiviifolia* were observed and assessed.

### 2.2.6 Observation and evaluation of chloroplast positioning

The chloroplast positionings in the thalli of *A. endiviifolia* were observed under an MZ16F fluorescence stereomicroscope (Leica Microsystems). A 480/40-nm excitation filter and LP510-nm barrier filter were used to observe the chlorophyll autofluorescence of the chloroplasts (Ogasawara et al., 2013). The chloroplast positionings were captured in RGB digital images (800 × 600 pixels) with a DP73 digital camera (Olympus). Each image was analysed with ImageJ software (http://rsb.info.nih.gov/ij/) (Rasband, 1997–2018). To evaluate the induced chloroplast repositioning, the chlorophyll fluorescence brightness ratio at the periclinal wall (the cellular middle region that parallels the cell surface; P) and anticlinal wall (region along the edge of the cell that is perpendicular to the cell surface; A) was calculated (P/A ratio quantification) (Kodama et al., 2008). Fluorescence intensities from 30 areas (196 $\mu m^2$ each) and 30 points (42 μm each) along the periclinal and anticlinal cell walls were selected randomly for the P/A ratio quantification. The average P/A ratio with standard deviation (N=3) was calculated from three replicated experiments. All statistical analyses were performed by GraphPad Prism 8.0. Multiple comparisons between all means were performed through unpaired t-test and Tukey's HSD test in one-way ANOVA with a significance level of 0.05. The adjusted p-value of ANOVA was also quantified from each comparison. Additionally, chlorophyll autofluorescence from chloroplasts from *A. endiviifolia* and *M. polymorpha* thalli were observed under an SP8X confocal laser scanning microscope (Leica Microsystems) with excitation at 488 nm and emission at 641 to 721 nm.

### 2.2.7 Observation of chloroplast positioning under red light microbeam irradiation

A temperature-regulated microscope with blue light (BL) microbeam irradiation system (Fujii et al., 2017; Tanaka et al., 2017) was modified to use red-light (RL) LED microbeam (632 nm, FOLS-01-632 nm-600 μm, Pi Photonics) irradiation. Thallus tissue of *A. endiviifolia* was fixed in microscope slides and observed under the microscope without any treatment for 30 min. This is to ensure the thallus piece adapts to the controlled condition and settled down on the microscope slide for better observation. After that, a thallus cell was focused and irradiated by the RL microbeam with approximately 10 μm in diameter for 90 min. Weak RL of 9 μmol photons $m^{-2}$ $s^{-1}$ and strong RL of 227 μmol photons $m^{-2}$ $s^{-1}$ microbeams were applied in the irradiation. Images of chloroplast positioning in the thallus cell before and after 90 min of RL microbeam irradiation were captured and compared.

### 2.2.8 Time-lapse observation of chloroplast movements under blue light microbeam irradiation

The temperature-regulated microscope with a BL LED microbeam irradiation system and charge-coupled device camera was used to construct the time-lapse visualisation of chloroplast movements (Fujii et al., 2017; Tanaka et al., 2017). Thallus tissue of *A. endiviifolia* was fixed in microscope slides and maintained under the temperature-regulated microscope at 22°C without any treatment for 30 min. After that, a thallus cell was focused and irradiated by the BL microbeam with a diameter of around 10 μm and the images were captured at the same time. Here, three different chloroplast movements were induced under the temperature-regulated microscope: the accumulation response by weak BL (30 μmol photons $m^{-2}$ $s^{-1}$) at 22°C, avoidance response by strong BL of (430 μmol photons $m^{-2}$ $s^{-1}$) at 22°C, and cold-avoidance response by weak BL at 5°C. A total of 90 images were taken every minute for 90 min in the accumulation and avoidance responses, and 138 images were taken every 5 min for 690 min in the cold-avoidance response (Sakata et al., 2019). The taken images were later compiled to form a time-lapse video with Fiji software (Schindelin et al., 2012). Five randomly selected chloroplasts were tracked and analysed in each time-lapse video with Fiji software to determine the distances they moved from the microbeam. The correlation coefficient (r) between the average distance of chloroplasts moved from the microbeam against time was calculated with GraphPad Prism 8.0.

### 2.2.9 Next-generation RNA sequencing analysis of *A. endiviifolia*

RNA of *A. endiviifolia* was used to construct mRNA-Seq libraries with a KAPA Stranded mRNA-Seq Kit (Illumina® Platforms). The size of the DNA fragments was verified using an Agilent 2100 bioanalyzer (Agilent Technologies) with an Agilent DNA 1000 Kit (Agilent Technologies). By using a Lightcycler 96 (Roche) with KAPA Library Quantification Kits (Illumina® Platforms), the DNA library concentration was quantified and diluted to 4 nM with elution buffer. The diluted library then proceeded to next-generation sequencing (NGS) by MiSeq Reagent Kit v3 (150 cycles; Illumina® Platforms). The obtained raw reads were quality trimmed with Trimmomatic version 0.39 to remove the adapter and low-quality ends(<QV30) in sequence, also remove reads with not more than 50 bp (Bolger et al., 2014; Suzuki et al., 2016). This trimming process resulted in 10,482,145 clean reads which were then proceeded to the de novo transcript assembly using Trinity version 2.8.5 (Suzuki et al., 2016; Haas et al., 2013). A total of 29,034 contigs were obtained from the assembly process with a total length of 27,508,784 bp. These RNA-Seq reads of *A. endiviifolia* were registered to the DDBJ Sequence Read Archive (DRA) under the accession number DRA011765.

### 2.2.10 Cloning and analysis of the Ae*PHOT* gene from *A. endiviifolia*

Referring to the phototropin gene sequence of *M. polymorpha* (*MpPHOT*; accession no. AHZ63885), the *PHOT* gene sequence of *A. endiviifolia* (*AePHOT*) in the mRNA-Seq libraries (accession no. DRA011765) was identified. Multiple alignments between the nucleotide (*AePHOT* and *MpPHOT*) sequences and protein (AePHOT and MpPHOT) sequences were performed with ClustalW. The aligned sequences were shaded using ESPript 3.0 (Robert & Gouet, 2014). Primer set (attB1_AePHOT_F and attB2_AePHOT_R) to amplify and clone *AePHOT* of *A. endiviifolia* was designed based on the alignments (Table 1). For PCR amplification, the cDNA of *A. endiviifolia* was prepared from the extracted RNA using ReverTra Ace® (Toyobo Co. Ltd). The *AePHOT* was amplified by PCR with the primer set and PrimeSTAR® Max DNA Polymerase (Takara Bio). The size of the amplified *AePHOT* was verified by 1% TAE agarose gel electrophoresis with 1 kbp DNA Ladder (NEB3232; NEB). The PCR product of *AePHOT* was extracted, purified, and checked in sequencing as described in Chapter 2.2.3. After that, 150 ng/uL of the PCR product was cloned into the pDONR™/ZEO vector in BP reaction using Gateway cloning technology (Invitrogen) and transformed into the competent cell of *Escherichia coli*. Successful transformed competent cell colonies were grown on the LB culture media with Zeocin antibiotic. Several transformed cells were randomly selected and checked in the colony PCR by EmeraldAmp® PCR Master Mix (Takara Bio). As the size of the gene carried in the transformed cells matched with the expected size of *AePHOT*, the transformed cells were re-cultured in the LB liquid culture with Zeocin. The pDONR™/ZEO-AePHOT plasmid was extracted by the Fast Gene Plasmid Mini Kit (Nippon Genetics) and the yield and purity were quantified by Nanodrop One Spectrophotometers (Thermo Fisher Scientific Inc.). The *AePHOT* sequence in the plasmid was confirmed by sequencing and stored at -25°C. The *AePHOT* sequence information in mRNA was registered to the DDBJ database under the accession number LC589979. Furthermore, the *AePHOT* sequence was subjected to a phototropin sequence alignment test with other plant species in the Basic Local Alignment Search Tool (BLAST). The results were used to construct a maximum likelihood phylogenetic tree using Mega7 (Kumar et al., 2016).

### 2.2.11 Southern blot analysis of *AePHOT*

In the mRNA region of *AePHOT*, the restriction sites of EcoRI and EcoRV were found to have only a single site in the gene (Figure 3A). Therefore, these restriction sites could confirm the *AePHOT* gene number in the genome of *A. endiviifolia*. One milligram of genomic DNA from *A. endiviifolia* was digested with the restriction enzyme EcoRI-HF or EcoRV-HF in 10×CutSmart Buffer (NEB) at 37°C overnight (Tsuboyama & Kodama, 2014). The digested DNA was electrophoresed in 1% TAE agarose gel with a 1-kb DNA ladder (NEB3232; New England Biolabs). The DNA in the agarose gel was transferred to a Hybond-N+ nylon membrane (GE Healthcare) using a vacuum transfer device (Bio Craft). Subsequently, probe labelling and hybridisation of the blot were conducted by AlkPhos Direct Labelling Reagents kits (GE Healthcare). A DNA fragment (583 bp) (Figure 3B; Table 1) was amplified by PCR from genomic DNA between LOV2 and kinase coding regions of *AePHOT* and used as a probe for labelling during the hybridisation at 60°C. Lastly, the CDP-Star Detection Reagent (GE Healthcare) was applied on the blot to detect the hybridised probes from chemiluminescence using LuminoGraph III (WSE-6300; ATTO Corporation).

### 2.2.12 Quantitative real-time PCR of *AePHOT*

To quantify the *AePHOT* expression under the dark, weak WL (60 μmol photons $m^{-2}$ $s^{-1}$), strong WL (200 μmol photons $m^{-2}$ $s^{-1}$) and low temperature (5°C) with weak WL conditions, four culture plates of 1-month-old *A. endiviifolia* were incubated in the four conditions for 24 h. The cultures of *A. endiviifolia* have been preincubated in the dark at 22°C for 24 h before transfer to the four conditions. After incubation, RNA was extracted from the cultures as described in Chapter 2.2.2. The RNA was reversed transcribed to cDNA using ReverTra Ace™ qPCR RT Master Mix with gRNA Remover (Toyobo). A primer set (AePHOT_111bp_F and AePHOT_111bp_R) was designed to amplify a fragment of 111 bp from *AePHOT* (Table 1). The actin gene (*PenB_ACT1*; accession number: DQ100290) of *A. endiviifolia* was used as the reference gene. Real-time PCR was conducted in a final volume of 20 μL containing FastStart Universal SYBR Green Master (Rox) (Roche), cDNA and gene-specific primers (10 μM) in the LightCycler®96 System (Roche) under the following cycling conditions: pre-incubation at 95°C for 10 min, 45 cycles of 95°C for 15 s, and 60°C for 1 min. High-resolution melting peak analysis was performed after the thermal cycles. The results were analysed with LightCycler®96 Software 1.1 (Roche) and Microsoft Excel. The Cq values of all transcripts were normalised to *PenB_ACT1*, and the relative *AePHOT* expression levels (fold change values) were calculated using the comparative ΔΔCq method (Regier & Frey, 2010). An average of three technical replicates was obtained for each treatment, and three biological replicates were performed. The statistical analysis was performed by GraphPad Prism 8.0. Multiple comparisons between all means were performed through Tukey's HSD test in one-way ANOVA with a significance level of 0.05.

## 2.3 Results

### 2.3.1 Sex determination of *A. endiviifolia*

As *A. endiviifolia* is a dioecious liverwort, the sex of the isolated *A. endiviifolia* was identified through PCR with specific primer sets that amplify expressed genes in the male and female gametophytes (Table 1) (Sierocka et al., 2011, 2014). In the cDNA of *A. endiviifolia*, only the expressed genes in male gametophytes, *PenB_Tua1* and *PenB_Raba1/11* were amplified (Figure 4A), indicating the sample used in the present study is a male strain. Notably, two expressed genes in female gametophytes, *PenB_MT3* and *PenB_CYSP*, were also amplified with *PenB_Tua1* and *PenB_Raba1/11* from the genomic DNA of *A. endiviifolia* (Figure 4B), consistent with the previous study (Sierocka et al., 2011). The identification of *PenB_MT3* and *PenB_CYSP* in the genome of the male strain of *A. endiviifolia* may be due to their possible involvement in the development of male thalli (Sierocka et al., 2011). Based on the PCR results, this *A. endiviifolia* strain was named the Utsunomiya male 1 (UTm1) strain.

### 2.3.2 Morphological characteristics of *A. endiviifolia* thallus

To assess the polymorphisms between the simple and complex thalloid thallus of *A. endiviifolia* (Jungermanniopsida) and *M. polymorpha* (Marchantiopsida), detached thalli of these liverworts were fixed and transversely sectioned to compare the cell layer morphology (Figure 5A and 5B). The cell walls were stained red with Safranin O, and the intracellular contents were stained blue with Alcian blue counterstain. The transverse sections of the simple thalloid thallus of *A. endiviifolia* showed chloroplasts developed uniformly in the parenchyma cell layer, and no air chambers developed above the parenchyma cell layer (Figure 5C and 5E). However, the transverse sections of the complex thalloid thallus of *M. polymorpha* showed chloroplasts developed unevenly within the thallus, where most chloroplasts were developed in the upper parenchyma layer than the lower parenchyma layer (Figure 5D and 5F). Additionally, multiple air chambers were developed above the parenchyma cell layer (Figure 5D and 5F). These morphologies observed in the simple and complex thalloid thalli are consistent with previous reports (Alaba et al., 2015; He-Nygrén et al., 2006; Shimamura, 2016; Sierocka et al., 2011, 2014). The results have highlighted the benefits of the simple thalloid thallus of *A. endiviifolia*, as uniformly developed chloroplasts could be observed through the chlorophyll fluorescence without disturbances from air chambers as in the complex thalloid thallus of *M. polymorpha* (Figure 5G and 5H). In short, a clear observation of chloroplast positionings in *A. endiviifolia* thallus was confirmed.

### 2.3.3 Chloroplast responses of *A. endiviifolia*

With the simple thalloid thallus of *A. endiviifolia*, four known chloroplast responses: dark-positioning, accumulation, avoidance and cold-avoidance have been analysed. The chloroplast positioning was evaluated using the P/A ratio quantification, which is the ratio of chlorophyll fluorescence intensities from chloroplasts near the periclinal wall (P) to the anticlinal wall (A) (Kodama et al., 2008). Taken an example in the dark-positioning response, fewer chloroplasts accumulated near the periclinal wall, giving a low chlorophyll fluorescence intensity from the periclinal wall to the anticlinal wall, thus resulting in a low P/A ratio.

Dark-positioning response of *A. endiviifolia* after incubation in the dark for 24, 48 and 72 h at 22°C was observed (Figure 6A). Initially, chloroplasts accumulated at the periclinal wall under weak WL (60 µmol photons $m^{-2}$ $s^{-1}$) with a P/A ratio of 1.3 before the dark incubation (Figure 6A and 6B). When the light-adapted thalli transferred to the dark conditions, chloroplasts moved to the anticlinal wall bordering with neighbouring cells in the first 24 h, significantly reducing the P/A ratio to 0.9 (adjusted p-value < 0.0001) (Figure 6A and 6B). In the following 48 h and 72 h of dark incubation, the chloroplasts continually shifted along the anticlinal wall, resulting in a P/A ratio of 0.8 and 0.9, respectively (Figure 6A and 6B). Note that chloroplasts were not localised to the outermost anticlinal wall near the edge of the thallus, as there are no neighbouring cells (Figure 7). This chloroplast movement pattern is unique and consistent with the dark-positioning responses in *A. capillus-veneris* and *M. polymorpha* (Komatsu et al., 2014; Tsuboi & Wada, 2012a). Next, dark-adapted thalli were irradiated with 10 to 210 µmol photons $m^{-2}$ $s^{-1}$ of white light (WL) to determine the light intensities that induce the accumulation and avoidance responses in *A. endiviifolia* (Figure 6C). The transition phase of accumulation to avoidance responses was observed when the light intensity was switched from 110 to 120 µmol photons $m^{-2}$ $s^{-1}$ of WL (Figure 6C). Accumulation response where chloroplasts localised along the periclinal wall was observed under weak WL with intensities up to 110 µmol photons $m^{-2}$ $s^{-1}$ (Figure 6C). Average P/A ratios ranging from 1.3 to 1.8 has resulted in this response (Figure 6D). When the light intensities reached 120 µmol photons $m^{-2}$ $s^{-1}$ and above, chloroplasts moved to the anticlinal wall, showing the avoidance response against the strong light (Figure 6C). This chloroplast response consequence the average P/A ratios ranging from 0.3 to 0.7, which are significantly different to the accumulation response (Figure 6D). Referring to the observed accumulation and avoidance responses of *A. endiviifolia* in the present study, the light intensity range of weak WL is from 10 to 110 µmol photons $m^{-2}$ $s^{-1}$ and strong WL is above 120 µmol photons $m^{-2}$ $s^{-1}$. Lastly, the cold-avoidance response was observed in the thalli of *A. endiviifolia* after incubation under weak WL (60 µmol photons $m^{-2}$ $s^{-1}$) at low-temperature (5°C) condition for 24 h. When the incubation temperature dropped to 5°C from the pre-incubation at 22°C, chloroplasts moved to the anticlinal wall despite the weak WL irradiation (Figure 6E). The response resulted in an average P/A ratio of 0.3, which significant contrast to the accumulation response at 22°C (p-value = 0.0007) (Figure 6F). Taken together, the four known chloroplast responses were observed in *A. endiviifolia*.

### 2.3.4 Blue light-dependent chloroplast movements in *A. endiviifolia*

After observing the accumulation, avoidance and cold-avoidance responses in *A. endiviifolia* under WL, a combination of different light spectra, blue light (BL) or red light (RL) was applied separately to determine the type of photoreceptor that induces the chloroplast movements in *A. endiviifolia*. Here, different intensities of BL were used to incubate the dark-adapted thalli of *A. endiviifolia*, and the accumulation and avoidance responses were induced as the WL incubation (Figure 8A, 6C and 6D). Under 10 to 30 μmol photons $m^{-2}$ $s^{-1}$ of BL irradiation, the accumulation response was induced and resulted in average P/A ratios of 1.5 to 1.6 (Figure 8A). The avoidance response was observed instantly when the BL intensities reached 40 μmol photons $m^{-2}$ $s^{-1}$ and above, indicating the transition phase of accumulation to avoidance response was between 30 and 40 μmol photons $m^{-2}$ $s^{-1}$ (Figure 8A). On the other hand, inconsistent chloroplast movements were observed under the RL irradiation, resulting in fluctuating average P/A ratios along the light intensities (Figure 8B). No transition phase of accumulation to avoidance response was observed in the RL-irradiated thalli as those shown in the WL- and BL- irradiated thalli (Figure 8 and 6D). These inconsistent P/A ratios resulted under different intensities of RL are unable to be repeated in a similar experiment. Therefore, RL was suggested to not be involved in mediating the chloroplast movements of *A. endiviifolia*. To verify this hypothesis, weak (9 μmol photons $m^{-2}$ $s^{-1}$) or strong (227 μmol photons $m^{-2}$ $s^{-1}$) RL microbeam was irradiated into a thallus cell of *A. endiviifolia*, and no specific chloroplast movement was induced from the microbeam (Figure 9). These results confirmed that the chloroplast movements in *A. endiviifolia* did not react to RL, but to BL irradiation only.

To further validate the BL-dependent chloroplast movements in *A. endiviifolia*, a BL microbeam was applied to make the time-lapse imaging of chloroplast movements. By using weak BL microbeam irradiation (30 μmol photons $m^{-2}$ $s^{-1}$), an accumulation response was mediated where the chloroplasts moved towards the microbeam spot (Figure 10A). To quantify the chloroplast movement, an average distance of five randomly selected chloroplasts moved from the centre of the microbeam spot was calculated. A strong negative correlation was observed between the average moving distance and irradiation period ($r = -0.95$) (Figure 10B). On the other hand, strong BL microbeam irradiation (430 μmol photons $m^{-2}$ $s^{-1}$) has stimulated the chloroplasts to move away from the microbeam spot (Figure 10C), indicating the avoidance response. A strong positive correlation was detected between the average moving distance and irradiation period ($r = 0.95$) (Figure 10D). Based on quantitative analysis of the accumulation and avoidance responses in *A. endiviifolia*, chloroplasts reacted strongly during the first 60 min of microbeam treatment and moved steadily in the following 30 min (Figure 10B and 10D). Moreover, weak BL microbeam irradiation at 5°C was applied to analyse the BL dependency of the cold-avoidance response in *A. endiviifolia*. The chloroplasts aggregated into groups and moved away from the weak BL microbeam, resulting in a positive correlation between the average moving distance and irradiation period ($r = 0.95$) (Figure 10E and 10F). This observation is consistent with the cold-avoidance response in *A. capillus-veneris* and *M. polymorpha* where chloroplast aggregated and moved significantly slower than accumulation and avoidance responses at room temperature (Figure 10E) (Fujii et al., 2017; Kodama et al., 2008; Tanaka et al., 2017). Overall, the light-dependent chloroplast responses including accumulation, avoidance, and cold-avoidance of *A. endiviifolia* were mediated in a BL-dependent manner, suggesting that a BL photoreceptor (i.e., phot) should be responsible for the movements.

### 2.3.5 Single copy phototropin gene of *A. endiviifolia* (*AePHOT*)

Next-generation mRNA sequencing of *A. endiviifolia* was performed to identify the *PHOT* genes. Only a single copy *AePHOT* gene was identified in the mRNA sequencing libraries of *A. endiviifolia* by referring to the *MpPHOT* gene sequence of *M. polymorpha* (Figure 11A) (Komatsu et al., 2014). Multiple alignments between *AePHOT* and *MpPHOT* (nucleotide sequences) showed 73% similarity, and AePHOT and MpPHOT (protein sequences) showed 71% similarity (Figure 12 and 13) (Komatsu et al., 2014). The coding region including the LOV1, LOV2 and kinase domains of AePHOT has been identified through the sequence alignments (Figure 12 and 13). Matching with MpPHOT, the cysteine residues for flavin mononucleotide (FMN) binding in the LOV domains, and the aspartic acid residue for the functionality of serine/threonine kinase domain were found in AePHOT (Figure 13) (Komatsu et al., 2014; Fujii et al., 2017). The similarity of the functional amino acids, cysteine and asparagine between AePHOT and MpPHOT suggests that the function of the LOV and kinase domains of MpPHOT were conserved in AePHOT. Besides that, in the maximum likelihood phylogenetic tree, *A. endiviifolia* was separated from the vascular plants and categorised into the liverwort family, Marchantiophyta which is characterised by a single copy *PHOT* gene (Figure 11B) (Komatsu et al., 2014; Li et al., 2015). The phylogenetic analysis also showed that *A. endiviifolia* shares the same clade with the close-related species *Pellia neesiana* that has a single copy *PHOT* gene (Figure 11B) (Li et al., 2015). These results convinced that *A. endiviifolia* contains only one *AePHOT* gene in the genome. To confirm the number of *AePHOT* gene, Southern blot analysis was performed using genomic DNA from *A. endiviifolia* and targeting two single restriction sites of EcoRI and EcoRV in the *AePHOT* gene (Figure 3A). Only a single band was detected in the blots from each EcoRI- and EcoRV- digested genomic DNA, indicating a single copy *AePHOT* gene in *A. endiviifolia* (Figure 11C). Although the full-length genomic DNA sequence of *AePHOT* was not obtained in the present study, this traditional method has been used to detect gene copy numbers from previous studies, like the single copy *MpPHOT* gene in *M. polymorpha* (Southern, 2006; McCabe et al., 1997; Komatsu et al., 2014). Taken together with all the evidence pointing to *A. endiviifolia* carrying a single copy of *AePHOT*, a simple phototropin signalling pathway may be employed to regulate the chloroplast movements.

### 2.3.6 Relative quantification of *AePHOT* expression level in different chloroplast responses

To understand the expressions of *AePHOT* during the dark-positioning, accumulation, avoidance and cold-avoidance responses, quantitative real-time PCR analysis of *A. endiviifolia* was performed using four templates extracted from cultures incubated under four conditions: dark at 22°C, weak WL (60 µmol photons $m^{-2}$ $s^{-1}$) at 22°C, strong WL (200 µmol photons $m^{-2}$ $s^{-1}$) at 22°C, and weak WL at 5°C. The lowest expression level of *AePHOT* was detected in the dark-positioning response under dark conditions, whereas high *AePHOT* expression levels were detected under light conditions (Figure 14). Indeed, accumulation response under weak WL at 22°C has resulted in the highest *AePHOT* expression levels, while similar expression levels of *AePHOT* have been detected in the avoidance and cold-avoidance responses under strong WL at 22°C and weak WL at 5°C, respectively (Figure 14). The results showed that *AePHOT* expression rises when exposed to light irradiation and does not rely on temperature variation. This expression pattern of *AePHOT* is consistent with the increased expression of *AtPHOT1* and *AtPHOT2* in *A. thaliana* under light irradiation and unaffected *MpPHOT* expression of *M. polymorpha* in low-temperature conditions (Fujii et al., 2020; Jarillo et al., 2001; Kagawa et al., 2001; Łabuz et al., 2015).

## 2.4 Discussion

Our findings in the present study prove the beneficial characteristics of *A. endiviifolia*, which refer to the simple thalloid thallus with clear chloroplast views and a single copy Ae*PHOT* gene. To date, no other plant species have been reported to carry the two beneficial characteristics together. Although the hornwort *Anthoceros punctatus* was known for a single copy *PHOT* gene, it also contains a PHOT derivative gene (*NEOCHROME* gene) (Li et al., 2014, 2015). The *NEOCHROME* gene comprises a fusion of the *PHOT* and *PHYTOCHROME* sequences, pointing to its involvement in chloroplast movements (Li et al., 2014). Therefore, the analysis of *PHOT* in hornwort is complicated by the presence of *NEOCHROME*, as presented in a study of *A. capillus-veneris* (Tsuboi et al., 2007). Additionally, *A. punctatus* cells contain only one large chloroplast with a pyrenoid, thus the chloroplast response can hardly be observed (Li et al., 2014; Vaughn et al., 1990). Besides that, the liverwort *M. polymorpha* was reported to contain only a single copy *PHOT* gene without the derivative gene, but chloroplasts were hard to observe from the complex thalloid thallus due to the developed multiple tissues and air chambers (Figure 5F and 5H) (Komatsu et al., 2014; Li et al., 2015; Shimamura, 2016). This kind of hindrance in chloroplast observation can be avoided by using morphologically simple photosynthetic organs likes the single cell layer tissue of the moss *Physcomitrella patens* and the simple thalloid thallus of *A. endiviifolia* (Figure 5E and 5G) (Buda et al., 2013). While *P. patens* provide a perfect view of chloroplast positioning, the high genetic redundancy has produced seven copies of *PHOT* genes (*PpPHOT1A-1*, *PpPHOT1A-2*, *PpPHOT1A-3*, *PpPHOT1B*, *PpPHOT2B*, *PpPHOT2C-1* and *PpPHOT2C-2*) to regulate the chloroplast movements (Kasahara et al., 2004; Li et al., 2015). The multiple gene traits require the silencing of other copy genes before analysing the gene of interest which will be cost- and time-consuming. In the present study, the single copy *AePHOT* gene implies a simple phototropin signalling pathway as *MpPHOT*, which could ease the gene analysis of chloroplast movements in *A. endiviifolia*.

Different chloroplast movement patterns were observed in the avoidance and cold-avoidance responses of *A. endiviifolia*, as described in previous studies of *M. polymorpha* (Tanaka et al., 2017). Indeed, chloroplasts spread

out and move to the nearest anticlinal wall of the cells in the avoidance response, whereas chloroplasts aggregate into groups and then move to all sides of the anticlinal wall in the cold-avoidance response (Tanaka et al., 2017). Here, similar chloroplast movement patterns during the avoidance and cold-avoidance responses of *A. endiviifolia* were observed through the time-lapse observation (Figure 10C, 10E and 15). Note that, the behaviour of chloroplast aggregation before migration in the cold-avoidance response was also observed in the fern *A. capillus-veneris* (Kodama et al., 2008). Furthermore, the dark-positioning response of *A. endiviifolia* showed chloroplasts moved and accumulated at the anticlinal wall bordering with neighbouring cells, but not to the outermost anticlinal wall of the thallus (Figure 7). This chloroplast movement pattern distinguishes the response with the avoidance and cold-avoidance response and is consistent with the dark-positioning response in *A. capillus-veneris* and *M. polymorpha* (Tsuboi & Wada, 2012a; Komatsu et al., 2014). Overall, the movement patterns of all chloroplast responses observed in *A. endiviifolia* match those reported in the model plants *M. polymorpha*, *A. capillus-veneris* and *A. thaliana*, showing these manners have been highly conserved throughout the evolution from non-vascular to vascular plants.

In the quantitative real-time PCR analysis of *AePHOT*, light exposures in the accumulation, avoidance and cold-avoidance responses have raised the expression level of *AePHOT* (Figure 14). These results are similar to the *PHOT* expressions in *A. thaliana* and *M. polymorpha* that enhance when exposed to light, suggesting the light-dependency of *PHOT* expression is conserved in *A. endiviifolia* (Jarillo et al., 2001; Kagawa et al., 2001; Łabuz et al., 2015; Komatsu et al., 2014). At 22°C, *AePHOT* was expressed at lower levels under strong white light (WL) than weak WL, showing the deterioration of *AePHOT* expression by strong light intensity to induce avoidance response (Figure 14). Similarly, a low expression level of *AePHOT* was detected in the cold-avoidance response under weak WL at 5°C (Figure 14). These results have pictured the accumulation response maintaining a high *AePHOT* expression level than the avoidance and cold-avoidance responses. According to the properties of the photocycle of LOV domains, the photoactivation level of *AePHOT* in the avoidance response and cold-avoidance response appears to be higher than that in the accumulation response (Christie, 2007; Salomon et al., 2000). Therefore, the expression level of *AePHOT* dropped when the photoactivated form is accumulated. Perhaps a feedback control mechanism exists in which the *PHOT* expression level is adjusted relative to the level of the photoactivated *PHOT*.

## 2.5 Summary of key findings

In this chapter, the transverse section of the simple thalloid thallus of *A. endiviifolia* showed uniformly developed chloroplasts and no air chamber developed within. The morphological simple thallus provides clear and direct observations of chloroplast positioning from the thallus surface. The ranges of light intensities and temperatures used to induce the dark-positioning, accumulation, avoidance and cold-avoidance responses in *A. endiviifolia* were fully elucidated. After the blue light (BL)-dependency of the chloroplast movements was determined, a single copy of the BL photoreceptor phototropin gene (*AePHOT*) was identified in *A. endiviifolia*. The similarities between *AePHOT* and *MpPHOT* suggest *A. endiviifolia* might employ a simple *AePHOT* signalling pathway as the *MpPHOT* in *M. polymorpha* to induce chloroplast movements (Fujii et al., 2017; Komatsu et al., 2014). Overall, the simple thalloid thallus and single copy *AePHOT* gene of *A. endiviifolia* have made it beneficial to be used to discover and understand the mechanisms of chloroplast movements.

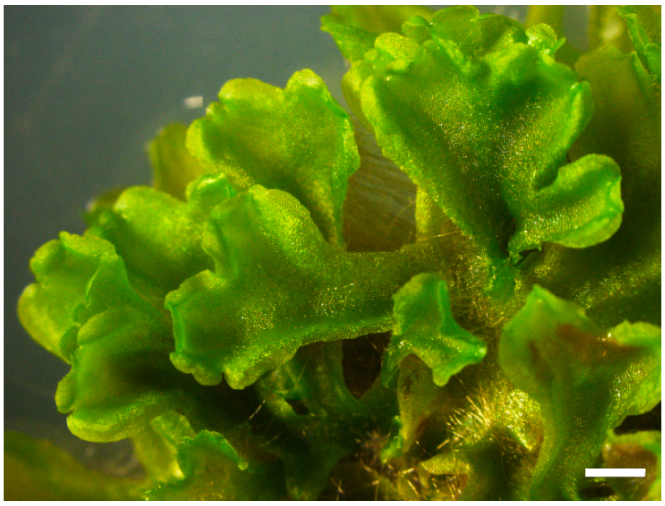

**Figure 1.** Simple thalloid liverwort, *Apopellia endiviifolia*. Scale bar, 1 mm.

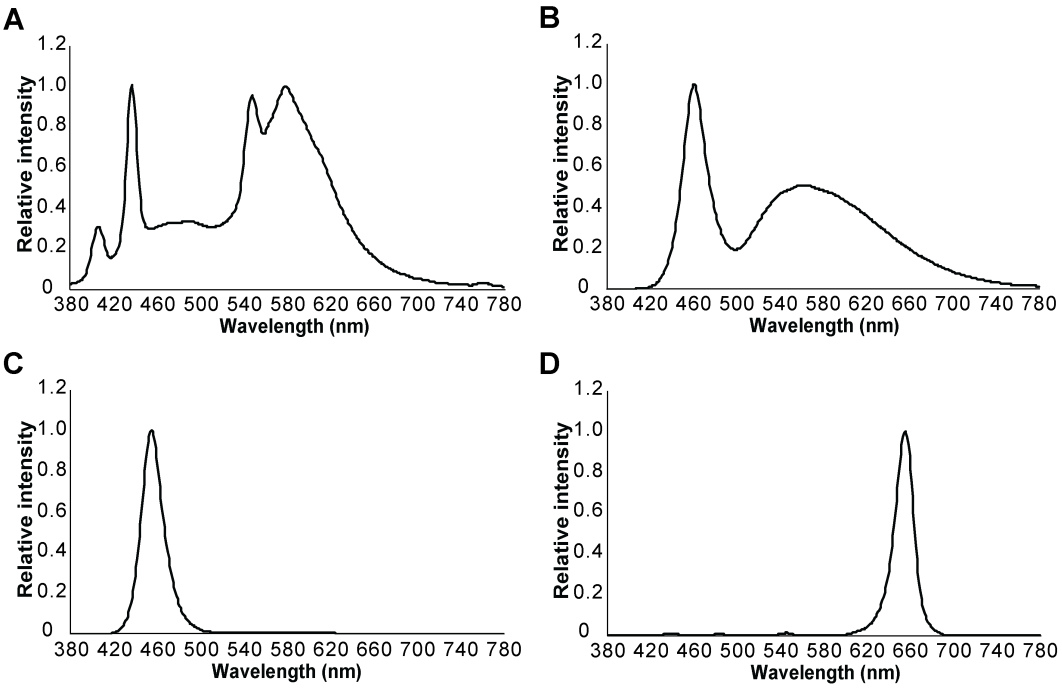


**Figure 2.** Light spectra of the light sources used in the present study. **A,** Light spectrum of white fluorescent light. **B,** Light spectrum of white LEDs. **C,** Light spectrum of blue LEDs. **D,** Light spectrum of red LEDs.

**A**


**B**

5'-GGCATCCTAACAGACCGATAGATTTGAACCTTATTTCTACATGGCTGATAAAAGG
GTACTAGCCATCCCCGTGTTTGGTAACCCAATTTTGGCCCTTGAGTGAGAAGGGCT
GGGTGTAGCTCCGGAAGGGACAGTGTCCCTTCCAGAGCCTCATTCATACTAGTACT
AGTTTTTTATGCTTTTCTTTTTCCCGCTCATGGGTTGATATTCTGGTGTCTTAGGCGT
GGAGGAGCCACACCAATCCATACCGAACTTGGTGGTGAAACTCCATTGCGGTGAC
GATACTATGGGGGAAGCCCCATGGAAAAATAGCTCGATGCCAGGATGAAAAAAACT
TAACGTTTCCGGGTCGTCTCGTTCAAAACCACAAAAAATTTGAACTTTATTTTCTACT
CCACGCTTCAAAATACATTCTTATGAAGAAAAACTTTTGAACTTCCGCGCATTGCCT
CGAATCCAAGTGGAGGCGGGGCCTGTAGCTCATGGAGGCGGGGCCTGTAGCTCA
TAGGATTAGAGCACGTGGCTACGAACCTCGGTGTCGGGGGTTCGAATCCCTCCTC
GCACTTACGTGGACAGTAATTGC-3'

**Figure 3.** Restriction sites and probe for the Southern blot analysis of *AePHOT*. **A,** Two single restriction sites, EcoRV and EcoRI in the *AePHOT* mRNA were targeted to identify the *AePHOT* gene copy number. Black line, protein coding region; Blue lines, untranslated region (UTR); Red bars, restriction sites. **B,** Probe (583 bp DNA fragment) used for labelling was amplified from genomic DNA between LOV2 and kinase coding regions of *AePHOT*.

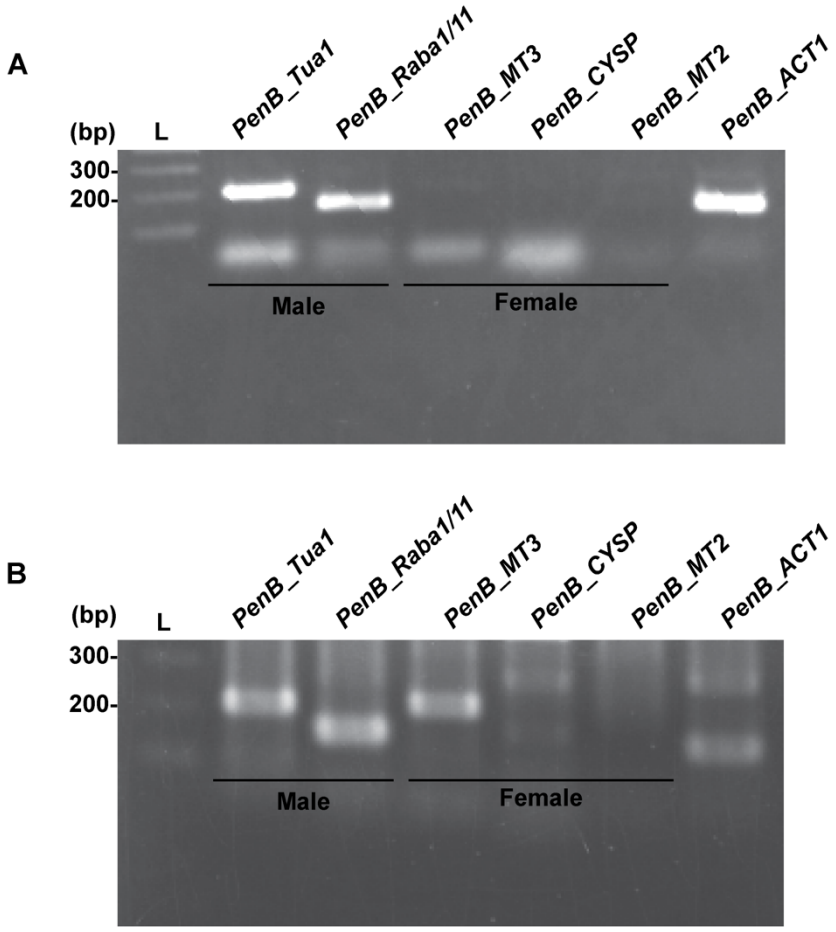


**Figure 4.** Sex determination of the isolated *A. endiviifolia*. PCR amplification was performed using primers for genes expressed in male (*PenB_Tua1* and *PenB_Raba1/11*) and female (*PenB_MT3*, *PenB_CYSP* and *PenB_MT2*) gametophytes with cDNA (**A**) and genomic DNA (**B**) from *A. endiviifolia*. The *Actin* gene (*PenB_ACT1*; accession number: DQ100290) of *A. endiviifolia* was used as a positive control. A 100-bp ladder (L) was used in the 2% TAE gel electrophoresis.

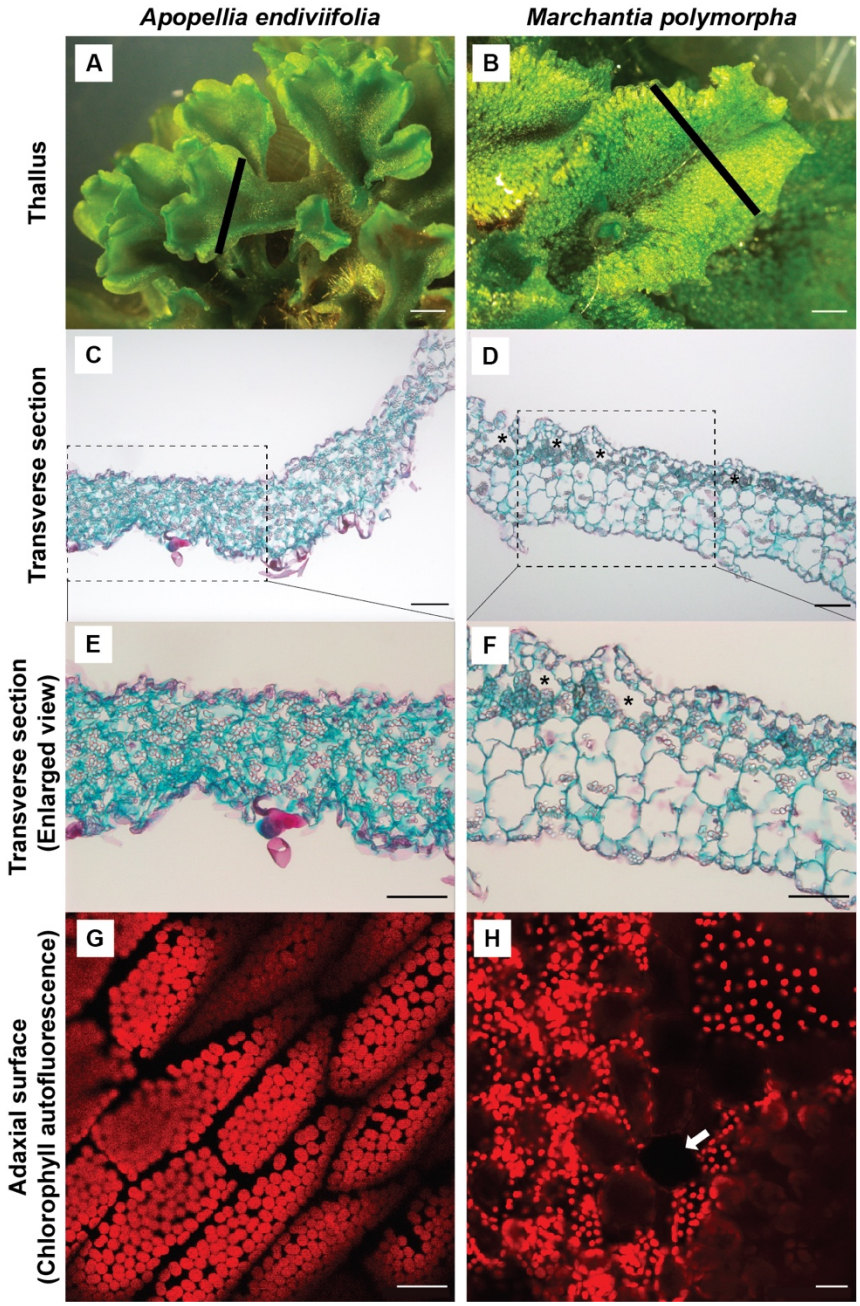


**Figure 5.** Transverse sections and chloroplast observation in *A. endiviifolia* and *M. polymorpha* thalli. **A**–**B,** Representative images of *A. endiviifolia* (**A**) and *M. polymorpha* (**B**) thalli. Black lines indicate the sectioning of the thallus. Scale bar, 1 mm. **C**–**F**, Transverse sections of *A. endiviifolia* (**C, E**) and *M. polymorpha* (**D, F**) thalli. Safranin red staining indicates the cell wall, and Alcian blue counterstaining indicates the intracellular contents. Scale bar, 200 μm. Asterisks indicate the developed air chamber in *M. polymorpha* thallus (**D, F**). **G**–**H,** Observation of chloroplasts through chlorophyll autofluorescence (red) by confocal laser scanning microscopy. The adaxial sides of *A. endiviifolia* (**G**) and *M. polymorpha* (**H**) thalli were observed. An arrow indicates the developed air chamber in *M. polymorpha* thallus (**H**). Scale bars, 20 μm.

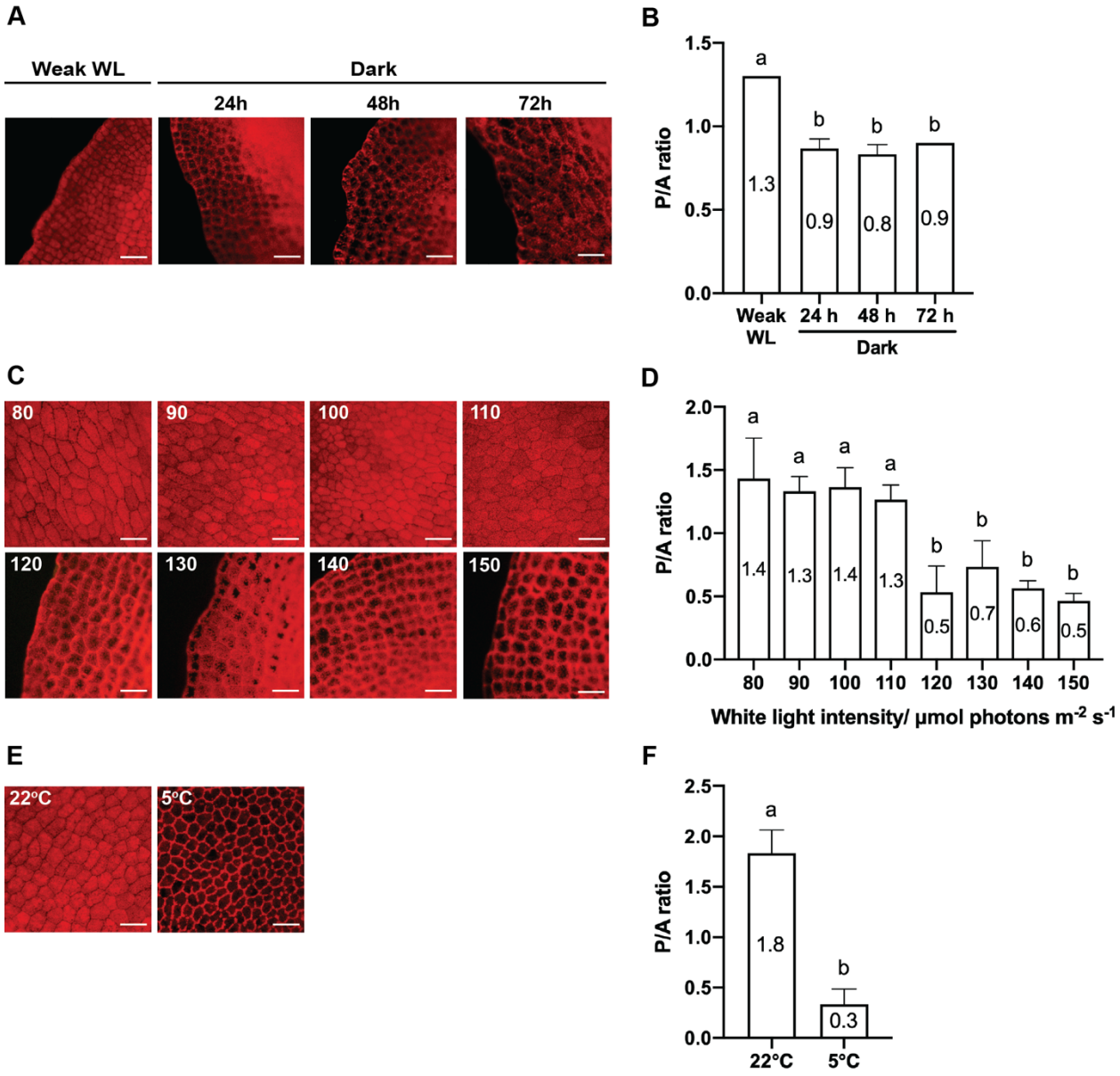


**Figure 6.** Chloroplast responses of *A. endiviifolia* under the dark, different light intensity and low-temperature conditions. **A,** Dark-positioning response of *A. endiviifolia*. Detached thalli were incubated in the dark at 22°C, and the dark-positioning response was observed after 24 h, 48 h and 72 h. The accumulation response under 60 µmol photons $m^{-2}$ $s^{-1}$ of white light (weak WL) was observed before dark incubation. **B,** Evaluation of the dark-positioning response by the P/A ratio quantification. The graph shows a quantitative analysis of the chloroplast positioning in (**A**) based on the average P/A ratio from three replicates. **C**, Accumulation and avoidance responses of *A. endiviifolia*. Detached thalli were incubated under 10 to 210 µmol photons $m^{-2}$ $s^{-1}$ of WL at 22°C for 24 h; only representative images from thallus incubated under 80 to 150 µmol photons $m^{-2}$ $s^{-1}$ of WL were presented. The accumulation response was observed at <110 µmol photons $m^{-2}$ $s^{-1}$, and the avoidance response was observed at >120 µmol photons $m^{-2}$ $s^{-1}$ of WL irradiation. **D,** Evaluation of the accumulation and avoidance responses by the P/A ratio quantification. The graph shows a quantitative analysis of the chloroplast positioning in (**C**) based on the average

P/A ratio from three replicates. The average P/A ratio of the dark-adapted thallus before treatment can be referred to the average P/A ratio of dark-positioning response at 24 h in (**B**). **E,** Cold-avoidance response in *A. endiviifolia*. Detached thalli were incubated under 60 µmol photons $m^{-2}$ $s^{-1}$ of WL at 22°C and 5°C for 24 h. The cold-avoidance response was induced at 5°C, whereas the accumulation response was induced at 22°C. **F,** Evaluation of the cold-avoidance response by the P/A ratio quantification. The graph shows a quantitative analysis of the chloroplast positioning in (**E**) based on the average P/A ratio from three replicates. Scale bars, 50 µm. Error bars represent standard deviation (N=3). Different alphabets (a and b) above the graph bars indicate significant differences (Tukey's HSD test for (**B**, **D**); Unpaired t-test for (**F**); $\alpha < 0.05$).

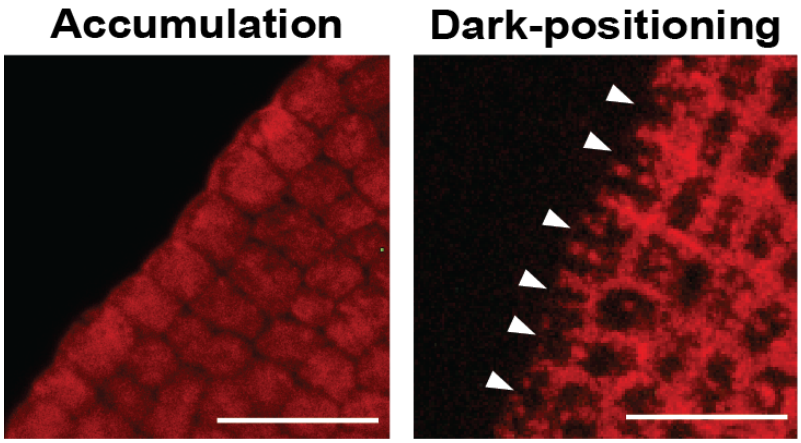


**Figure 7.** Dark-positioning response near the outermost anticlinal wall of *A. endiviifolia* thallus. Accumulation and dark-positioning response were induced after incubation under 60 µmol photons $m^{-2}$ $s^{-1}$ of white light and in the dark, respectively, for 24 h at 22°C. Arrowheads indicate no chloroplast localisation at the outermost anticlinal wall in the dark-positioning response. Scale bars, 50 µm.

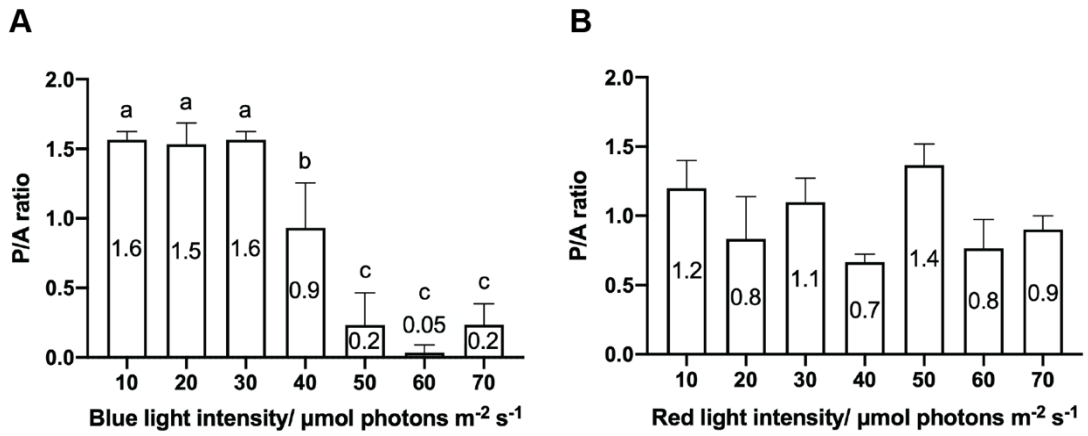


**Figure 8.** Blue light-dependent chloroplast movements in *A. endiviifolia*. Detached thalli were incubated under 10 to 70 µmol photons $m^{-2}$ $s^{-1}$ of blue and red light at 22°C for 24 h. **A,** Quantitative analysis of chloroplast positioning resulting from blue light irradiation based on the average P/A ratio from three replicates. Different alphabets (a, b and c) above the graph bars indicate significant differences (Tukey's HSD test; $\alpha < 0.05$). **B,** Quantitative analysis of chloroplast positioning resulting from red light irradiation based on the average P/A ratio from three replicates in this study. The average P/A ratio of the dark-adapted thallus before treatment can be referred to the average P/A ratio of dark-positioning response at 24 h in Figure 6B.

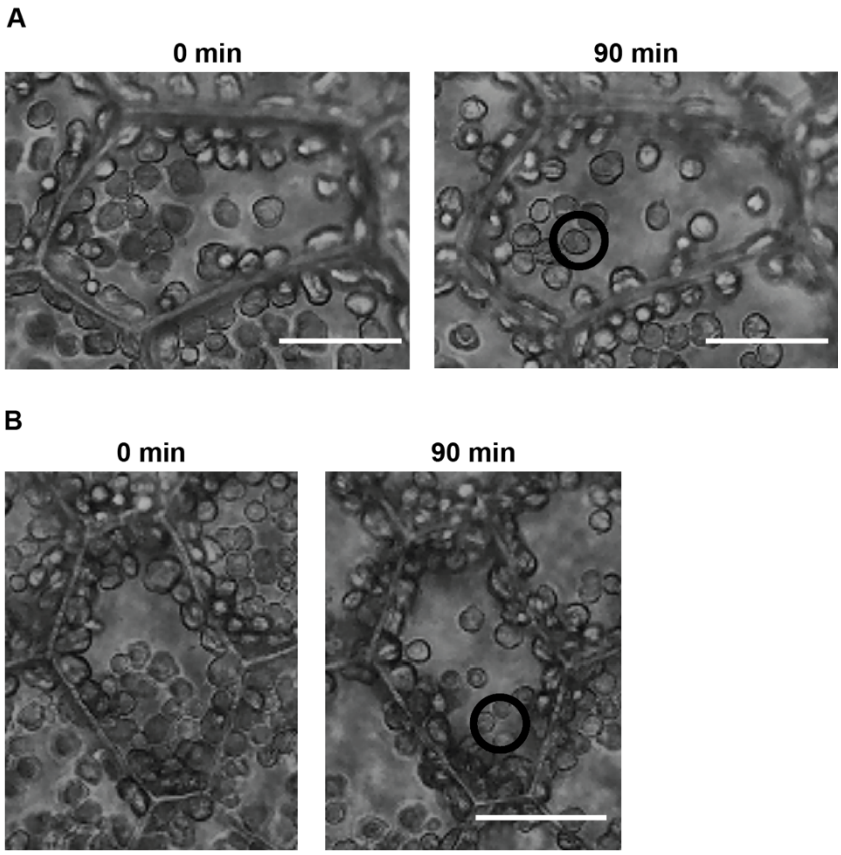


**Figure 9.** Chloroplast movements in *A. endiviifolia* after red light (RL) microbeam irradiation. **A,** Observation of chloroplast positioning in the thallus cell before and after 90 min irradiation of weak RL microbeam (9 μmol photons $m^{-2}$ $s^{-1}$) at 22°C. **B,** Observation of chloroplast positioning in the thallus cell before and after 90 min irradiation of strong RL microbeam (227 μmol photons $m^{-2}$ $s^{-1}$) at 22°C. Scale bars, 30 μm. The black circle indicates the RL microbeam-irradiated spot.

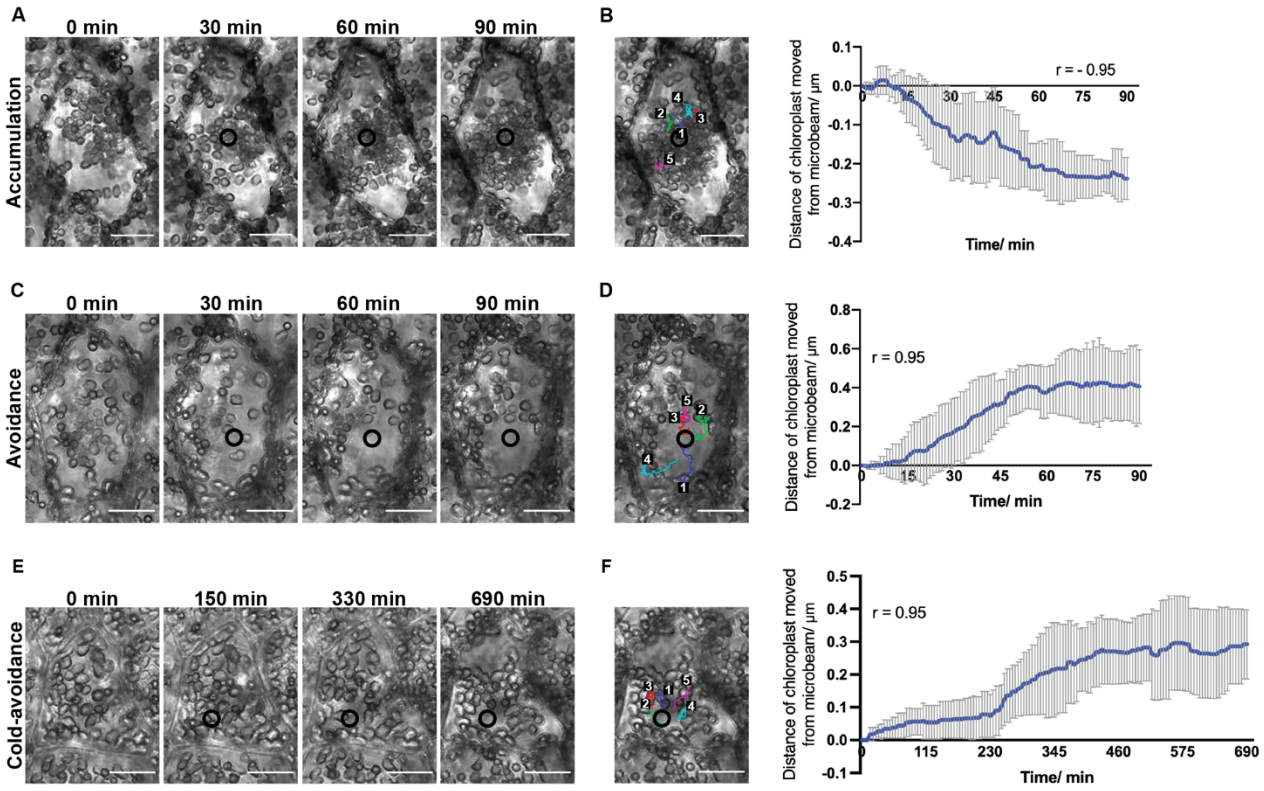


**Figure 10.** Time-lapse imaging of chloroplast movements in *A. endiviifolia* under blue light (BL) microbeam irradiation. **A,** Accumulation response of chloroplasts towards the weak BL (30 µmol photons $m^{-2}$ $s^{-1}$) microbeam-irradiated spot in the thallus cell at 22°C. **B,** Quantitative analysis of the chloroplast moving distance in (**A**) calculated from the five numbered chloroplasts; the average distance of chloroplasts moved against time is shown in the graph. **C,** Avoidance response of the chloroplasts away from the strong BL (430 µmol photons $m^{-2}$ $s^{-1}$) microbeam-irradiated spot in the thallus cell at 22°C. **D,** Quantitative analysis of the chloroplast moving distance in (**C**) calculated from the five numbered chloroplasts; the average distance of chloroplasts moved against time is shown in the graph. **E,** Cold-avoidance response of the chloroplasts away from the weak BL (30 µmol photons $m^{-2}$ $s^{-1}$) microbeam-irradiated spot in the thallus cell at 5°C. **F,** Quantitative analysis of the chloroplast moving distance in (**E**) calculated from the five numbered chloroplasts; the average distance of chloroplasts moved against time is shown in the graph. Scale bars, 30 µm. The black circle indicates the BL microbeam-irradiated spot. Error bars represent standard deviation. The "r" indicates the correlation coefficient between the average distances of chloroplasts moved from the microbeam and irradiation time.

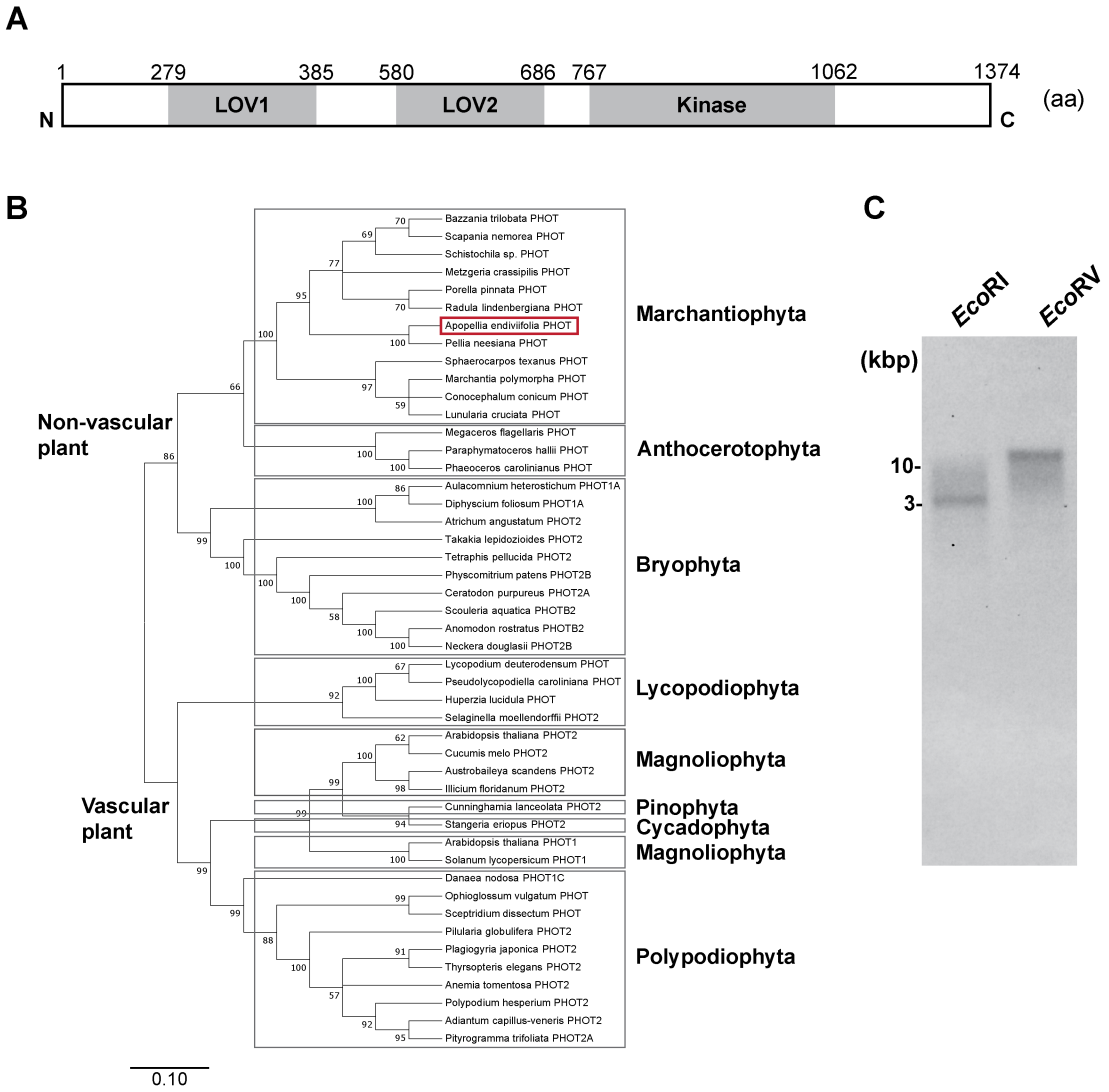


**Figure 11.** A single copy *PHOTOTROPIN* gene (*AePHOT*) of *A. endiviifolia*. **A,** Schematic illustration of AePHOT protein. aa, amino acids. **B,** Maximum likelihood phylogenetic tree of *A. endiviifolia*. Through the alignment of *AePHOT* sequences with ClustalW in Mega 7, phylogenetic relationships of *A. endiviifolia* (red border) with 47 non-vascular and vascular plants had assembled. The bootstrap values are indicated at the nodes. The bar represents 0.10 substitutions in each site. **C,** Southern blot analysis of *AePHOT*. A single band was shown in the lane denoted with EcoRI and EcoRV in the blot that was generated from EcoRI- and EcoRV-digested DNA products, respectively. The blot was hybridised by a probe of the *AePHOT* genomic fragment between the LOV2 and kinase coding regions (Figure 3B).

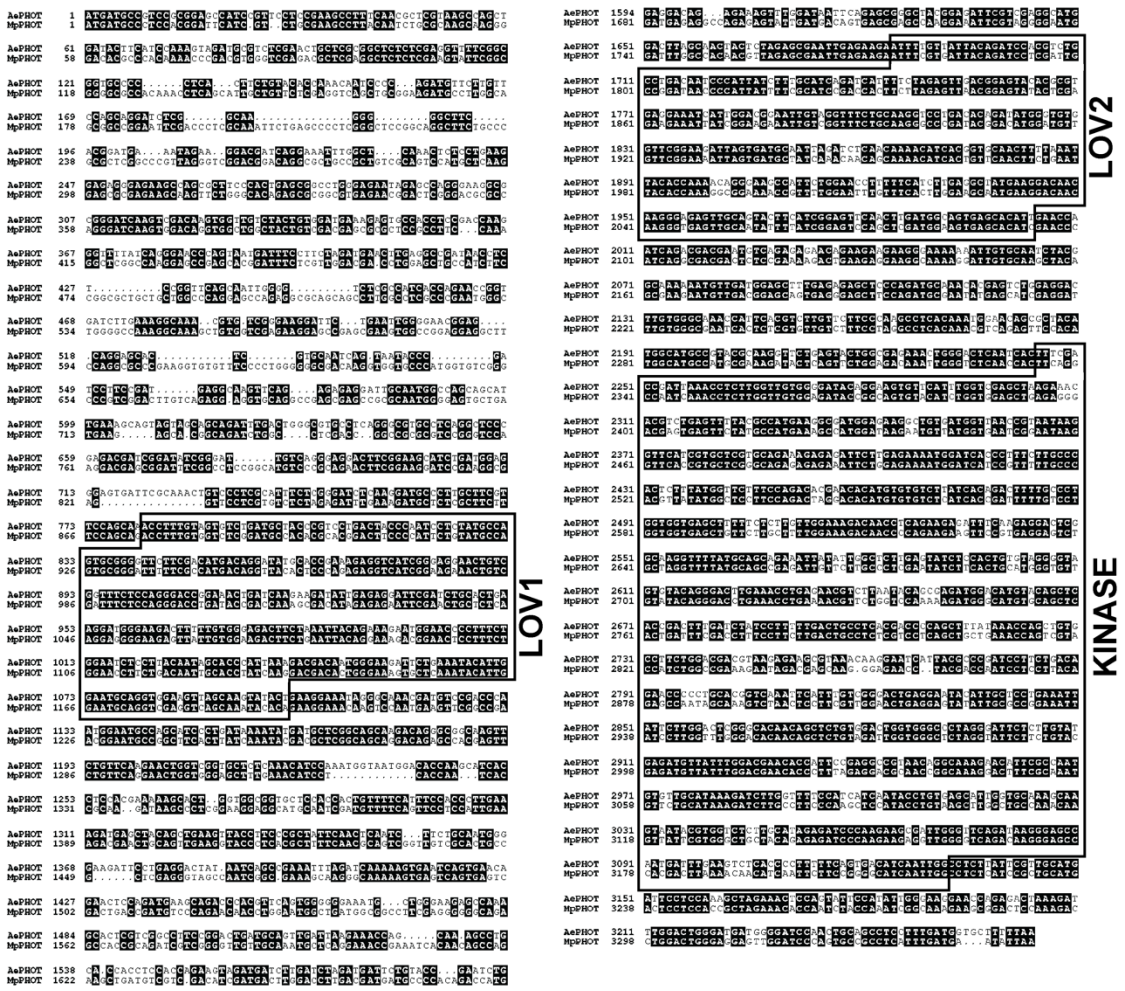


**Figure 12.** Alignment of *AePHOT* and *MpPHOT* nucleotide sequences (cDNA). The dark-shaded sequences indicate identical nucleotides between *AePHOT* and *MpPHOT*. The boxes indicate the coding regions of LOV1, LOV2, and kinase domains.

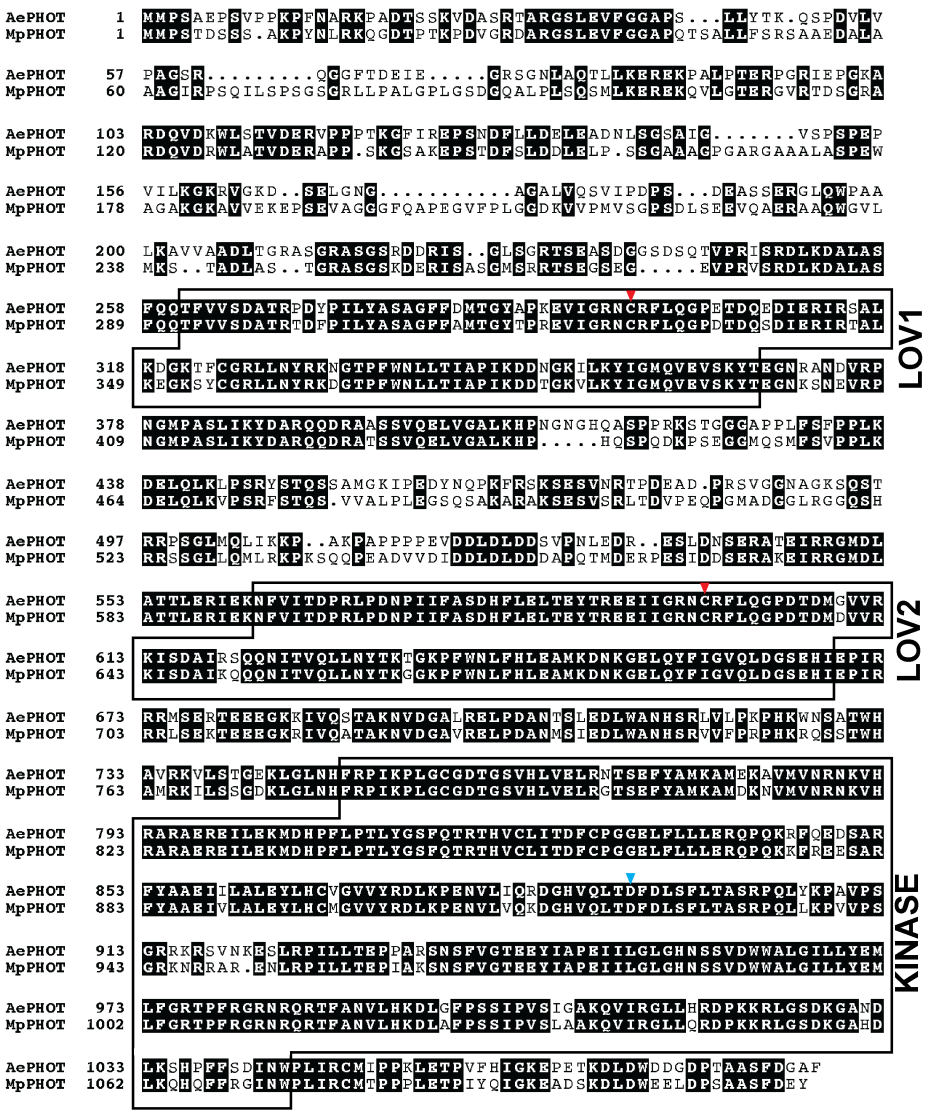


**Figure 13.** Alignment of AePHOT and MpPHOT protein sequences. The dark-shaded sequences indicate identical amino acids between AePHOT and MpPHOT. The boxes indicate the LOV1, LOV2, and kinase domains. Red arrowheads indicate the cysteine residues for FMN binding in the LOV1 and LOV2 domains of AePHOT and MpPHOT. The blue arrowhead indicates the aspartic acid residue, which is essential for the kinase function of AePHOT and MpPHOT.

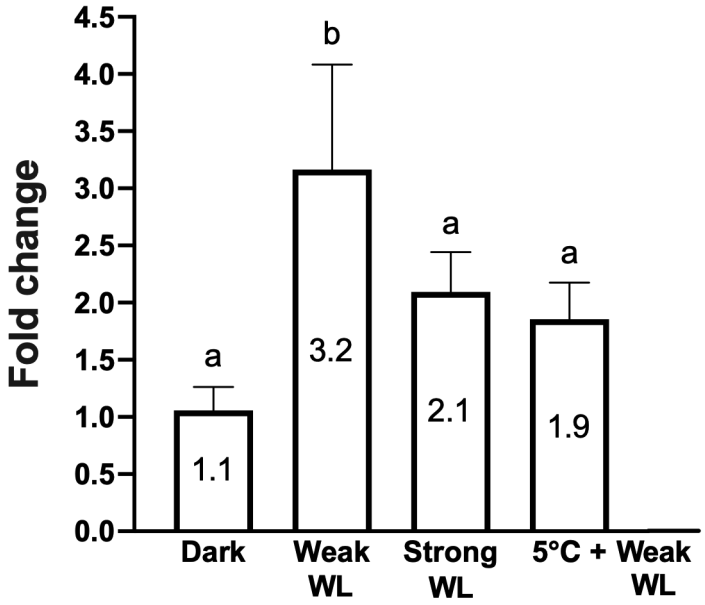


**Figure 14.** Quantitative real-time PCR analysis of *AePHOT* gene expression. Relative expression levels (fold change values) of *AePHOT* in the dark, weak white light (WL), strong WL, and low temperature (5°C) with weak WL are shown in the graph. All transcript levels were normalised against *PenB_ACT1*. Error bars represent standard deviation. Different alphabets (a and b) above the graph bars indicate significant differences (Tukey's HSD test; $\alpha < 0.05$).

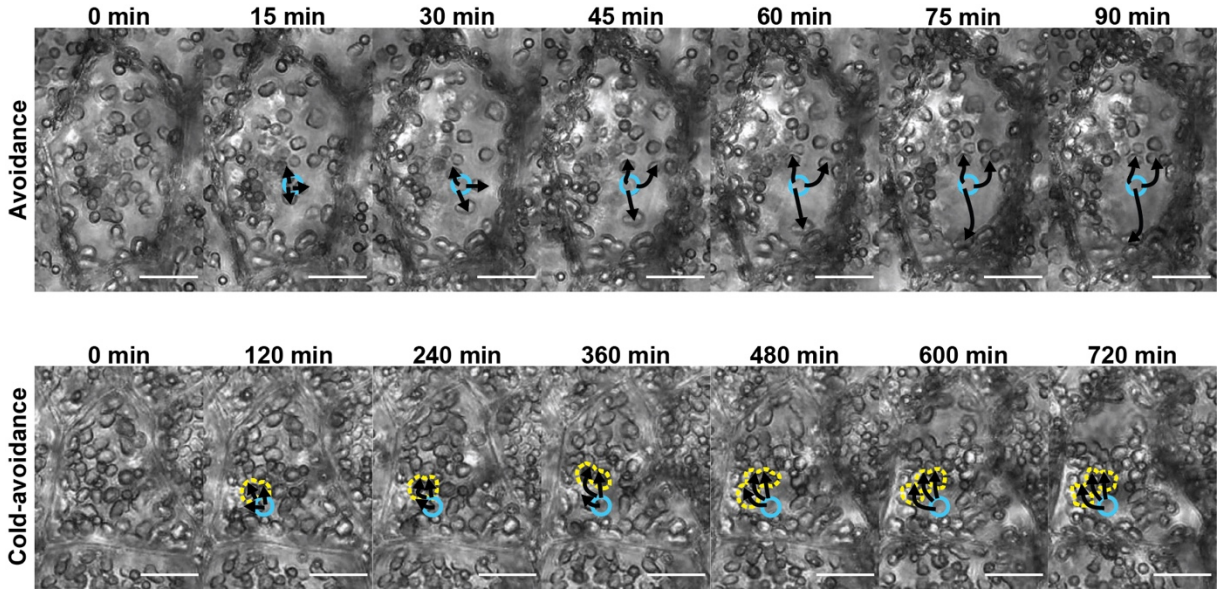


**Figure 15.** Time course of the avoidance and cold-avoidance responses of *A. endiviifolia*. **A,** Avoidance response of chloroplasts moving away from the irradiated strong BL microbeam (430 μmol photons $m^{-2}$ $s^{-1}$) in the thallus cell at 22°C. The arrows show chloroplasts moving towards the anticlinal wall separately. **B,** Cold-avoidance response of chloroplasts moving away from the irradiated weak BL microbeam (30 μmol photons $m^{-2}$ $s^{-1}$) in the thallus cell at 5°C. The arrows show chloroplasts gathering into a group (yellow dashed line) and moving away from the microbeam spot. Scale bars, 30 μm. The blue circle indicates the BL microbeam-irradiated spot. Images shown in this figure are taken from the time-lapse imaging in Figure 10C and 10E.

**Table 1.** Primers used in the experiments described in Chapter 2.

| Primer name | Sequence from 5′ to 3′ direction | Purpose |
|---|---|---|
| PeTUA1_F (Male) | GTATGTAAGCACCCCACCCTAACCTG | Sex determination of the isolated *A. endiviifolia* |
| PeTUA1_R (Male) | TGAGTGATTTGTGTTCTGGTTCTGCC | |
| PeRABa1/11_F (Male) | GATCATACTGACTCCAACATTGTG | |
| PeRABa1/11_R (Male) | CACATTCGTAGATTCAAGAGCAGAC | |
| PeMT3 _F (Female) | ACAACATGCAGCAACACCTC | |
| PeMT3_R (Female) | TCGAGCCCCAGTAGAAGGT | |
| PeCYSP_F (Female) | AGAGTCCTCCGTGTCGAGTC | |
| PeCYSP_R (Female) | ATCCTGCTGGGCATTCAGT | |
| PeMT2_F (Female) | AATAACATAGCTGCGGTGCAT | |
| PeMT2_R (Female) | ACGGCAAAGGGGATTTAGTT | |
| PeACT1_F (Actin) | CTAGATACCGCTCGGACCAG | *Actin* gene (accession number: DQ100290) |
| PeACT1_R (Actin) | GCTTCCATCCCGATTAGTGA | |
| attB1_AePHOT_F | GGGGACAAGTTTGTACAAAAAAGCAGGCTTCCGACACCTCGTTCTTTAT | Cloning of *PHOT* gene from *A. endiviifolia* |
| attB2_AePHOT_R | GGGGACCACTTTGTACAAGAAAGCTGGGTCAAGGAATTCCCAGTGGAGC | |
| AePHOT_Probe_F | GGCATCCTAACAGACCGATAG | Probe labelling of Southern blot analysis of *A. endiviifolia* |
| AePHOT_Probe_R | GCAATTACTGTCCACGTAAGT | |
| AePHOT_111bp_F | ATGATGCCGTCCGCGGAGCC | Quantification RT-PCR of *AePHOT* |
| AePHOT_111bp_R | CTCGAGAGAGCCGCGAGCAG | |

# CHAPTER 3

# COMPARATIVE ANALYSIS OF *AEPHOT* AND *MPPHOT* EXPRESSIONS IN *APOPELLIA ENDIVIIFOLIA* AND *MARCHANTIA POLYMORPHA*

## 3.1 Background overview

Blue light photoreceptor, phototropin (phot) was first identified in plants to be responsible for the phototropic response in *Arabidopsis thaliana* (Liscum & Briggs, 1995). The phot functions were later extensively studied and proved to regulate the stomatal opening, leaf orientation, cotyledon expansion and chloroplast movements (Kinoshita et al., 2001; Sakai et al., 2001; Christie, 2007). These functions play important role in photosynthesis for plant growth and development. Phot originated in a single copy from Viridiplantae (a combination of land plants and green algae) and was duplicated into different homologs and paralogs in various plants after countless evolution in the plant lineages (Li et al., 2015). Major duplication of *PHOT* genes in the evolution like *A. thaliana* (*AtPHOT1* and *AtPHOT2*) and *Physcomitrella patens* (*PpPHOT1A*-1, *PpPHOT1A*-2, *PpPHOT1A*-3, *PpPHOT1B*, *PpPHOT2B*, *PpPHOT2C*-1 and *PpPHOT2C*-2) have resulted in the overlapped and diverged functions among the *PHOT* paralogs under different conditions, as mentioned in Chapter 1.2 (Li et al., 2015; Sakai et al., 2001).

Meanwhile, no duplication of the *PHOT* gene from Viridiplantae in the evolutionary lineage of liverworts, resulting in the single *PHOT* gene trait in liverworts to regulate all the chloroplast movements (Li et al., 2015). For instance, the *AePHOT* in *Apopellia endiviifolia* and *MpPHOT* in *Marchantia polymorpha* (Yong et al., 2021; Komatsu et al., 2014). These two species are closely related in the family of Marchantiophyta and their *PHOT* genes share high similarities (Yong et al., 2021). However, their morphological characteristics are different where *A. endiviifolia* grows a simple thalloid thallus with chloroplasts developed uniformly and no air chamber within, contrary to the complex thalloid thallus of *M. polymorpha* with chloroplasts developed unevenly and air chambers within (Yong et al., 2021). Therefore, the two species were sub-classified into Jungermanniopsida and Marchantiopsida, respectively (Crandall-Stotler et al., 2005; He-Nygren et al., 2006). The simple thalloid thallus of *A. endiviifolia* is more useful for clear chloroplast observations than that in *M. polymorpha*. Therefore, if both *AePHOT* and *MpPHOT* are compatible with each other, the idea of using *A. endiviifolia* as a chloroplast observation tool in the analysis of *MpPHOT* was proposed. Here, I performed a cross-introduction of *AePHOT* and *MpPHOT* into *A. endiviifolia* and *M. polymorpha*, to verify the signalling of *AePHOT* in chloroplast movements of *A. endiviifolia* and check the compatibility of *AePHOT* and *MpPHOT* between *A. endiviifolia* and *M. polymorpha*. The resulting chloroplast positionings in the transformed cells of *A. endiviifolia* and *M. polymorpha* were observed and assessed.

## 3.2 Methodology

### 3.2.1 Plant materials and growth conditions

The Utsunomiya male 1 (UTm1) strain of *A. endiviifolia* and the male strain (Tak-1) of *M. polymorpha* were used in this study. The subcultures of *A. endiviifolia* and *M. polymorpha* were propagated on mineral culture media and half-strength B5 culture media, respectively, under continuous 60 μmol photons $m^{-2}$ $s^{-1}$ white light (FL40SW; NEC Corporation) at 22°C. The mineral culture medium and half-strength B5 culture media were prepared as described in Chapter 2.2.1. One- to two-month-old thalli of *A. endiviifolia* and three-day-old gemmalings of *M. polymorpha* were used for all experiments.

### 3.2.2 Plasmid construction

To generate the plasmids of 35S-AePHOT and 35S-MpPHOT for cell transformation of *A. endiviifolia* and *M. polymorpha*, the pDONR™/ZEO-AePHOT (Yong et al., 2021) and pDONR207-MpPHOT (Addgene: 100600; Kodama, 2016) were used. Both the plasmids were cloned into the pGWT35S vector (Addgene: 182790; Fujii et al., 2018), a destination vector for cellular transient expression, by LR reaction of Gateway cloning technology (Invitrogen). The plasmids of 35S-AePHOT and 35S-MpPHOT were generated from the transformed *Escherichia coli* colonies which were selected from LB culture media with kanamycin antibiotic. Each plasmid was extracted from the LB liquid culture of 35S-AePHOT and 35S-MpPHOT and the concentration was quantified as described in Chapter 2.2.10. Each plasmid was sent for gene sequencing to confirm the AePHOT and MpPHOT sequences and stored at -25°C.

### 3.2.3 Particle bombardment of *A. endiviifolia* and *M. polymorpha*

Detached *A. endiviifolia* thalli with the adaxial surface facing upwards were placed flat in the centre of a 60-mm culture medium. Each bombardment shot applied 0.1 mg of gold particles (1 μm in diameter) and a Citrine fluorescent marker. One microgram of the *AePHOT* or *MpPHOT* with *Citrine* plasmids was brought to a total volume of 10 μL by sterile water and mixed with 10 μL of 2.5 M $CaCl_2$ and 4 μL of 0.1 M of spermidine to coat the gold particles. In the control experiment, 1 μg of *Citrine* plasmid was used in the gold particle coating. A PDS-1000/He™ Biolistic Particle Delivery System (Bio-Rad) was employed to perform each bombardment. For *A. endiviifolia*, the plasmid-coated gold particles were spread on a 450-psi rupture disc and bombarded at a pressure of 4.5 MPa to the detached thalli. For *M. polymorpha*, the plasmid-coated gold particles were spread on a 650-psi rupture disc and bombarded at a pressure of 5.9 MPa to the gemmalings. The thallus pieces and gemmalings were incubated in the dark overnight after bombardment, then incubated under weak blue light (25 μmol photons $m^{-2}$ $s^{-1}$) condition at 22°C for 24 h before observation.

### 3.2.4 Observation and assessment of chloroplast positionings in transformed cell

To observe the expression of *AePHOT* and *MpPHOT* through the Citrine fluorescence in the transformed cells of *A. endiviifolia* and *M. polymorpha*, an SP8X confocal laser scanning microscope (Leica Microsystems) was used with excitation at 513 nm obtained from the white light laser and emission from 517 nm to 546 nm (Osaki & Kodama, 2017). Time-gating filter with a gating time set to 0.5 was enabled during observation, to avoid interferences from the chlorophyll autofluorescence (Kodama, 2016). The chlorophyll autofluorescence from *A. endiviifolia* thalli and *M. polymorpha* gemmalings were observed by excitation at 488 nm and emission from 641 nm to 721 nm. The resulting chloroplast positionings in the transformed cells of *A. endiviifolia* and *M. polymorpha* under the weak blue light (25 μmol photons $m^{-2}$ $s^{-1}$) at 22°C were observed and assessed. If an avoidance response has formed instead of the accumulation response which would normally be induced, indicating the transient overexpression from the introduced *PHOT* to the chloroplast responses (Fujii et al., 2020). The number of transformed cells that showed avoidance response was counted and the ratio against all observations was quantified.

## 3.3 Results

### 3.3.1 AePHOT and MpPHOT functions in *A. endiviifolia*

To understand the function of *AePHOT* in regulating chloroplast movement of *A. endiviifolia*, AePHOT plasmid with Citrine (fluorescent marker) was introduced into the thallus cells by particle bombardment. For the control experiment, only Citrine was introduced into the thallus cells (mock cells). Under weak blue light (BL; 25 μmol photons $m^{-2}$ $s^{-1}$) at 22°C, chloroplasts moved to the anticlinal wall and formed avoidance responses in 26 out of 35 (74%) AePHOT-transformed cells of *A. endiviifolia* (Figure 16 and Table 2). The observation is contrasted with the accumulation response observed in the mock cells, suggesting the endogenous *AePHOT* expression has been promoted from the introduced *AePHOT*, thus avoidance response from the transient overexpression induced in the transformed cells (Figure 16). These results confirmed the *AePHOT* functional role in *A. endiviifolia* to mediate the chloroplast movements. Furthermore, to determine whether the phototropin of *M. polymorpha* (*MpPHOT*) functions similarly as *AePHOT* in *A. endiviifolia*, MpPHOT plasmid with Citrine was introduced into the thallus cells of *A. endiviifolia*. Under weak BL at 22°C, avoidance responses were observed in 33 out of 35 (94%) MpPHOT-transformed cells of *A. endiviifolia*, contrasting to the accumulation response in the mock cells (Figure 16 and Table 2). This result shows the transient overexpression of *MpPHOT* in inducing avoidance response in the transformed cells, thus confirming the compatible *MpPHOT* signalling in *A. endiviifolia*.

### 3.3.2 AePHOT and MpPHOT functions in *M. polymorpha*

To determine whether *AePHOT* can regulate chloroplast movements in *M. polymorpha* as *MpPHOT* did in *A. endiviifolia* (Figure 16), AePHOT plasmid with Citrine was introduced into the gemmaling cells of *M. polymorpha* by particle bombardment. For the control experiment, only Citrine was introduced into the gemmaling cells (mock cells). After weak BL incubation at 22°C, avoidance responses were observed in only 4 out of 34 (12%) AePHOT-transformed cells of *M. polymorpha*, while accumulation responses were induced in most of the observed cells as in the mock cells (Figure 17 and Table 3). The observation suggests the endogenous *MpPHOT* expression was not promoted by the introduced *AePHOT* to induce an avoidance response in *M. polymorpha*, indicating the incompatible *AePHOT* signalling in *M. polymorpha*. Moreover, to rule out the possibility of ineffective particle bombardment transformation in *M. polymorpha*, the MpPHOT plasmid with Citrine was bombarded into the gemmaling cells of *M. polymorpha*. Under weak BL at 22°C, avoidance response was induced in 27 out of 32 (84%) MpPHOT-transformed cells of *M. polymorpha*, in contrast to the accumulation response in the mock cells and AePHOT-transformed cells (Figure 17 and Table 3). The transient overexpression of the introduced *MpPHOT* in chloroplast responses confirmed the particle bombardment transformation is effective for *M. polymorpha*. Therefore, the incompatibility of *AePHOT* in *M. polymorpha* was not due to the transformation method, but to the species specificity of *AePHOT*.

## 3.4 Discussion

A single copy *AePHOT* gene of *A. endiviifolia* was identified and suggested to regulate the chloroplast movements (Yong et al., 2021). Here, the *AePHOT* function in relocating the chloroplast movements, and the compatibility test of *AePHOT* and *MpPHOT* in *A. endiviifolia* and *M. polymorpha* were investigated. The transient overexpression of *AePHOT* and *MpPHOT* in *A. endiviifolia* have shown in the transformed cells through the induced avoidance response under the weak blue light conditions at 22°C (Figure 16). However, the introduction of AePHOT into *M. polymorpha* failed to promote the endogenous *MpPHOT* expression in *M. polymorpha*, hence avoidance response was not induced in the transformed cells (Figure 17). These results show the compatible function of *MpPHOT* in *A. endiviifolia* and the incompatible *AePHOT* function in *M. polymorpha*. These phenomena may relate to the phylogenetical relation between *A. endiviifolia* and *M. polymorpha*, where the *Pellia* genus of *A. endiviifolia* was located at the subsequent diverging lineage of *M. polymorpha* (Crandall-Stotler et al., 2005). In evolution, phot paralogs developed in different species to adapt to their habitat and some minor polymorphism in the amino acids of PHOT may result in unforeseen functional divergences (Li et al., 2015). Therefore, the minor polymorphism between AePHOT and MpPHOT may be the reason that *AePHOT* did not function in *M. polymorpha* (Yong et al., 2021).

### 3.5 Summary of key findings

In this chapter, the role of *AePHOT* in regulating the chloroplast movements was verified through the transient overexpression of the chloroplast response in AePHOT-transformed cells of *A. endiviifolia*. Moreover, the incompatible *AePHOT* signalling in the transformed cells of *M. polymorpha* has shown the species specificity of *AePHOT* that only functions on its own. Besides that, the compatibility of *MpPHOT* in *A. endiviifolia* was proved through the transient overexpression on the chloroplast response in the MpPHOT-transformed cells of *A. endiviifolia*.

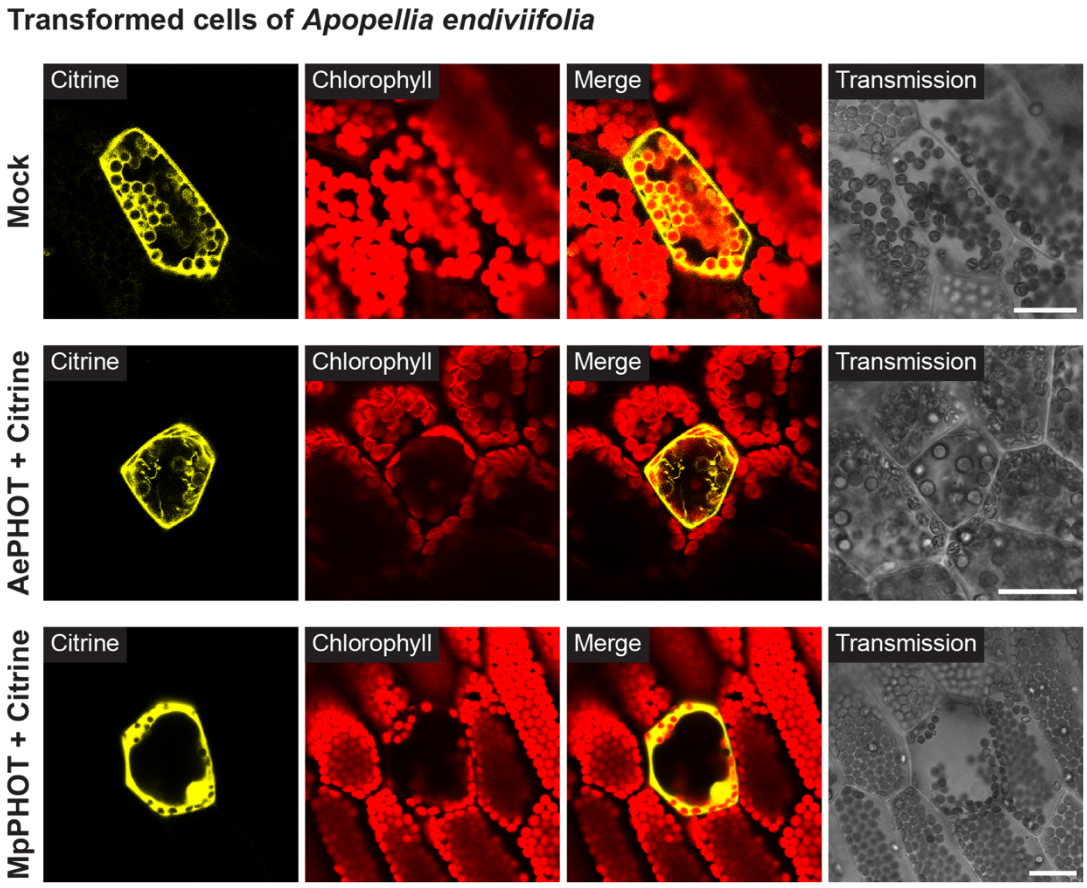


**Figure 16.** Observation of chloroplast positionings formed in the AePHOT- and MpPHOT-transformed cells of *A. endiviifolia* under weak blue light (25 μmol photons $m^{-2}$ $s^{-1}$) at 22°C. The AePHOT and MpPHOT with Citrine fluorescent marker were introduced into *A. endiviifolia* by particle bombardment. Mock refers to the control experiment that only introduced Citrine into *A. endiviifolia*. Citrine and chlorophyll fluorescence are shown as yellow and red, respectively. Scale bars, 25 μm.

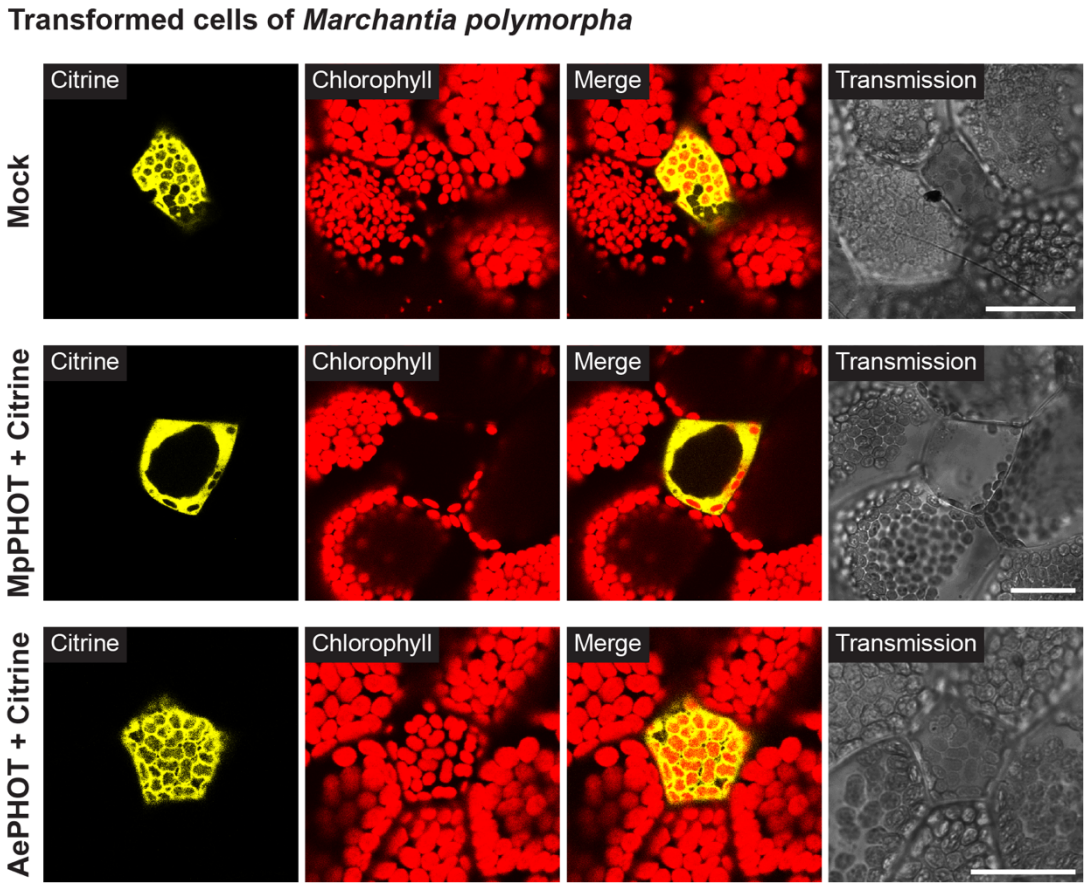


**Figure 17.** Observation of chloroplast positionings formed in the MpPHOT- and AePHOT-transformed cells of *M. polymorpha* under weak blue light (25 μmol photons $m^{-2}$ $s^{-1}$) at 22°C. The MpPHOT and AePHOT with Citrine fluorescent marker were introduced into *M. polymorpha* by particle bombardment. Mock refers to the control experiment that only introduced Citrine into *M. polymorpha*. Citrine and chlorophyll fluorescence are shown as yellow and red, respectively. Scale bars, 25 μm.

**Table 2.** Quantification of chloroplast positionings resulted in the transformed cells of *A. endiviifolia* after incubation under weak blue light (25 μmol photons $m^{-2}$ $s^{-1}$) at 22°C for 24 h.

| | Avoidance | Accumulation | Undefined | Total observation | Avoidance/ Total observation (%) |
|---|---|---|---|---|---|
| **Mock** | 4 | 31 | 3 | 38 | 11 |
| **AePHOT + Citrine** | 26 | 7 | 2 | 35 | 74 |
| **MpPHOT + Citrine** | 33 | 1 | 1 | 35 | 94 |

*Note*: Mock refers to the control experiment that only introduced the fluorescent marker, Citrine into *A. endiviifolia*.

**Table 3.** Quantification of chloroplast positionings resulted in the transformed cells of *M. polymorpha* after incubation under weak blue light (25 μmol photons $m^{-2}$ $s^{-1}$) at 22°C for 24 h.

| | Avoidance | Accumulation | Undefined | Total observation | Avoidance/ Total observation (%) |
|---|---|---|---|---|---|
| **Mock** | 3 | 27 | 2 | 32 | 9 |
| **MpPHOT + Citrine** | 27 | 3 | 2 | 32 | 84 |
| **AePHOT + Citrine** | 4 | 28 | 2 | 34 | 12 |

*Note*: Mock refers to the control experiment that only introduced the fluorescent marker, Citrine into *M. polymorpha*.

## CHAPTER 4

## ANALYSIS OF CYTOSKELETONS INVOLVED IN CHLOROPLAST MOVEMENTS OF *APOPELLIA ENDIVIIFOLIA*

### 4.1 Background overview

As *AePHOT* signalling in the chloroplast movements of *A. endiviifolia* was confirmed, the cytoskeleton components employed in the downstream signalling to regulate chloroplast movements in *A. endiviifolia* became my next focus. To date, the cytoskeleton components, microtubules and/or actin filaments have been reported to regulate the chloroplast movements in plants (Komatsu et al., 2014; Kasahara et al., 2004; Tsuboi et al., 2007; Sato et al., 2001; Takagi, 2003). In *Physcomitrella patens*, microtubules and actin filaments function redundantly in the accumulation and avoidance responses (Sato et al., 2001; Yamashita et al., 2011). In the dark-positioning response of *P. patens*, microtubules are responsible for the longitudinal orientation of chloroplasts and actin filaments control the direction of chloroplast motions (Sato et al., 2001; Yamashita et al., 2011). The utilisation of both microtubules and actin filaments in chloroplast movements of *P. patens* is indeed a rare case, while many plants like *Arabidopsis thaliana*, *Adiantum capillus-veneris* and *Marchantia polymorpha* are regulating chloroplast movements by actin filaments only (Kadota et al., 2009; Tsuboi & Wada, 2012b; Kimura & Kodama, 2016). Actin filaments are shown in the long filamentous actin (F-actin) and the short chloroplast (cp-) actin filaments near the chloroplast periphery, anchoring chloroplasts to the cellular plasma membrane (Kimura & Kodama, 2016; Kadota et al., 2009). Through the phot signalling, cp-actin filaments associate the directional chloroplast motility in cells, that gather at the side of the chloroplast periphery parallel to the leading direction of movement during accumulation and avoidance responses (Kadota et al., 2009; Yamashita et al., 2011; Tsuboi & Wada, 2012b). This behavioural action of cp-actin shows an obvious distinction from the long filaments of F-actin.

Although the characteristics and functions of microtubules and actin filaments have been well-studied in model plants, the activities of these cytoskeleton components were primarily observed from the light-dependent chloroplast responses of accumulation, avoidance and cold-avoidance responses. Therefore, the roles of the cytoskeleton components in the dark-positioning response were left unclear, particularly to plants that employ only actin filaments for chloroplast movements. The insufficient study of dark-positioning response could be due to the requirement of a prolonged dark incubation period to complete the response (Moore, 1888; Senn, 1908). For instance, dark incubation for 72 h in *M. polymorpha*, 36 h in *A. capillus-veneris*, 24 h in *P. patens* and 12 h in *A. thaliana* (Sato et al., 2001; Komatsu et al., 2014; Tsuboi & Wada, 2012b; Suetsugu et al., 2005). In the responses, chloroplasts move slowly and take a long time to complete their movements. This hinders the observation process and likely explains why less is known about the dark-positioning response than the light-dependent chloroplast responses. In this study, I coincidentally noticed that the dark-positioning response of *A. endiviifolia* can be completed within a short period of dark incubation, which shows the potential uses of *A. endiviifolia* in understanding dark-positioning responses. Therefore, the required time for a complete dark-positioning response of *A. endiviifolia* in the dark incubation was identified through the time-tracking observation in the present study.

Moreover, the roles of microtubules and actin filaments in all chloroplast movements including the light-dependent chloroplast responses and dark-positioning responses of *A. endiviifolia* were also investigated. Visualisation of the microtubules and actin filaments in *A. endiviifolia* was performed through the immunofluorescence staining and localisation of the fluorescent protein probe, respectively (Kimura & Kodama, 2016; Du et al., 2021). To determine the responsible cytoskeleton component of the chloroplast movements in *A. endiviifolia*, microtubule and actin filament depolymerisation inhibitors, oryzalin and latrunculin A (lat-A) was applied and the chloroplast positioning formed in the inhibitor-treated thalli will be observed and assessed.

## 4.2 Methodology

### 4.2.1 Plant materials and growth conditions

The Utsunomiya male 1 (UTm1) strain of *A. endiviifolia* was used in this study. The subcultures of *A. endiviifolia* were propagated on mineral culture media under continuous 60 μmol photons $m^{-2}$ $s^{-1}$ white light (FL40SW; NEC Corporation) at 22°C. The mineral culture medium was prepared as described in Chapter 2.2.1. One- to two-month-old, detached thalli were used for all experiments.

### 4.2.2 Time-tracking observation of the dark-positioning response of *A. endiviifolia*

To determine the time needed for complete dark-positioning response in *A. endiviifolia*, light-adapted thallus pieces were incubated in the dark at 22°C and observed for 6 h in 30 min intervals. The detached thalli were also incubated for 24 h in the dark at 22°C to induce a complete dark-positioning response (Yong et al., 2021). Before dark incubation, light-adapted thallus was prepared by incubating under 60 μmol photons $m^{-2}$ $s^{-1}$ of white light (FL40SW; NEC Corporation) at 22°C for 2 h.

### 4.2.3 Treatments of microtubule and actin filament polymerisation inhibitors

Two cytoskeleton polymerisation inhibitors were applied in this study. For microtubule polymerisation inhibitor, 10 μM oryzalin (Sigma-Aldrich) was prepared from the stock solution of 10 mM oryzalin in dimethyl sulfoxide (DMSO; Sigma-Aldrich). For actin filament polymerisation inhibitors, 1 μM latrunculin A (lat-A; Sigma Aldrich) was prepared from the stock solution of 0.1 mM lat-A in ethanol (EtOH). For the control experiment, 0.25% of DMSO and EtOH were used. A total volume of 5 mL of the inhibitor (oryzalin or lat-A) was poured into a 60-mm diameter Petri dish containing culture medium with five detached thalli in each treatment. The submerged thalli were incubated for 2 h to complete the depolymerisation.

### 4.2.4 Immunofluorescence staining of microtubules

Immunofluorescence staining of microtubules of *A. endiviifolia* was performed as previously described with some modifications (Du et al., 2021). Detached *A. endiviifolia* thalli were pre-treated with the microtubule depolymerisation inhibitor oryzalin, and DMSO (control experiment) as described in Chapter 4.2.3. The untreated and treated thalli were fixed by fixative made from 4% paraformaldehyde in 100 mL of microtubule stabilising buffer (MTSB) solution with 1 mL of 50% glutaraldehyde (Sigma Aldrich), 300 µL of Tween 20 and 300 µL of Triton X-100, adjusted to pH 7. The MTSB solution was prepared by dissolving 7.56 g PIPES, 0.62 g $MgSO_4 \cdot 7H_2O$ and 0.95 g EGTA in sterile water, adjusted to pH 6.9 to a final volume of 500 mL. All thalli were submerged in the fixative and vacuumed for 10 min for three cycles; the fixative was renewed in each cycle. Following an additional 3 h incubation of the thalli in new fixative, and then replaced the fixative to MTSB for 20 min incubation in three cycles; the MTSB was renewed in each cycle. After that, the fixed thalli were embedded into 6% low melting agarose and incubated at 4°C for 15 min. After the agarose gel solidified, thallus tissue was sectioned horizontally to 100 µm thickness by an RM2245 rotary microtome (Leica Biosystems) and placed to the MTSB droplets in the PAP circle drawn on poly-L-lysine coated glass slides. Next, the thallus sections were treated with 1% (w/v) hemicellulose with 1% (v/v) Triton X-100 in MTSB solution for 15 min. Subsequently, the thallus sections were washed with 1×Tris-buffered saline (TBS) for 5 min in three cycles; the 1×TBS was renewed in each cycle. The 1×TBS solution was prepared by dissolving 8.8 g NaCl and 20 mL of 1 M Tris-HCl (pH=8.0) in 1 L of water and autoclaved for 15 min at 121°C. After washing, the thallus section was incubated with primary antibody (T5168 Monoclonal Anti-α-Tubulin antibody produced in mouse; Sigma Aldrich) with 1% bovine serum albumin (BSA) in 1×TBS at 1: 800 dilutions for overnight at 4°C. Next, the primary antibody was removed, and the thallus sections were washed with 1×TBS for 10 min in three cycles; the 1×TBS was renewed in each cycle. After washing, the thallus sections were treated with secondary antibody (A-21202 Donkey anti-Mouse IgG (H+L) Highly Cross-Adsorbed Secondary Antibody, Alexa Fluor™ 488; Thermo Fisher) with 1% BSA in 1×TBS at 1: 500 dilutions at 37°C for 2 h in the dark. Following the removal of the second antibody, the thallus sections were washed with 1×TBS for 10 min in three cycles; the 1×TBS was renewed in each cycle. Finally, the slides with fluorescent-stained thallus sections were mounted with ProLong™ Gold Antifade Mountant (Sigma Aldrich) before observation.

### 4.2.5 Actin filament fluorescent marker amplification

To observe actin filaments in *A. endiviifolia* cells, the actin filament marker, a plasmid encoding pMpGWB403-Lifeact-Citrine (Addgene: 100582) was introduced into the detached thalli of *A. endiviifolia* by particle bombardment (Kimura & Kodama, 2016). The plasmid of pMpGWB403-Lifeact-Citrine with spectinomycin resistance was generated and extracted as described in Chapter 3.2.2 and stored at -25°C.

### 4.2.6 Particle bombardment

Detached *A. endiviifolia* thalli with the adaxial surface facing upwards were placed flat in the centre of a 60-mm culture medium. For each bombardment shot, 0.1 mg of gold particles (1 μm in diameter) was applied. One microgram of the *Lifeact-Citrine* plasmid was brought to a volume of 10 μL by sterile water and mixed with 10 μL of 2.5 M $CaCl_2$ and 4 μL of 0.1 M of spermidine to coat the gold particles. The plasmid-coated gold particles were bombarded into the detached thalli as described in Chapter 3.2.3. After the bombardment, the detached thalli were incubated in the dark overnight, treated with actin filament depolymerisation inhibitor latrunculin A, and EtOH (control experiment), and then observed the following day.

### 4.2.7 Visualisation of microtubules and actin filaments of *A. endiviifolia*

To observe microtubules and actin filaments through the expression of Alexa Fluor 488 immunofluorescence in the stained thallus sections and *Lifeact-Citrine* in the transformed cells of *A. endiviifolia*, an SP8X confocal laser scanning microscope (Leica Microsystems) was used. For Alexa Fluor 488 fluorescence, observations were obtained with excitation at 488 nm and emission from 500 to 530 nm (Du et al., 2021). For Lifeact-Citrine transient expression, observations were obtained with excitation at 513 nm and emission from 517 to 546 nm (Kimura & Kodama, 2016). During the observation, the time-gating function was employed with a gating time set to 0.5, to avoid interferences from chloroplast autofluorescence (Kodama, 2016). Moreover, the chlorophyll autofluorescence from *A. endiviifolia* thalli was observed by excitation at 488 nm and emission from 641 to 721 nm. The confocal z-stack images of microtubules and actin filaments were captured.

### 4.2.8 Induction of chloroplast movements in *A. endiviifolia*

A series of incubation conditions were utilised to analyse chloroplast movements during the dark-positioning, accumulation, avoidance, and cold-avoidance responses in inhibitor-treated *A. endiviifolia* thalli. Pre-incubation conditions before inhibitor treatment were contrasted with the incubation conditions after inhibitor treatment, to observe changes in chloroplast movements before and after inhibitor treatment. Initially, five detached thalli were pre-incubated for 24 h under weak blue light (BL; 25 μmol photons $m^{-2}$ $s^{-1}$) at 22°C before the subsequent induction of the dark-positioning, avoidance, or cold-avoidance response, and in darkness at 22°C before the subsequent induction of the accumulation response. After 24 h, the pre-incubated thalli were treated with microtubule or actin filament polymerisation inhibitor for 2 h in the pre-incubated conditions. The treated thalli were then transferred to incubate in conditions that induced the subsequent chloroplast responses: 3 h in darkness at 22°C for the dark-positioning response, 24 h under weak BL at 22°C for the accumulation response, 24 h under strong BL (50 μmol photons $m^{-2}$ $s^{-1}$) for the avoidance response, and 24 h under weak BL at 5°C for the cold-avoidance response. These treated thalli were observed after the incubation.

### 4.2.9 Observation and evaluation of chloroplast positioning

Chloroplast positionings formed in the thalli of *A. endiviifolia* were observed under the MZ16F fluorescence stereomicroscope (Leica Microsystems) and evaluated by the P/A ratio quantification as described in Chapter 2.2.6 (Ogasawara et al., 2013; Kodama et al., 2008). Along the periclinal and anticlinal cell walls, 30 areas (196 $\mu m^2$ each) and 30 points (42 μm each) of fluorescence intensities were selected randomly for the P/A ratio quantification. The experiment was repeated three times independently, and the average P/A ratio with standard deviation (N=3) was calculated. All statistical analyses were performed by GraphPad Prism 8.0. Multiple comparisons between all means were performed through Tukey's HSD test in one-way ANOVA with a significance level of 0.05. The adjusted p-value of ANOVA was also quantified from each comparison.

## 4.3 Results

### 4.3.1 Timeline of the dark-positioning response of *A. endiviifolia*

To construct a timeline of the dark-positioning response of *A. endiviifolia*, the P/A ratio of the chloroplast positionings in dark-incubated thalli of every 30 min was quantified (Kodama et al., 2008). After the first 30 min of dark incubation, partial chloroplasts moved to the anticlinal wall bordering with neighbouring cells from the periclinal wall, resulting in a P/A ratio of 1.3 (Figure 18). The P/A ratio was 0.4 lesser than that before dark incubation, indicating the dark-positioning response has been initiated (Figure 18B). Subsequently, most of the chloroplasts were aggregating along the anticlinal wall, leaving nearly no chloroplast positionings at the periclinal wall (Figure 18A). These chloroplast positionings showed a sharp decline in the P/A ratio from 1.3 at 60 min to 0.6 at 180 min of dark incubation, achieving the dark-positioning response (Figure 18B). In the following dark incubation period (up to 24 h), chloroplasts were moving along the anticlinal wall, resulting in fluctuating P/A ratios within the range of 0.5 to 0.7 (Figure 18). These observations suggest that the dark-positioning response of *A. endiviifolia* is completed after incubation in the dark for 180 min (3 h).

### 4.3.2 Visualisation of microtubules and actin filaments in *A. endiviifolia*

For visualisation of the microtubules and actin filaments, the microtubules of *A. endiviifolia* were stained by microtubule immunofluorescence of Alexa Fluor 488, and actin filament fluorescence marker Lifeact-Citrine was introduced to the thalli of *A. endiviifolia* by particle bombardment to localise the actin filaments. Through the Alexa Fluor 488 fluorescence, microtubules were observed as filamentous signals covering the chloroplasts and extended from plasma membranes in the stained thallus cell (Figure 19A). Through the *Lifeact-Citrine* transient expression, long filamentous actin (F-actin) was observed anchoring around the chloroplasts as filamentous signals in the transformed cells (Figure 19B). During the avoidance response under the strong blue light (BL), short chloroplast (cp-) actin filaments concentrated at the heading side of the chloroplast periphery parallel to the moving direction toward the anticlinal wall were detected (Figure 19C). Therefore, both microtubules and actin filaments were visualised in *A. endiviifolia*.

### 4.3.3 Depolymerisation of microtubules and actin filaments in *A. endiviifolia*

To depolymerise the microtubules and actin filaments in *A. endiviifolia*, the microtubule and actin filament polymerisation inhibitors oryzalin and latrunculin A (lat-A) were applied, respectively. In the oryzalin-treated thallus sections, the Alexa Fluor 488 filamentous signals of microtubules were not observed, and the fluorescence signals were localised to the cytosol instead (Figure 20A). While in the DMSO-treated thallus section which is the control experiment resembled those of the untreated thallus section (Figure 19A and 20A). These results indicate the specific depolymerisation of microtubules by oryzalin. Furthermore, when the *A. endiviifolia* transformed cells expressing *Lifeact-Citrine* were treated with lat-A, the expression size of the filamentous signal anchoring around the chloroplasts was reduced, and the fluorescent signals were localised to the cytosol instead (Figure 20B). In contrast, the actin filaments of *A. endiviifolia* transformed cells expressing *Lifeact-Citrine* in the control experiment treated with EtOH resembled those in untreated transformed cells (Figure 19B and 20B). These results show the specific depolymerisation of actin filaments by lat-A.

### 4.3.4 Chloroplast movements of *A. endiviifolia* are actin filament dependent

To investigate the unidentified cytoskeleton components employed in the light-dependent chloroplast responses including accumulation, avoidance and cold-avoidance of *A. endiviifolia*, chloroplast movements were analysed after the depolymerisation of microtubules and actin filaments by oryzalin or lat-A, respectively. The P/A ratio quantification was applied to evaluate the resulting chloroplast positionings (Kodama et al., 2008). To analyse the accumulation response, the thalli were pre-induced to dark-positioning response and treated with oryzalin or lat-A, following a final incubation under the weak BL (25 μmol photons $m^{-2}$ $s^{-1}$) at 22°C. Accumulation responses were shown in the oryzalin-treated thalli as the DMSO-treated thalli (control treatment), resulting in P/A ratios of 1.5 and 1.6 (Figure 21A). However, the pre-induced dark-positioning response remained in the lat-A-treated thalli with a significantly low P/A ratio of 0.3 (adjusted p-value = 0.0003) and did not show accumulation response as observed in the EtOH-treated thalli (control treatment) (Figure 21A). These results confirm that only the disrupted actin filaments have inhibited the accumulation response in *A. endiviifolia*. Next, in the avoidance response analysis, the thalli were pre-induced to accumulation response and treated with oryzalin or lat-A, followed by a final incubation under the strong BL (50 μmol photons $m^{-2}$ $s^{-1}$) at 22°C. Oryzalin-treated thalli showed an avoidance response as the DMSO-treated thalli, which resulted in P/A ratios of 0.2 and 0.3 (Figure 21B). By contrast, the accumulation response continued in lat-A-treated thalli with a significantly high P/A ratio of 1.3 (adjusted p-value < 0.0001) and did not show avoidance responses as the EtOH-treated thalli (Figure 21B). These observations indicate that only the disrupted actin filaments have inhibited the avoidance response in *A. endiviifolia*. Subsequently, to analyse the cold-avoidance response, the thalli were pre-induced to accumulation response and treated with oryzalin or lat-A, followed by a final incubation under weak BL at 5°C. Both oryzalin-treated and DMSO-treated thalli showed cold-avoidance responses, resulting in the same P/A ratio of 0.2 (Figure 21C). Yet, the lat-A-treated thalli still showed the pre-induced accumulation response with a significantly high P/A ratio of 1.0 (adjusted p-value < 0.0001) and did not show the cold-avoidance response as the EtOH-treated thalli (Figure 21C). These results indicate that only

the disrupted actin filaments have inhibited the cold-avoidance response in *A. endiviifolia*. Overall, the actin filaments regulation in the light-dependent chloroplast responses of *A. endiviifolia* was verified.

Furthermore, the dark-positioning response of *A. endiviifolia* was analysed to determine the regulatory roles of microtubules or actin filaments in the response. The thalli were pre-induced to accumulation response and treated with oryzalin or lat-A, followed by a final incubation under dark conditions at 22°C. Dark-positioning responses were observed in both oryzalin-treated and DMSO-treated thalli with a similar P/A ratio of 0.7 (Figure 22). While in the lat-A-treated thalli, dark-positioning responses were not observed, instead the pre-induced accumulation response remained in the cells with a significantly high P/A ratio of 1.2 (adjusted p-value < 0.0001), in contrast to the EtOH-treated thalli (Figure 22). These results are similar to the light-dependent chloroplast responses, where only the disrupted actin filaments have restricted the chloroplast mobility and inhibited the dark-positioning response in *A. endiviifolia*. Hence, the dark-positioning response of *A. endiviifolia* was proved to be regulated by actin filaments.

### 4.4 Discussion

After confirming the Aephot signalling in *A. endiviifolia*, I continue my analysis of understanding the chloroplast movements by investigating the microtubules or actin filaments employed in the downstream signalling to regulate chloroplast movements. Here, the microtubules and actin filaments of *A. endiviifolia* were observed and the dependency of actin filaments in the light-dependent chloroplast responses and dark-positioning response were identified.

Through the transient expression of the actin filament fluorescent marker Lifeact-Citrine, the actin filaments including the long filamentous actin (F-actin) and short chloroplast (cp-) actin filaments of *A. endiviifolia* were visualised in the transformed cells (Figure 19B and 19C). The long filamentous network structure of F-actin in *A. endiviifolia* was consistent with that in *Marchantia polymorpha* (Kimura & Kodama, 2016). However, the short filament structures of cp-actin filaments associated with chloroplast motion in *A. endiviifolia* are unable to be compared with *M. polymorpha*, as cp-actin filaments were not observed in *M. polymorpha* in a previous study (Kimura & Kodama, 2016). In the present study, the cp-actin filaments of *A. endiviifolia* were detected during the avoidance response after an hour of strong blue light incubation at 22°C (Figure 19C). This observation reveals the involvement of cp-actin filaments in chloroplast movements of liverwort species, although these filaments have yet to be observed in *M. polymorpha* (Kimura & Kodama, 2016). Indeed, the frequent disappearance and reappearance behaviour of cp-actin filaments at the edges of chloroplasts makes them difficult to detect (Kadota et al., 2009; Kimura & Kodama, 2016). Hence, optimisation of the incubation duration and observation time should be crucial for capturing and analysing cp-actin filaments in the future. Although I did not fully analyse the cp-actin filaments of *A. endiviifolia*, as this was not the main purpose of this study, such observations could highlight the conservation of cp-actin filaments from non-vascular to vascular plants throughout evolution.

Much is known about the roles of actin filaments in the light-dependent chloroplast responses of accumulation, avoidance and cold-avoidance, yet the dark-positioning response remains to be elucidated. When the dark-positioning response was first identified in the 19$^{th}$ century, it was shown to require a prolonged dark incubation

period, with periods of up to 10 weeks for meadow saxifrage (*Saxifraga granulata*) and the fern *Pteris serrulata* and 10 days for vernal water-starwort (*Callitriche verna*) and wood sorrel (*Oxalis acetosella*) (Moore, 1888; Senn, 1908). This prolonged dark incubation would be expected to weaken plants by causing starvation in the dark, hence hampering observations (Moore, 1888). In recent studies, several plant species have been found to complete dark-positioning in a relatively short period, but at least 12 h are needed to complete the response like the *Arabidopsis thaliana* (Suetsugu et al., 2005). In *A. endiviifolia*, the dark-positioning response was completed after 3 h of dark incubation, a much faster response than those reported in other plant species (Figure 18). This characteristic highlights the potential use of *A. endiviifolia* for studying the dark-positioning response. Based on limited data about the dark-positioning response, the speed of this rapid response is perhaps related to the type of tissues used for observation. Mature simple thalloid tissues are used to observe the dark-positioning response in *A. endiviifolia* (Yong et al., 2021), whereas previous studies have observed this response in premature structures, such as the protonemata of *Physcomitrella patens*, prothalli of *Adiantum capillus-veneris*, gemmalings of *Marchantia polymorpha*, and seedlings of *A. thaliana* (Sato et al., 2001; Komatsu et al., 2014; Tsuboi & Wada, 2012b; Suetsugu et al., 2005). Therefore, possibly an as-yet-unidentified component of the morphological development determines the speed of the dark-positioning response. Also, differences in experimental conditions between the present and previous studies might be one of the reasons for the rapid dark-positioning response of *A. endiviifolia*.

Chloroplast movements in most plants are dependent on actin filament motility systems (e.g., *A. thaliana*, *A. capillus-veneris*, and *M. polymorpha*), whereas some plants also employ microtubule motility systems (e.g., *P. patens* and *Bryopsis plumosa*) (Oikawa et al., 2003, 2008; Kimura & Kodama, 2016; Tsuboi & Wada, 2012b; Sato et al., 2001; Kasahara et al., 2004; Mizukami & Wada, 1981). Actin filaments regulate BL-mediated chloroplast movements via the phototropin (phot) signalling pathway, and microtubules regulate red light (RL)–mediated chloroplast movements via phot in the phytochrome signalling pathway (Sato et al., 2001; Kasahara et al., 2004). These reported data support my results of actin filament regulation in the light-dependent chloroplast responses of *A. endiviifolia*, as these movements were only induced by BL (Figure 21) (Yong et al., 2021). Furthermore, the dark-positioning response of *A. endiviifolia* was also regulated by actin filaments, partly similar to *P. patens* which employ microtubules and actin filaments to regulate the dark-positioning response (Figure 22) (Sato et al., 2001; Kasahara et al., 2004). Therefore, the light- and dark-induced chloroplast responses are suggested to use the same chloroplast motility mechanism in plant cells. To date, delayed and inhibited dark-positioning responses were observed in *phot2* mutant cells of *A. capillus-veneris* and *A. thaliana*, pointing to the involvement of phot signalling in this response (Tsuboi et al., 2007; Tsuboi & Wada, 2012a; Suetsugu et al., 2005). However, the signalling mechanism or relation of phot with actin filaments in inducing the dark-positioning responses is still a mystery and will be interesting to find out in the future.

### 4.5 Summary of key findings

In this chapter, microtubules and actin filaments of *A. endiviifolia* were visualised through the expressions of the respective fluorescent probes. Moreover, the dark-positioning response of *A. endiviifolia* can be achieved rapidly within 3 h of dark incubation, significantly faster than any reported plant species. Hereafter, the involvement of actin filament in the light-dependent chloroplast responses of accumulation, avoidance and cold-avoidance, and the dark-positioning response of *A. endiviifolia* were confirmed.

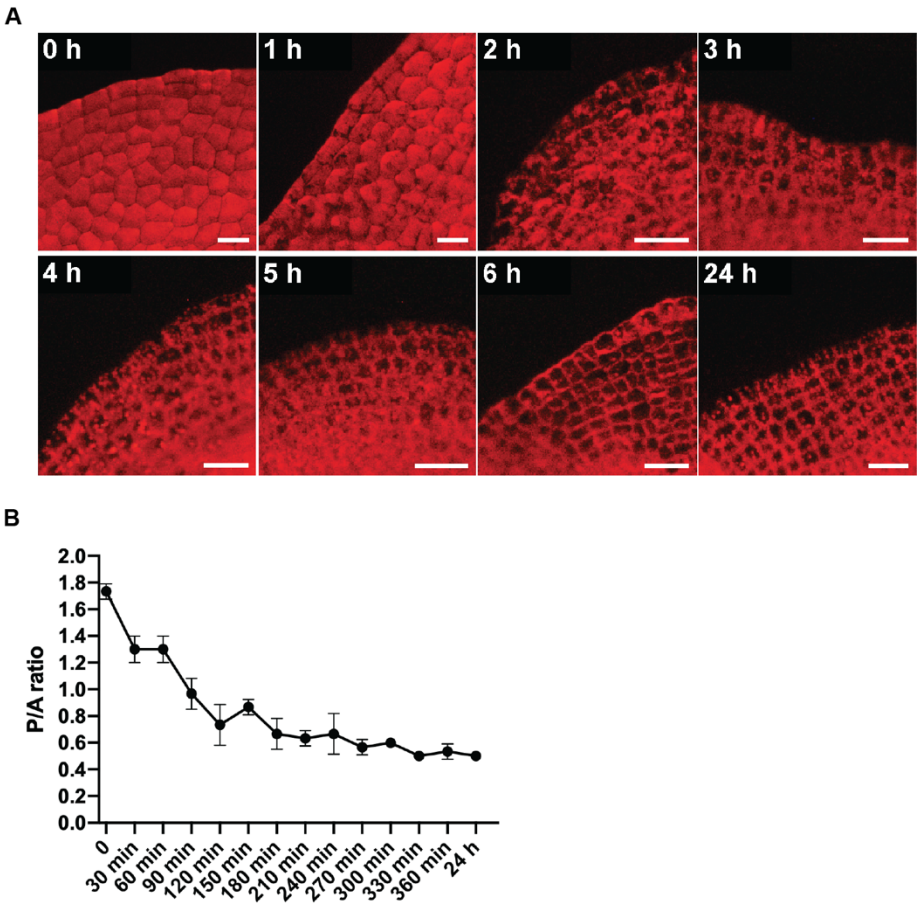


**Figure 18.** Timeline of the dark-positioning response of *A. endiviifolia*. **A,** Representative images of the hourly dark induction of dark-positioning response in *A. endiviifolia* thalli. Scale bars, 50 µm. **B,** Evaluation of chloroplast positioning by the P/A ratio quantification. The average P/A ratio of chloroplasts positioning from the periclinal wall to the anticlinal wall in the dark-positioning response after every 30 min of dark incubation was tracked and quantified from three replicates. The declining P/A ratio implied the process of chloroplast movements in the dark-positioning response. Error bars represent standard deviation (N=3). Significant differences from 0 min with the range of 30 min ≤ t (time) ≤ 24 h ($P < 0.05$), 90 min ≤ t ≤ 24 h ($P < 0.01$), and 180 min ≤ t ≤ 24 h ($P < 0.001$); Tukey's HSD test; $\alpha < 0.05$.

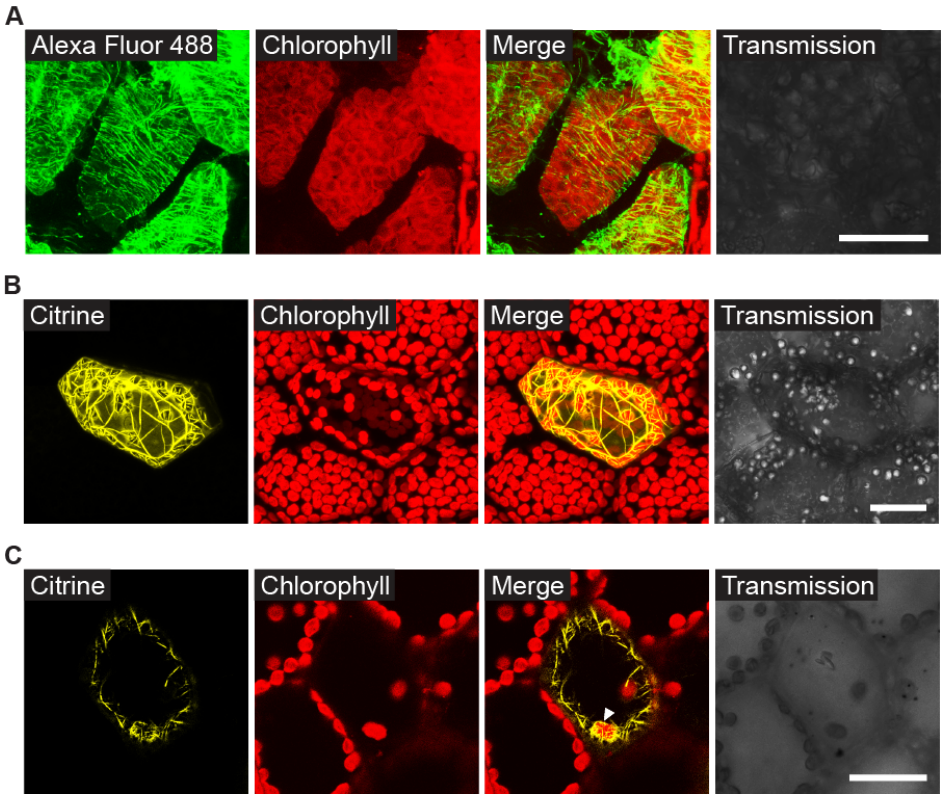


**Figure 19.** Visualisation of microtubules and actin filaments in *A. endiviifolia*. **A**, Confocal z-stack image of microtubules in fluorescent-stained thallus section of *A. endiviifolia*. The thallus section of *A. endiviifolia* was stained by Alexa Fluor 488 fluorescent probe in immunofluorescence staining. **B**, Confocal z-stack image of actin filaments in *A. endiviifolia* transformed cells transiently expressing *Lifeact-Citrine*. **C**, Visualisation of chloroplast (cp-) actin filaments (white arrowhead) during the avoidance response of *A. endiviifolia* through *Lifeact-Citrine* expression. (**B, C**) The *Lifeact-Citrine* construct was introduced into *A. endiviifolia* by particle bombardment. Alexa Fluor 488, Lifeact-Citrine and chlorophyll fluorescence are shown as green, yellow, and red, respectively. Scale bars, 25 μm.

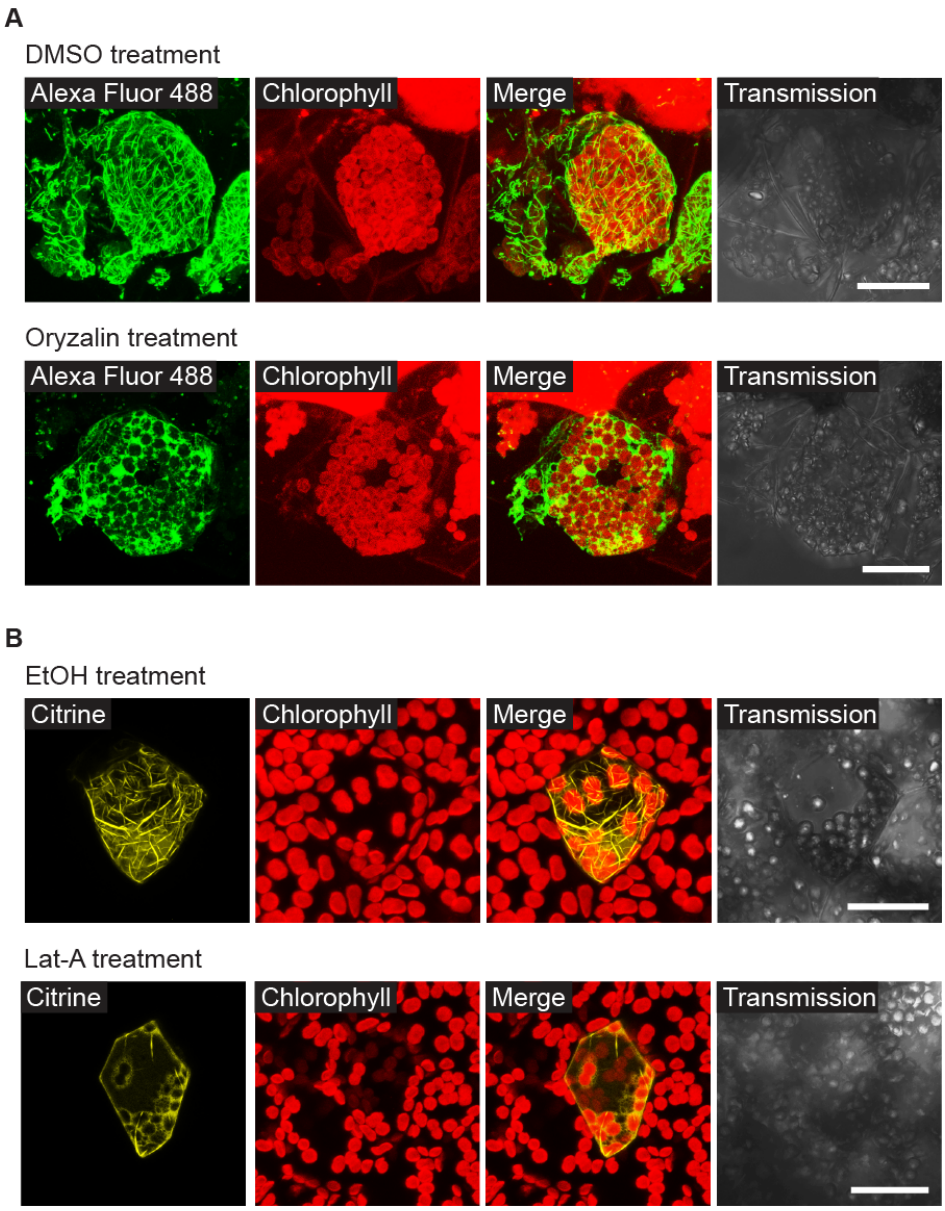


**Figure 20.** Depolymerisation of microtubules and actin filaments of *A. endiviifolia* by their respective inhibitors. **A**, Confocal z-stack image of microtubules in fluorescent-stained thallus section that pre-treated with dimethyl sulfoxide (control experiment) or oryzalin (microtubule depolymerisation inhibitor). **B**, Confocal z-stack image of actin filaments in *A. endiviifolia* transformed cells expressing *Lifeact-Citrine* treated with ethanol (control experiment) or latrunculin A (actin filament depolymerisation inhibitor). DMSO, 0.25% (v/v) dimethyl sulfoxide solution; Oryzalin, 10 µM oryzalin; EtOH, 0.25% (v/v) ethanol solution; Lat-A, 1 µM latrunculin A. Alexa Fluor 488, Lifeact-Citrine and chlorophyll fluorescence are shown as green, yellow, and red, respectively. Scale bars, 25 µm.

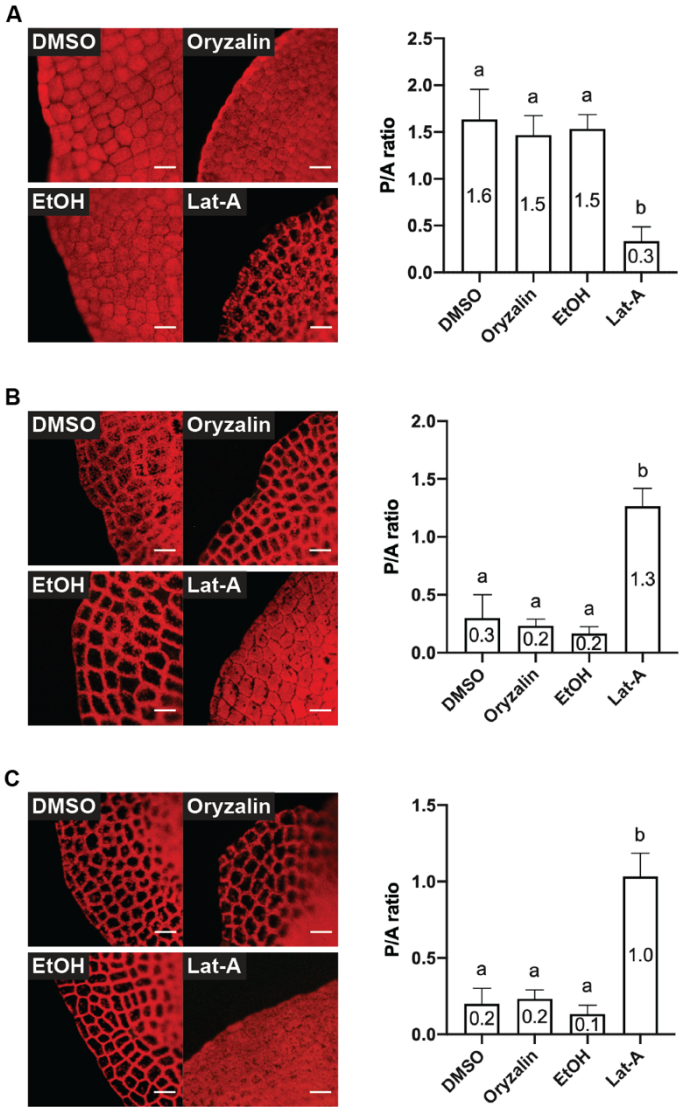


**Figure 21.** Determination of actin filament dependency of the accumulation, avoidance and cold-avoidance responses of *A. endiviifolia*. **A,** Representative images of chloroplast positioning induced in the inhibitor-treated thalli after incubation under weak blue light (25 µmol photons $m^{-2}$ $s^{-1}$) at 22°C for 24 h. The graph showed the quantitative analysis of the resulting chloroplast positionings based on the average P/A ratio from three replicates. **B,** Representative images of chloroplast positioning induced in the inhibitor-treated thalli after incubation under strong blue light (50 µmol photons $m^{-2}$ $s^{-1}$) at 22°C for 24 h. The graph showed the quantitative analysis of the resulting chloroplast positionings based on the average P/A ratio from three replicates. **C,** Representative images of chloroplast positioning induced in the inhibitor-treated thalli after incubation under weak blue light (25 µmol photons $m^{-2}$ $s^{-1}$) at 5°C for 24 h. The graph showed the quantitative analysis of the resulting chloroplast positionings based on the average P/A ratio from three replicates. DMSO, 0.25% (v/v) dimethyl sulfoxide solution; Oryzalin, 10 µM oryzalin; EtOH, 0.25% (v/v) ethanol solution; Lat-A, 1 µM latrunculin-A. Scale bars, 50 µm. Error bars represent standard deviation (N=3). Different alphabets (a and b) above the graph bars indicate significant differences (Tukey's HSD test; $\alpha < 0.05$).

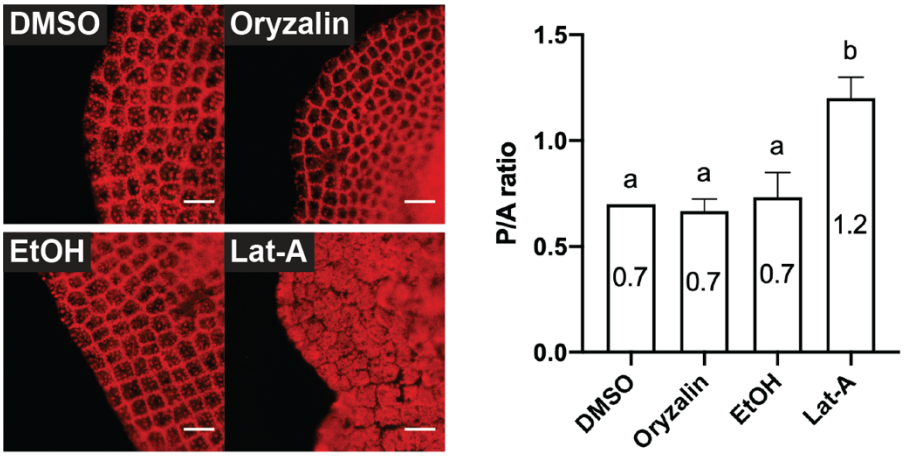


**Figure 22.** Determination of actin filament dependency of the dark-positioning response of *A. endiviifolia*. **A,** Representative images of chloroplast positioning induced in the inhibitor-treated thalli after incubation in the dark at 22°C for 3 h. The graph showed the quantitative analysis of the resulting chloroplast positionings based on the average P/A ratio from three replicates. DMSO, 0.25% (v/v) dimethyl sulfoxide solution; Oryzalin, 10 μM oryzalin; EtOH, 0.25% (v/v) ethanol solution; Lat-A, 1 μM latrunculin A. Scale bars, 50 μm. Error bars represent standard deviation (N=3). Different alphabets (a and b) above the graph bar indicate significant differences (Tukey's HSD test; $\alpha < 0.05$).

# CHAPTER 5

## CONCLUSION AND PROSPECT FOR FUTURE STUDY

The physiological and molecular properties of the chloroplast movements of *A. endiviifolia* were investigated. The simple thalloid thallus with uniformly developed chloroplast and no air chambers has provided clear chloroplast observation in the present study. This beneficial characteristic has facilitated the subsequent analysis of observing the four chloroplast responses: dark-positioning, accumulation, avoidance and cold-avoidance under dark, weak light, strong light and low-temperature conditions, respectively. The blue light dependency of chloroplast responses of *A. endiviifolia* has proved and directed the identification of a single copy phototropin gene (*AePHOT*). The *AePHOT* signalling was therefore verified through the transiently overexpressed chloroplast responses in the AePHOT-transformed cells of *A. endiviifolia* under weak blue light conditions at 22°C. Additionally, the species specificity of the *AePHOT* gene was identified after the incompatible *AePHOT* signalling in the AePHOT-transformed cells of *M. polymorpha* was observed. Furthermore, *MpPHOT* has transiently overexpressed the chloroplast responses in both MpPHOT-transformed cells of *A. endiviifolia* and *M. polymorpha* under weak BL conditions. This finding shows the compatibility of *MpPHOT* with *A. endiviifolia*, also supports the notion of using *A. endiviifolia* as a chloroplast observation tool in the future analysis of *MpPHOT*.

Furthermore, the rapid dark-positioning response of *A. endiviifolia* completed after 3 h of dark incubation was demonstrated in the present study. This movement speed in the dark was considered the fastest than any reported data. The rapid dark-positioning response can be a useful trait of *A. endiviifolia* and highlights the potential uses in future studies of the response. Indeed, the physiological significance of the dark-positioning response remains a mystery since it was first observed by Bernhard Frank in 1872. Perhaps this issue will be elucidated by analysing the rapid dark-positioning response of *A. endiviifolia*. Finally, microtubules and actin filaments were visualised through the respective fluorescent probes in *A. endiviifolia* and were precisely disrupted by the microtubule and actin filament polymerisation inhibitors, oryzalin and latrunculin A. Only the depolymerised actin filaments have restricted the chloroplast mobility in the light-dependent chloroplast response of accumulation, avoidance and cold-avoidance of *A. endiviifolia*, proving actin filaments were responsible for the chloroplast responses. Additionally, the dark-positioning response was also inhibited by the disruption of actin filaments only, indicating the dark-positioning response of *A. endiviifolia* depends solely on the actin filament-associated motility mechanism. This is the first report to describe actin filament dependency of the rapid dark-positioning response in *A. endiviifolia*, and I hope this will be a good start to elucidate the response in the future.

Overall, the physiological properties of chloroplast movements in *A. endiviifolia* have been conclusively analysed and understood. However, the molecular analysis of the chloroplast movements of *A. endiviifolia* was not conducted as much as the physiological analysis. The reason was due to the incomplete transformation technique developed in *A. endiviifolia*. Unlike many well-known model plants, *A. endiviifolia* was not much reported or involved in research, and most of the reported studies are about sex determination and phylogenetical analysis (Sierocka et al., 2011, 2014, 2020; Alaba et al., 2015; Newton, 1981). Therefore, the development of genetic

transformation technology using *A. endiviifolia* was limited. Despite the particle bombardment transformation that has successfully transformed the thallus cells for transient expression in the present study, a stable genetic transformation technique is still desired and would expand the experimental options to understand the chloroplast movements in *A. endiviifolia*. Therefore, a stable genetic transformation method like the Agrobacterium-mediated transformation method should be developed for better utilisation of *A. endiviifolia* in future studies.

**LIST OF REFERENCES**


Alaba, S., Piszczalka, P., Pietrykowska, H., Pacak, A. M., Sierocka, I., Nuc, P. W., Singh, K., Plewka, P., Sulkowska, A., Jarmolowski, A., Karlowski, W. M., & Szweykowska-Kulinska, Z. (2015). The liverwort *Pellia endiviifolia* shares microtranscriptomic traits that are common to green algae and land plants. *New Phytologist*, *206*(1), 352–367.

Bolger, A. M., Lohse, M., & Usadel, B. (2014). Trimmomatic: a flexible trimmer for Illumina sequence data. *Bioinformatics*, *30*(15), 2114–2120.

Briggs, W. R., Beck, C. F., Cashmore, A. R., Christie, J. M., Hughes, J., Jarillo, J. A., Kagawa, T., Kanegae, H., Liscum, E., Nagatani, A., Okada, K., Salomon, M., Rüdiger, W., Sakai, T., Takano, M., Wada, M., & Watson, J. C. (2001). The phototropin family of photoreceptors. *Plant Cell*, *13*(5), 993–997.

Buda, G. J., Barnes, W. J., Fich, E. A., Park, S., Yeats, T. H., Zhao, L., Domozych, D. S., & Rose, J. K. C. (2013). An ATP binding cassette transporter is required for cuticular wax deposition and desiccation tolerance in the moss *Physcomitrella patens*. *Plant Cell*, *25*(10), 4000–4013.

Chomczynski, P. (1993). A reagent for the single-step simultaneous isolation of RNA, DNA and proteins from cell and tissue samples. *BioTechniques*, *15*(3), 532–537.

Christie, J. M., Salomon, M., Nozue, K., Wada, M., & Briggs, W. R. (1999). LOV (light, oxygen, or voltage) domains of the blue-light photoreceptor phototropin (nph1): Binding sites for the chromophore flavin mononucleotide. *Proceedings of the National Academy of Sciences of the United States of America*, *96*(15), 8779–8783.

Christie, J. M. (2007). Phototropin blue-light receptors. *Annual Review of Plant Biology*, *58*(1), 21–45.

Crandall-Stotler, B. J., Forrest, L. L., & Stotler, R. E. (2005). Evolutionary trends in the simple thalloid liverworts (Marchantiophyta, Jungermanniopsida subclass Metzgeriidae). *Taxon*, *54*(2), 299.

Du, F., Zhao, F., Traas, J., & Jiao, Y. (2021). Visualization of cortical microtubule networks in plant cells by live imaging and immunostaining. *STAR Protocols*, *2*(1), 100301.

Frank, B. (1872). Über die Veränderung der Lage der Chlorophyllkörner und des Protoplasmas in der Zelle und deren innere und äußere Ursachen. Jb. wiss. Bot. 8, 216–303.

Fujii, Y., Ogasawara, Y., Takahashi, Y., Sakata, M., Noguchi, M., Tamura, S., & Kodama, Y. (2020). The cold-induced switch in direction of chloroplast relocation occurs independently of changes in endogenous phototropin levels. *PLoS ONE*, *15*(5), 1–15.

Fujii, Y., Tanaka, H., Konno, N., Ogasawara, Y., Hamashima, N., Tamura, S., Hasegawa, S., Hayasaki, Y., Okajima, K., & Kodama, Y. (2017). Phototropin perceives temperature based on the lifetime of its photoactivated state. *Proceedings of the National Academy of Sciences of the United States of America*, *114*(34), 9206–9211.

Fujii, Y., Yoshimura, A., & Kodama, Y. (2018). A novel orange-colored bimolecular fluorescence complementation (BiFC) assay using monomeric Kusabira-Orange protein. *BioTechniques*, *64*(4), 153–161.

Gotoh, E., Suetsugu, N., Yamori, W., Ishishita, K., Kiyabu, R., Fukuda, M., Higa, T., Shirouchi, B., & Wada, M. (2018). Chloroplast accumulation response enhances leaf photosynthesis and plant biomass production. *Plant Physiology*, *178*(3), 1358–1369.

Haas, B. J., Papanicolaou, A., Yassour, M., Grabherr, M., Philip, D., Bowden, J., Couger, M. B., Eccles, D., Li, B., Macmanes, M. D., Ott, M., Orvis, J., Pochet, N., Strozzi, F., Weeks, N., Westerman, R., William, T., Dewey, C. N., Henschel, R., … Regev, A. (2013). De novo transcript sequence reconstruction from RNA-Seq: reference generation and analysis with Trinity. *Nature protocols, 8*(8), 1494–1512.

He-Nygrén, X., Juslén, A., Ahonen, I., Glenny, D., & Piippo, S. (2006). Illuminating the evolutionary history of liverworts (Marchantiophyta)-Towards a natural classification. *Cladistics*, *22*(1), 1–31.

Hikawa, M., Nishizawa, K., & Kodama, Y. (2019). Prediction of prospective leaf morphology in lettuce based on intracellular chloroplast position. *Scientia Horticulturae, 251*, 20–24.

Izumi, M., Ishida, H., Nakamura, S., & Hidema, J. (2017). Entire photodamaged chloroplasts are transported to the central vacuole by autophagy. *The Plant Cell, 29*(2), 377–394.

Jarillo, J. A., Gabrys, H., Capel, J., Alonso, J. M., Ecker, J. R., & Cashmore, A. R. (2001). Phototropin-related NPL1 controls chloroplast relocation induced by blue light. *Nature*, *410*(6831), 952–954.

Kadota, A., Sato, Y., & Wada, M. (2000). Intracellular chloroplast photorelocation in the moss *Physcomitrella patens* is mediated by phytochrome as well as by a blue-light receptor. *Planta*, *210*(6), 932–937.

Kadota, A., Yamada, N., Suetsugu, N., Hirose, M., Saito, C., Shoda, K., Ichikawa, S., Kagawa, T., Nakano, A., & Wada, M. (2009). Short actin-based mechanism for light-directed chloroplast movement in *Arabidopsis*. *Proceedings of the National Academy of Sciences of the United States of America*, *106*(31), 13106–13111.

Kagawa, T., Kasahara, M., Abe, T., Yoshida, S., & Wada, M. (2004). Function analysis of phototropin2 using fern mutants deficient in blue light-induced chloroplast avoidance movement. *Plant and Cell Physiology*, *45*(4), 416–426.

Kagawa, T., Sakai, T., Suetsugu, N., Oikawa, K., Ishiguro, S., Kato, T., Tabata, S., Okada, K., & Wada, M. (2001). *Arabidopsis* NPL1: A phototropin homolog controlling the chloroplast high-light avoidance response. *Science*, *291*(5511), 2138–2141.

Kagawa, T., & Wada, M. (1994). Brief irradiation with red or blue light induces orientational movement of chloroplasts in dark-adapted prothallial cells of the fern *Adiantum*. *Journal of Plant Research*, *107*(4), 389–398.

Kasahara, M., Kagawa, T., Sato, Y., Kiyosue, T., & Wada, M. (2004). Phototropins mediate blue and red light-induced chloroplast movements in *Physcomitrella patens*. *Plant Physiology*, *135*(3), 1388–1397.

Kasahara, M., Swartz, T. E., Olney, M. A., Onodera, A., Mochizuki, N., Fukuzawa, H., Asamizu, E., Tabata, S., Kanegae, H., Takano, M., Christie, J. M., Nagatani, A., & Briggs, W. R. (2002). Photochemical properties of the flavin mononucleotide-binding domains of the phototropins from Arabidopsis, rice, and *Chlamydomonas reinhardtii*. *Plant Physiology*, *129*(2), 762–773.

Kataoka, H. (1980). Photoorientation movement of chloroplasts. In M. Furuya (Ed.), *Light and Life in Nature (Hikari-undoh-hannoh, in Japanese)* (pp. 206–241). Kyoritsu-Shuppan, Tokyo.

Kimura, S., & Kodama, Y. (2016). Actin-dependence of the chloroplast cold positioning response in the liverwort *Marchantia polymorpha* L. *PeerJ 4:e2513*.

Kinoshita, T., Doi, M., Suetsugu, N., Kagawa, T., Wada, M., & Shimazaki, K. (2001). Phot1 and phot2 mediate blue light regulation of stomatal opening. *Nature*, *414*(6864), 656–660.

Kodama, Y. (2016). Time gating of chloroplast autofluorescence allows clearer fluorescence imaging in planta. *PLoS ONE*, *11*(3), 1–8.

Kodama, Y., Tsuboi, H., Kagawa, T., & Wada, M. (2008). Low temperature-induced chloroplast relocation mediated by a blue light receptor, phototropin 2, in fern gametophytes. *Journal of Plant Research*, *121*(4), 441–448.

Komatsu, A., Terai, M., Ishizaki, K., Suetsugu, N., Nishihama, R., Yamato, K. T., Kohchi, T., Tsuboi, H., & Wada, M. (2014). Phototropin encoded by a Single-Copy gene mediates chloroplast photorelocation movements in the liverwort *Marchantia polymorpha*. *Plant Physiology*, *166*(1), 411–427.

Kumar, S., Stecher, G., & Tamura, K. (2016). MEGA7: Molecular evolutionary genetics analysis version 7.0 for bigger datasets. *Molecular Biology and Evolution*, *33*(7), 1870–1874.

Łabuz, J., Hermanowicz, P., & Gabryś, H. (2015). The impact of temperature on blue light induced chloroplast movements in *Arabidopsis thaliana*. *Plant Science*, *239*, 238–249.

Li, F. W., Villarreal, J. C., Kelly, S., Rothfels, C. J., Melkonian, M., Frangedakis, E., Ruhsam, M., Sigel, E. M., Der, J. P., Pittermann, J., Burge, D. O., Pokorny, L., Larsson, A., Chen, T., Weststrand, S., Thomas, P., Carpenter, E., Zhang, Y., Tian, Z., … Pryer, K. M. (2014). Horizontal transfer of an adaptive chimeric photoreceptor from bryophytes to ferns. *Proceedings of the National Academy of Sciences of the United States of America*, *111*(18), 6672–6677.

Li, F. W., Rothfels, C. J., Melkonian, M., Villarreal, J. C., Stevenson, D. W., Graham, S. W., Wong, G. K. S., Mathews, S., & Pryer, K. M. (2015). The origin and evolution of phototropins. *Frontiers in Plant Science*, *6*, 1–11.

Liscum, E., & Briggs, W. R. (1995). Mutations in the *NPH1* locus of Arabidopsis disrupt the perception of phototropic stimuli. *The Plant Cell, 7*(4), 473–485.

McCabe, M. S., Power, J. B., de Laat, A. M. M., & Davey, M. R. (1997). Detection of single-copy genes in DNA from transgenic plants by nonradioactive Southern blot analysis. *Molecular Biotechnology, 7*(1), 79–84.

Mizukami, M., & Wada, S. (1981). Action spectrum for light-induced chloroplast accumulation in a marine coenocytic green alga, *Bryopsis plumosa*. *Plant and Cell Physiology*, *22*(7), 1245–1255.

Moore, S. le M. (1888). Studies in vegetable biology. - IV. The influence of light upon protoplasmic movement, Part II. *Journal of the Linnean Society of London, Botany, 24*(163), 351–389.

Newton, M. E. (1981). Evolution and speciation in Pellia, With special reference to the Pellia megaspora-endiviifolia complex (Metzgeriales), II. Cytology. *Journal of Bryology*, *11*(3), 433–440.

Ogasawara, Y., Ishizaki, K., Kohchi, T., & Kodama, Y. (2013). Cold-induced organelle relocation in the liverwort *Marchantia polymorpha* L. *Plant, Cell and Environment*, *36*(8), 1520–1528.

Oikawa, K., Kasahara, M., Kiyosue, T., Kagawa, T., Suetsugu, N., Takahashi, F., Kanegae, T., Niwa, Y., Kadota, A., & Wada, M. (2003). CHLOROPLAST UNUSUAL POSITIONING1 is essential for proper chloroplast positioning. *Plant Cell*, *15*(12), 2805–2815.

Oikawa, K., Yamasato, A., Kong, S., Kasahara, M., Nakai, M., Takahashi, F., Ogura, Y., Kagawa, T. & Wada, M. (2008). Chloroplast outer envelope protein Chup1 is essential for chloroplast anchorage to the plasma membrane and chloroplast movement. *Plant Physiology, 148*, 829-842.

Osaki, Y., & Kodama, Y. (2017). Particle bombardment and subcellular protein localization analysis in the aquatic plant *Egeria densa*. *PeerJ* 5:e3779.

Parzych, A., Jonczak, J., & Sobisz, Z. (2018). *Pellia endiviifolia* (Dicks.) Dumort. Liverwort with a potential for water purification. *International Journal of Environmental Research*, *12*(4), 471–478.

Regier, N., & Frey, B. (2010). Experimental comparison of relative RT-qPCR quantification approaches for gene expression studies in poplar. *BMC Molecular Biology*, *11*.

Robert, X., & Gouet, P. (2014). Deciphering key features in protein structures with the new ENDscript server. *Nucleic Acids Research*, *42*(W1), 320–324.

Sakai, T., Kagawa, T., Kasahara, M., Swartz, T. E., Christie, J. M., Briggs, W. R., Wada, M., & Okada, K. (2001). *Arabidopsis* nph1 and npl1: Blue light receptors that mediate both phototropism and chloroplast relocation. *Proceedings of the National Academy of Sciences of the United States of America*, *98*(12), 6969–6974.

Sakata, M., Kimura, S., Fujii, Y., Sakai, T., & Kodama, Y. (2019). Relationship between relocation of phototropin to the chloroplast periphery and the initiation of chloroplast movement in *Marchantia polymorpha*. *Plant Direct*, *3*(8), 1–13.

Salomon, M., Christie, J. M., Knieb, E., Lempert, U., & Briggs, W. R. (2000). Photochemical and mutational analysis of the FMN-binding domains of the plant blue light receptor, Phototropin. *Biochemistry, 39*(31), 9401–9410.

Sato, Y., Wada, M., & Kadota, A. (2001). Choice of tracks, microtubules and/or actin filaments for chloroplast photo-movement is differentially controlled by phytochrome and a blue light receptor. *Journal of Cell Science*, *114*(2), 269–279.

Schindelin, J., Arganda-Carreras, I., Frise, E., Kaynig, V., Longair, M., Pietzsch, T., Preibisch, S., Rueden, C., Saalfeld, S., Schmid, B., Tinevez, J., White, D., Hartenstein, V., Eliceiri, K., Tomancak, P., & Cardona, A. (2012). Fiji: an open-source platform for biological-image analysis. *Nature Methods, 9*, 676–682.

Senn, G. (1908). Die Gestalts-und Lageveränderung der Pflanzen-Chromatophoren: mit einer Beilage: Die Lichtbrechung der lebenden Pflanzenzelle. W. Engelmann.

Shimamura, M. (2016). *Marchantia polymorpha*: Taxonomy, phylogeny and morphology of a model system. *Plant and Cell Physiology*, *57*(2), 230–256.

Sierocka, I., Alaba, S., Jarmolowski, A., Karlowski, W. M., & Szweykowska-Kulinska, Z. (2020). The identification of differentially expressed genes in male and female gametophytes of simple thalloid liverwort *Pellia endiviifolia* sp. B using an RNA-seq approach. *Planta*, *252*(2), 1–15.

Sierocka, I., Kozlowski, L. P., Bujnicki, J. M., Jarmolowski, A., & Szweykowska-Kulinska, Z. (2014). Female-specific gene expression in dioecious liverwort Pellia endiviifolia is developmentally regulated and connected to archegonia production. *BMC Plant Biology*, *14*(1), 1–14.

Sierocka, I., Rojek, A., Bielewicz, D., Karlowski, W., Jarmolowski, A., & Szweykowska-Kulinska, Z. (2011). Novel genes specifically expressed during the development of the male thalli and antheridia in the dioecious liverwort *Pellia endiviifolia*. *Gene*, *485*(1), 53–62.

Southern, E. (2006). Southern blotting. *Nature Protocols, 1*(2), 518–525.

Suetsugu, N., Kagawa, T., & Wada, M. (2005). An auxilin-like J-domain protein, JAC1, regulates phototropin-mediated chloroplast movement in Arabidopsis. *Plant Physiology*, *139*(1), 151–162.

Suzuki, K., Suzuki, T., Nakatsuka, T., Dohra, H., Yamagishi, M., Matsuyama, K., & Matsuura, H. (2016). RNA-seq-based evaluation of bicolor tepal pigmentation in Asiatic hybrid lilies (Lilium spp.). *BMC Genomics, 17*(1), 611.

Takagi, S. (2003). Actin-based photo-orientation movement of chloroplasts in plant cells. *Journal of Experimental Biology*, *206*(12), 1963–1969.

Tanaka, H., Sato, M., Ogasawara, Y., Hamashima, N., Buchner, O., Holzinger, A., Toyooka, K., & Kodama, Y. (2017). Chloroplast aggregation during the cold-positioning response in the liverwort *Marchantia polymorpha*. *Journal of Plant Research*, *130*(6), 1061–1070.

Trojan, A., & Gabryś, H. (1996). Chloroplast distribution in *Arabidopsis thaliana* (L.) depends on light conditions during growth. *Plant Physiology*, *111*(2), 419–425.

Tsuboi, H., Suetsugu, N., Kawai-Toyooka, H., & Wada, M. (2007). Phototropins and neochrome1 mediate nuclear movement in the fern *Adiantum capillus-veneris*. *Plant and Cell Physiology*, *48*(6), 892–896.

Tsuboi, H., & Wada, M. (2012a). Chloroplasts move towards the nearest anticlinal walls under dark conditions. *Journal of Plant Research*, *125*(2), 301–310.

Tsuboi, H., & Wada, M. (2012b). Distribution pattern changes of actin filaments during chloroplast movement in *Adiantum capillus-veneris*. *Journal of Plant Research*, *125*(3), 417–428.

Tsuboyama, S., & Kodama, Y. (2014). AgarTrap: A simplified Agrobacterium-mediated transformation method for sporelings of the liverwort *Marchantia polymorpha* L. *Plant and Cell Physiology*, *55*(1), 229–236.

Vaughn, K. C., Campbell, E. O., Hasegawa, J., Owen, H. A., & Renzaglia, K. S. (1990). The pyrenoid is the site of ribulose 1,5-bisphosphate carboxylase/oxygenase accumulation in the hornwort (Bryophyta: Anthocerotae) chloroplast. *Protoplasma*, *156*(3), 117–129.

Wada, M. (2016). Chloroplast and nuclear photorelocation movements. *Proceedings of the Japan Academy Series B: Physical and Biological Sciences*, *92*(9), 387–411.

Xin, P., Li, B., Zhang, H., & Hu, J. (2019). Optimization and control of the light environment for greenhouse crop production. *Scientific Reports, 9*(1), 8650.

Yamashita, H., Sato, Y., Kanegae, T., Kagawa, T., Wada, M., & Kadota, A. (2011). Chloroplast actin filaments organize meshwork on the photorelocated chloroplasts in the moss *Physcomitrella patens*. *Planta*, *233*(2), 357–368.

Yong, L. K., Tsuboyama, S., Kitamura, R., Kurokura, T., Suzuki, T., & Kodama, Y. (2021). Chloroplast relocation movement in the liverwort *Apopellia endiviifolia*. *Physiologia Plantarum*, *173*(3), 775–787.